Modeling, Design and Development of Frameless Stereotaxy in Robot Assisted Neurosurgery

By
GAURAV BHUTANI
(Enrolment No: ENGG01200804002)
Bhabha Atomic Research Centre, Mumbai, India

Under the guidance of:

Dr. T. A. Dwarakanath	**Dr. Aliasgar Moiyadi**	**Shri. D. Venkatesh**
Guide	Co-Guide	Technical Advisor

A thesis submitted to the
Board of Studies in Engineering Sciences

In partial fulfillment of the requirements for the Degree of

DOCTOR OF PHILOSOPHY
of
HOMI BHABHA NATIONAL INSTITUTE

July, 2015

Homi Bhabha National Institute

Recommendations of the Viva Voce Committee

As members of the Viva Voce Committee, we certify that we have read the dissertation prepared by Gaurav Bhutani entitled "**Modeling, Design and Development of Frameless Stereotaxy in Robot Assisted Neurosurgery**" and recommend that it may be accepted as fulfilling the thesis requirement for the Degree of Doctor of Philosophy.

Dated 8/6/15
Chairman: Prof. V.K. Suri

Dated 08/06/2015
Guide: Prof. T. A. Dwarakanath

Dated
Co-Guide: Prof. Aliasgar Moiyadi

Dated 8/6/2015
Technical Advisor: Shri. D. Venkatesh

Dated 8/6/2015
Examiner: Prof. Ashitava Ghosal

J. Chattopadhyay Dated 8/6/15
Member 1: Prof. J. Chattopadhyay

Dated 08/06/15
Member 2: Prof. R. K. Singh 08/06/15

Dated 08/06/15
Member 3: Prof. P. V. Varde

Dated 8/6/15
Member 4: Prof. Balasubramanium

Final approval and acceptance of the thesis is contingent upon the candidate's submission of the final copies of the thesis to HBNI.

We hereby certify that we have read this thesis prepared under our direction and recommend that it may be accepted as fulfilling the thesis requirement.

Date: June 8, 2015

Place: Mumbai

Dr. Aliasgar Moiyadi
Co-guide

Dr. T. A. Dwarakanath
Guide

Statement by Author

This dissertation has been submitted in partial fulfillment of requirements for an advanced degree at Homi Bhabha National Institute (HBNI) and is deposited in the library to be made available to borrowers under rules of the HBNI.

Brief quotations from this dissertation are allowable without special permission, provided that accurate acknowledgement of source is made. Requests for permission for extended quotation from or reproduction of this manuscript in whole or in part may be granted by the Competent Authority of HBNI when in his or her judgment the proposed use of the material is in the interests of scholarship. In all other instances, however, permission must be obtained from the author.

Gaurav Bhutani

Declaration

Myself Gaurav Bhutani (Enrolment No: **ENGG01200804002) o**f HBNI Mumbai, hereby certify that this research work “**Modeling, Design and Development of Frameless Stereotaxy in Robot Assisted Neurosurgery**” carried out by me and the report submitted in partial fulfillment of the requirements of the program is an original work of mine under the guidance of faculty mentors Dr. T. A. Dwarakanath, Dr. Aliasgar Moiyadi and Mr. D. Venkatesh. The study is not based or reproduced from any existing work of any other person or on any earlier work undertaken at any other time or for any other purpose, and has not been submitted as a whole or in part for a degree / diploma at this or any other institution / University.

Gaurav Bhutani

Dedicated

To

My Dear Parents

Acknowledgement

First and foremost, I thank the Almighty God for sustaining the enthusiasm with which I plunged into this endeavor.

I express special gratitude to my organization Bhabha Atomic Research Centre (BARC) for providing me an opportunity to undertake this research. Though, I have taken many efforts in carrying out this research work, it would not have been possible without the kind help and support of many individuals and institutions like Tata Memorial Hospital (TMH) and Advanced Centre for Treatment, Research & Education in Cancer (ACTREC). I would like to extend my sincere thanks to all of them.

I am highly indebted to Dr. T. A. Dwarakanath (Scientific Officer, DRHR, BARC & Professor, HBNI, Mumbai) for his invaluable guidance, and giving me an insight, encouragement and motivation during the course of the work. His ‘Never Say Die’ spirit, to try & try till one succeeds gave me immense motivation to complete the research work successfully. I take this opportunity to express my profound sense of sincere and deep gratitude to my co guide Dr. Aliasgar Moiyadi (Neurosurgeon TMH & Professor, HBNI, Mumbai) for his instrumental support, prompt and valuable guidance besides providing real exposure in the medical field of neurosurgery. I would like to express my deep gratitude to my technical advisor Shri. D. Venkatesh (Ex. Section Head, Electronics & Control Section, DRHR, BARC) for his inspirational support and valuable suggestions for the research work. I would like to thank them all and would like to remember them as a team who guided me to do research and development in an area which would be very helpful to mankind. Their valuable suggestions have ensured that the research work has seen the light of the day.

I would like to express my special gratitude and thanks to Prof. B. K. Dutta (Dean, HBNI), Prof. V. K. Suri (Chairman, Doctoral Committee, HBNI) and all the doctoral committee members, Prof. Balasubramaniam, Prof. J. Chattopadhyay, Prof. P. V. Varde, Prof. P. Chellapandi, Prof. R. Reddy and Prof. R. K. Singh for their valuable suggestions and support throughout the duration of my work. My special thanks to them for their valuable time attending my periodical doctoral committee meetings.

I have great pleasure in expressing my deep gratitude to Dr. D. N. Badodkar (Head, DRHR, BARC) and Dr. P. K. Pal (Head, Autonomous Robotics Section, DRHR, BARC) for permitting me to pursue this research work at the Division of Remote Handling and Robotics (DRHR) and providing the necessary information and the support without which this project would not have been successful. My thanks and appreciation to my colleagues, especially Prafulla A. Khadapkar, P. B. Patil, Hemanta Swain, S. K. Sinha and Venkata P. P. K. for their support and all the people who willingly helped me.

Last, but not the least I extend my gratitude towards my parents, my family members especially my wife Arshi, who helped me at various stages of my thesis and all my close friends for their kind co-operation and encouragement, which helped me in the completion of this work.

I give my sincere and heartfelt thanks to all the respondents who helped me to bring out the research work in a successful manner.

Gaurav Bhutani

Abbreviations

CT	Computerized Tomography
MRI	Magnetic Resonance Imaging
MR	Magnetic Resonance
DOF	Degree of Freedom
2D	Two Dimensional
3D	Three Dimensional
PKM	Parallel Kinematic Mechanism
SPKM	Spatial Parallel Kinematic Mechanism
6D-PKM	Six Degree of Freedom Parallel Kinematic Mechanism
3D-SPKM	Three Degree of Freedom Spatial Parallel Kinematic Mechanism
SCMM	Surgical Coordinate Measuring Mechanism
SCF	Stereotactic Coordinate Frame
FDA	Food and Drug Administration
AESOP	Automated Endoscopic System for Optimal Positioning
ZRSS	ZEUS Robotic Surgical System
UU	Universal-Universal
SPS	Spherical-Prismatic-Spherical
UPS	Universal-Prismatic-Spherical
UPU	Universal-Prismatic-Universal
RRPRR	Revolute-Revolute-Prismatic-Revolute-Revolute
AR	Anatomical Reference
RR	Robot Reference
TP	Target Point
DH	Denavit Hartenberg
OpenGL	Open Graphics Library
F-T Sensor	Force-Torque Sensor
PQP	Proximity Query Package
OBB	Oriented Bounding Boxes
STL	STereo Lithography
DICOM	Digital Imaging and Communications in Medicine
DRHR	Division of Remote Handling and Robotics

BARC	Bhabha Atomic Research Centre
TMH	Tata Memorial Hospital
ACTREC	Advanced Centre for Treatment, Research & Education in Cancer
API	Application Programming Interface
DKP	Direct Kinematics Problem
IKP	Inverse Kinematic Problem
LASER	Light Amplification by Stimulated Emission of Radiation
AACMM	Articulated Arm Coordinate Measuring Mechanism

Index

Abstract

Stereotactic surgery is an approach for the diagnosis of cancer and its treatment. It makes use of a system of three-dimensional coordinates to locate a site (generally within the brain) with utmost precision for a biopsy or surgery. Stereotactic surgery works on the principle of giving a minimal cut necessary for the surgical procedures. Frame and frameless stereotaxy are the two neurosurgical procedures undertaken for diagnostics and treatment of cancer. Many studies on the frame and frameless stereotaxy list the advantages and limitations of the procedures. The aim of the research work presented in this thesis is to develop a robot based frameless stereotactic neurosurgery system having the following features: (i) accuracy comparable to frame based stereotaxy (ii) patient comfort levels equivalent to frameless stereotaxy (iii) free of the line of sight problem existing in optical based frameless stereotaxy.

The objective of the research is to achieve frameless stereotaxy in robot assisted neurosurgery. The research objective is addressed in two parts. The first part of the proposed problem deals with eliminating the physical frames. A methodology is developed to provide a practical design solution to determine the relation of the tumor with respect to the robot frame of reference. A new method for the neuro-registration and the neuronavigation system for the frameless stereotaxy is established through the development of a 4 DOF Surgical Coordinate Measuring Mechanism (SCMM). The measurement of a set of anatomical coordinate data through the SCMM helps to determine the relation of the tumor with respect to the surgical tool. The surgical tool is attached to the Parallel Kinematic Mechanism based robot. This method results in a simpler and accurate system for the neuro-registration and tracking purposes. Experiments are performed to evaluate the performance characteristics and to validate the mechanism. The second part of the proposed problem deals with the mechanism synthesis, analysis, modeling, simulation and prototype development of the robot developed for the frameless stereotactic neurosurgery. The parallel mechanism based architecture is chosen for robot construction to meet the high precision requirement of the neurosurgery. The synthesis of the robot is carried out to meet the workspace and manipulability requirements of the neurosurgery. The mobility analysis, sensitivity analysis, error analysis, singularity analysis of the parallel mechanism based robot is undertaken. The engineering design considerations in the construction of prototypes are presented. The workspace analysis and motion simulation are performed to check the reachability and motion aspects of the robot in

the context of neurosurgery. The successful development of the prototype is reported. Experiments were conducted for the performance evaluation of the parallel mechanism based robot in neurosurgery. The experimental results validate the robot based frameless stereotactic neurosurgery.

List of Publications

International Journal: 03

1. Gaurav Bhutani and T A Dwarakanath, **"Practical Feasibility of High Precision 3-UPU Parallel Mechanism",***Robotica*, Vol. 32, pp. 341 - 355, Issue 3, 2014.
 (Link: http://dx.doi.org/10.1017/S0263574713000696)

2. Gaurav Bhutani and T A Dwarakanath, **"Novel Design Solution to High Precision 3 axes Translational Parallel Mechanism**", *Mechanism and Machine Theory* Journal, Vol. 75, pp 118-130, 2014.
(Link: http://dx.doi.org/10.1016/j.mechmachtheory.*2013.11.010)*

3. *T A Dwarakana*th and Gaurav Bhutani, **"Beam type hexapod structure based six component force-torque sensor",** *Mechatronics*, Volume 21, Issue 8, pp. 1279 – 1287, 2011.

Peer Reviewed National and International Conference: 07

1. T. A. Dwarakanath, Gaurav Bhutani, Anubhav, Aditya Agrawal, "**Spatial Remote Center Analysis of Parallel Robots**" Presented in 2nd *International Conference on Advances in Robotics (AIR-2013)* held at BITS, Goa from 2nd July to 4th July 2015.

2. Gaurav Bhutani, T. A. Dwarakanath, K D Lagoo, Aliasgar Moiyadi and Venkata P P K, "**Neuro-Registration and Navigation Unit for Surgical Manipulation**" Presented in *1st International and 16th National Conference on Machines and Mechanisms (iNaCoMM2013),* held at IIT Roorkee, from 18th Dec. to 20th Dec. 2013.

3. Varsha Shirwalkar, T. A. Dwarakanath, Gaurav Bhutani , "**Force-Torque Interpretation in Intermediary Telepresence for Remote Manipulation**" Presented in *1st International and 16th National Conference on Machines and Mechanisms (iNaCoMM2013),* held at IIT Roorkee, from 18th Dec. to 20th Dec. 2013.

4. Amar Banerji, T A Dwarakanath and Gaurav Bhutani, "**An Analog Computer for a 6-axes Force-Torque Sensor**", Presented in *1st International Conference on Advances in Robotics (AIR-2013)* held at R&DE (Engrs), DRDO, Pune from 4th July to 6th July 2013.

5. T A Dwarakanath and Gaurav Bhutani, "**Novel Design Solution to High Precision 3 axes Translational Parallel Mechanism**", Presented in *15th National Conference on Machines and Mechanisms (NaCoMM 2011)* held at Indian Institute of Technology Madras from 30th Nov. to 2nd Dec. 2011.

6. T A Dwarakanath, Gaurav Bhutani and Puneet Srivastava, "**Task space trajectory planning among cooperating robots through mirror motions**", Presented in *15thNational Conference on Machines and Mechanisms (NaCoMM 2011)* held at Indian Institute of Technology Madras from 30th Nov. to 2nd Dec. 2011.

7. Gaurav Bhutani, T A Dwarakanath, Aliasgar Moiyadi and D Venkatesh, "**Frame based to Frameless Stereotactic Neuro-Surgery**", Presented in *15th National Conference on Machines and Mechanisms (NaCoMM 2011)* held at Indian Institute of Technology Madras from 30th Nov. to 2nd Dec. 2011.

National Seminar: 01

1. T A Dwarakanath, G Bhutani, "**Intermediary Telepresence for Remote Manipulation**," Presented in *National Seminar on Recent Advances in PIE & Remote Technologies for Nuclear Fuel Cycle (RAPT-2010)* held at Indira Gandhi Centre for Atomic Research, Kalpakkam from 23rd Sep. to 24th Sep. 2010.

List of Figures

List of Tables

Chapter I

Introduction

1.1 Introduction to Stereotactic Surgery

The word *stereotactic* is formed by a combination of Greek and Latin words. *Stereo*, in Greek means "solid" or "having three dimensions" and the Latin word *tactus*, means "touch”. Literally, the stereotactic procedure involves identifying a target in three-dimensional coordinates by touching the target with a probe. Stereotactic surgery is an approach for performing targeted surgical procedures, and is often used in diagnosis and treatment of cancers, particularly brain tumors. It makes use of a system of three-dimensional coordinates to locate a site (generally within the brain) with utmost precision, which is a pre-requisite for a biopsy or surgery.

Brain tumors are detected using sophisticated computer technology that images the brain in various ways. Computerized tomography (CT) uses X-rays to develop a 3D-image of the brain. Magnetic resonance imaging (MRI) creates a brain image using magnetic fields and radio-waves. A CT Scan is best suited for viewing bone injuries, diagnosing lung and chest problems, and detecting cancers. A MRI is suited for examining soft tissue in ligament and tendon injuries, spinal cord injuries, brain tumors, etc. In this thesis, simply, ‘MRI’ is referred instead of referring to CT/MRI every time. For the context of the work in the thesis, either CT or MRI scan can be used.

Treatment of a brain tumor depends on its type and location in the body. Craniotomy is the surgical removal of the tumor which involves opening the skull as shown in figure 1.1. In craniotomy, the skin and the underlying tissues are incised in order to access the tumor and perform surgical treatment. The extent of the opening may vary depending on the location and nature of the disease being addressed. The MRI image aids the neurosurgeon to effectively estimate the location of the tumor and manipulate the surrounding structures ensuring safe removal. Often, the tumor is deep seated surrounded by very eloquent and critical structures. The above mentioned type of conventional surgery for the brain is associated with high risk and may lead to more complications besides longer healing time. Reaching these lesions accurately and with minimal disturbance to the surrounding structures is the key.

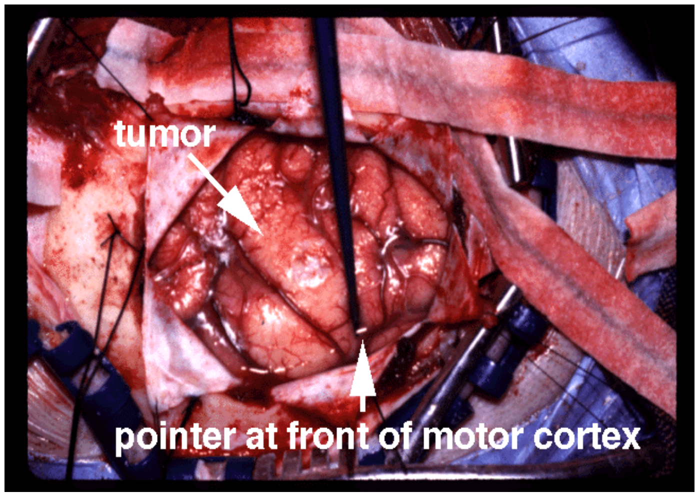

Figure 1.1: A tumor as seen in an open conventional surgery [1]

Stereotactic surgery works on the principle of minimal invasion, giving a minimal cut required for surgical procedures. In context of brain tumors, stereotactic surgery can be performed either to obtain a tissue sample for biopsy or for complete removal of the tumor. The advantage of stereotactic approach is that if the location of the tumor with respect to the base frame of surgical tool is known, then even deep tumors can be localized and approached through a small channel. As the stereotactic surgery is based on minimum invasion, the healing time is less in comparison to conventional craniotomy surgery. Thus surgical exposure shall be minimized and uninvolved areas of the brain can be protected against unwanted risk and complications associated with brain surgeries. Also, for procedures such as biopsy, the opening of the skull can be completely avoided. Even when a craniotomy is indeed required, stereotaxy provides neurosurgeons with a roadmap guiding the procedure and provides neurosurgeons with a confidence that tumor removal may be accomplished without developing any new neurological deficits in a patient.

The stereotactic surgery is a minimally invasive form of surgical intervention which makes use of a three dimensional frame of reference outside the body to locate the tumor within the body. The tumor position is determined with respect to the three dimensional body frame of reference. Also, the position of the surgical tool is determined with respect to the same body frame of reference as illustrated in figure 1.2. Thus, the position of the tumor is determined with respect to the base frame of surgical tool.

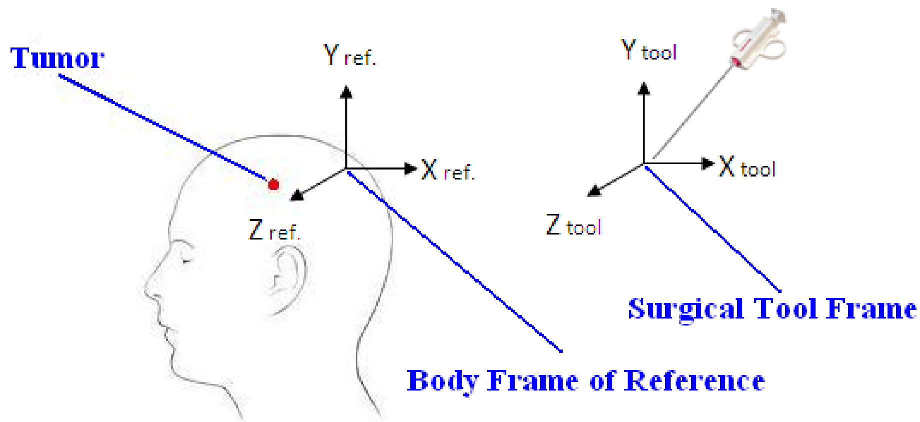

Figure 1.2: Schematic sketch of body and tool frame of reference

The research on frame based stereotaxy was evident in 1908, in which a rigid frame was attached to the patient for establishing a body frame of reference. Due to limitations of frame based stereotaxy systems; the research towards frameless stereotaxy procedures was initiated. The detailed discussion on frame based stereotaxy and frameless stereotaxy will be presented in Chapter 2. Frameless stereotaxy has generated a large interest in the field of medical science. Invasive surgery to minimally invasive and non-invasive surgery is an evolving research area utilizing engineering and technological advancements in imaging, tomography and surgical tooling.

A robot is an advanced tool to generate a precise spatial motion to reach discrete targets with utmost stability and reliability. Robotic surgery or robot-assisted surgery is a technological development that aids the surgeon to perform the surgical procedure with the assistance of robots. The aim of the research work involved in the presented thesis is to develop a prototype of a robot and the related essential setup which would aid the neurosurgeon for frameless stereotactic neurosurgery.

1.2 Organization of the Thesis

The ongoing chapter explains the concept of stereotaxy, stereotactic surgery, references needed for robot based surgery and arrangement of reference frames for localization.

The **second chapter** underscores the historical practices of frame and frameless stereotaxy procedures and the advent of engineering practices in neurosurgical procedures. The concept of stereotaxy in surgical procedures is explained. Building the same body frame of reference for the surgical tool and the tumor and the other important aspects of localization are discussed. The evolution of frame based stereotaxy procedures and recent research and development in the field of frameless stereotaxy are highlighted. The unresolved issues and the limitations of frame and frameless stereotaxy procedures are discussed. State of art robot based surgery and neurosurgery in particular is presented. Literature survey for the parallel mechanisms is presented. The emphasis has been on the suitability of three Degree of Freedom (DOF), six DOF parallel mechanisms and application based issues of parallel mechanisms. The scope of the work and the objectives for the research work is elaborated.

The **third chapter** presents a detailed analysis and synthesis of the robotic system based on the attributes required for the robot based frameless stereotactic neurosurgery. The details of the kinematic structure of 3 and 6 DOF parallel kinematic mechanisms; which are the candidates for robot development in neurosurgery, are presented. The mobility analysis of passive composite joints (used in parallel mechanisms) to arrive at the mobility and optimum orientation of passive composite joints are presented. Sensitivity analysis is undertaken to determine the rate of change of motion of the platform for the given rate of change of motion of each of its legs. Singularity analysis is presented to position the boundaries of the workspace farthest from singularities. Error analysis which deals with the posture error analysis at the platform of the parallel mechanism due to the inaccuracies in passive composite joints is presented. The above analysis aids in development of a high precision robot for performing neurosurgery.

The **fourth chapter** presents the engineering design considerations, workspace analysis, motion simulation, prototype development and experiments conducted for the performance evaluation of the 3 DOF parallel mechanisms. The design considerations which ensure negligible torsional backlash for the prototype design are presented. The development of the mechanism incorporating the design considerations and accounting for mechanical constraints, along with experimental results for the repeatability and trajectory following accuracy for various payloads are presented. The experiments undertaken to validate the frameless stereotactic neurosurgery procedure using the mechanism are presented.

The **fifth chapter** describes the analysis and design of a 6 DOF parallel kinematic mechanism to perform stereotactic procedures to circumvent the customized patient specific attachments, and to fulfill the additional dexterity to the reachable surgical workspace. The synthesis of the mechanism is carried out to fulfill the workspace and manipulability requirements. The properties and requirements including engineering design of the parallel mechanism based robot for frameless stereotactic neurosurgery are presented. The chapter presents the design basis of the mechanism, including workspace requirements; which is established in coordination with neurosurgeons. The 3D motion simulation of the mechanism which helps to effect corrections for interference free mobility and trajectory planning of the mechanism throughout its workspace are presented. Prototype development of 6 DOF parallel mechanism for neurosurgical procedures is presented.

The **sixth chapter** describes the development of a framework to determine the relation of the tumor with utmost precision with respect to the robot reference frame. The information used to formulate the relation between the tumor (Patient's body frame of reference) with respect to the robot base frame, is referred to as neuro-registration. The chapter presents a portable measuring mechanism; which is designed to localize an anatomical reference plane (body frame of reference) with respect to the robot reference coordinate system. A solid model and the working model of the mechanism are developed and presented. The experiments to evaluate the performance characteristics of the mechanism are presented. The chapter presents experimental results of marker based pair point registration and surface based registration procedures of the mechanism.

The thesis concludes in the **seventh chapter** giving an account of the contribution made towards robot based stereotactic neurosurgery. The chapter discusses a few open problems, which need near future solution. The chapter presents emerging trends in neurosurgery and likely practices in the next decade.

1.3 Contribution of the Work

The contribution of the thesis is development of a robot based frameless stereotactic neurosurgery system having the following features:

(i) accuracy comparable to frame based stereotaxy.

(ii) patient comfort levels equivalent to frameless stereotaxy.

(iii) free of the line of sight problem existing in optical based measuring devices.

The contribution of the research also includes formulating the structure of the various associated devices, detailed analysis and development of a robotic system for frameless stereotactic neurosurgery.

Chapter II

Historical Practices in Neurosurgery and State of the Art Engineering in Stereotactic Neurosurgery

2.1 Introduction

This chapter underscores historical practices of frame and frameless stereotaxy procedures and the advent of engineering practices in neurosurgical procedures. The evolution of frame based stereotaxy procedures and recent research and development in the field of frameless stereotaxy is highlighted. The problems and the limitations of frame and frameless stereotaxy procedures are addressed. State of the art robot based surgery and neurosurgery in particular is presented. Literature survey for the parallel mechanisms is presented. The emphasis has been on the suitability of three Degree of Freedom (DOF), six DOF parallel mechanisms and open issues in utilizing parallel mechanisms for surgical applications. The problem formulation and scope of the work is elaborated.

2.2 Evolution of Stereotaxy

Neurosurgeons aimed to develop a system, which can guide a surgical tool to the tumor inside the brain. This was called stereotactic system. The technological solution for the surgical problems has resulted in progress from multiple directions. The first practical stereotactic system was invented more than a century ago in 1908 by Victor Horsley and Robert Henry Clarke [2-10]. In 1908, they published a paper describing their system, atlas and methods for studying the brain functions of cats and monkeys. The system, (see figure 2.1) used by them implemented a Cartesian (Three Orthogonal Axis) system to locate the cerebral targets inside the brain. It assumed that the cerebral targets have a constant and fixed spatial relationship with the body structures in the brain and the external landmarks on the skull. These relations were not individual data of any patient but experience values combined into an atlas. The difficulty in using the Horsley-Clarke apparatus for the human brain is that there is a high variation of the spatial relation between the skull landmarks and the brain structures. Horsley-Clarke apparatus and its modifications were used only for animal experimentation [2-10].

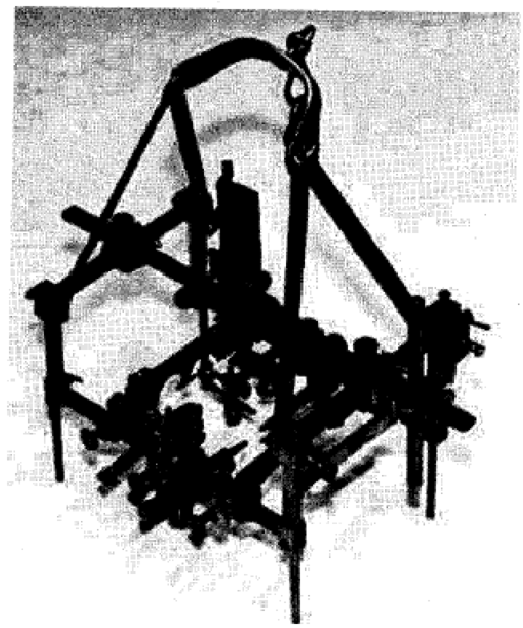

Figure 2.1: Horsley-Clarke stereotactic system [2]

In 1946, the first stereotactic setup, which could be used for the human brain was developed by Ernest A. Spiegel and Henry T. Wycis [11, 12]. A cap was attached to the frame (refer figures 2.2 and 2.3), which was casted for each individual patient and fitted to the patient's head. They used a Cartesian coordinate system for their device. In the Spiegel-Wycis methodology, inter-cerebral landmarks were used for localization of sub-cortical structures. The mentioned approach provided a modest accuracy. The instrument based on this methodology was used for treatment of chronic pain, tumor cysts and movement disorders including Parkinson's disease. Spiegel and Wycis duo further developed the first stereotactic human atlas that gave the relationship of various brain structures with respect to the reference landmarks. At the same time many other stereotactic apparatus were developed [11, 12].

Professor Lars Leksell developed a stereotactic device exclusively for human brain surgery in 1949 [13, 14, 15, 16, 17]. He used a polar coordinate system instead of the Cartesian coordinate system used till then. The Leksell systems were frequently upgraded and are in use till date. Figure 2.4 illustrates the Leksell frame manufactured by his Swedish company. Presently, there are numerous such stereotactic frames available for clinical use.

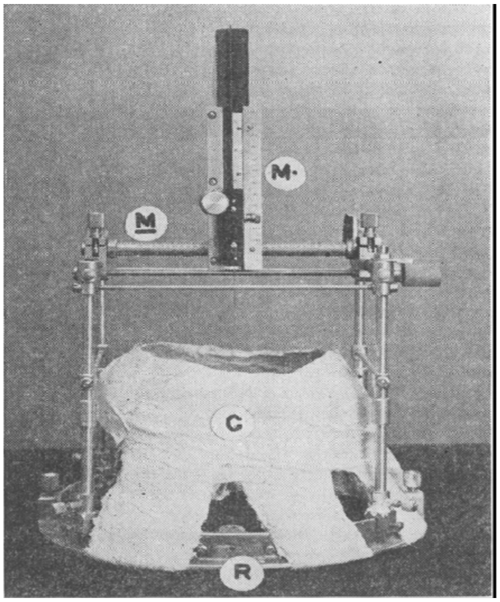

Figure 2.2: Spiegel-Wycis apparatus (side view) [11, 12]

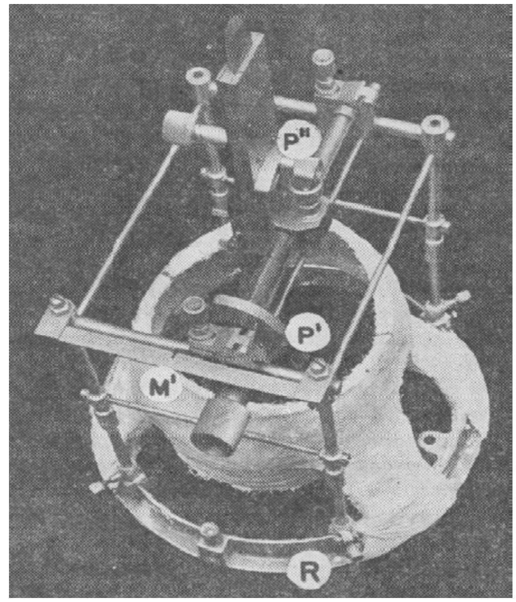

Figure 2.3: Spiegel-Wycis apparatus (top view) [11, 12]

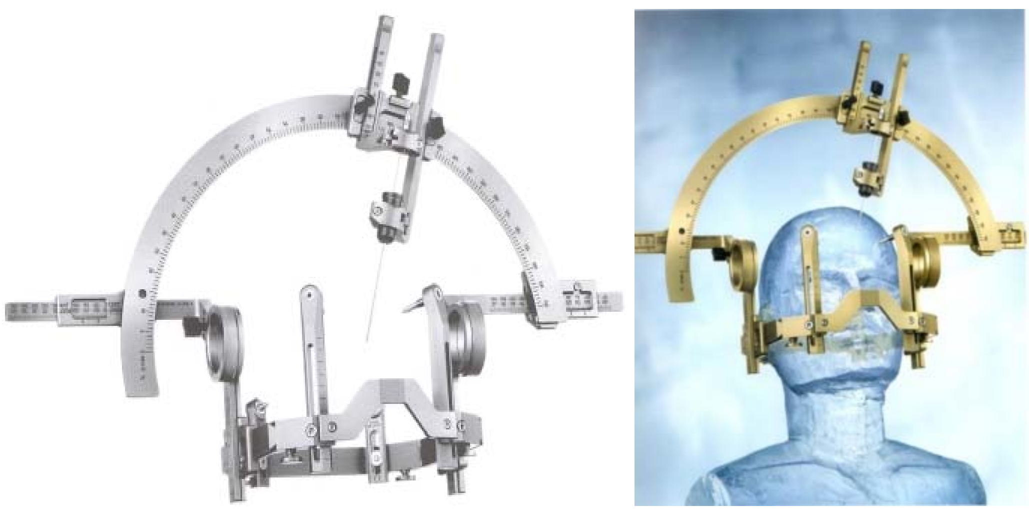

Figure 2.4: Leksell stereotactic frame with stereotactic arc attached [15, 16]

Before 1970's, the position of the tumor (or any other target) was calculated based on the brain atlas (developed on experience values) and X-ray images. These gave a two dimensional view (2D) view of the tumor. A 2D image does not give details of the coordinates of the tumor in the direction perpendicular to the imaging plane. Radiographic techniques give projection of the subject along one direction, thus a 3D view is not generated. Therefore the position of the structures perpendicular to the imaging plane were calculated by visually comparing the radiographic images taken in orthogonal planes and by prior knowledge of anatomical structures within the brain.

In 1970, Computer Tomography [18, 19] was invented. This technique was a revolution in the imaging procedures. Computer Tomography (CT) is an imaging method that uses X-rays to create cross-sectional pictures of the body. CT is a medical imaging method employing tomography created by computer processing. Three-dimensional models of organs can be created by stacking the individual slices of sections together. Later, Magnetic Resonance Imaging (MRI) provided fillip to the medical imaging, offering anatomical information superior to the CT especially for the brain. In a stereotactic procedure, first the stereotactic frame is attached to the patient and then the CT/MRI scan is taken with the frame. The stereotactic frame, besides the tumor is also visible in the CT/MRI scanned images. With the aid of the CT/MRI scan, the three-dimensional coordinates of any tumor inside the brain with relation to the stereotactic frame (rigidly attached to the skull) can be determined [18, 19].

2.3 Frame based Stereotaxy

This section describes the working of the Leksell stereotactic system. The stereotactic apparatus uses a set of three coordinates (x, y and z) in an orthogonal frame of reference (Cartesian coordinates), or, alternatively, a polar coordinates system, along with three coordinates namely angle, depth and antero-posterior location. The mechanical device is equipped with head-holding clamps and bars, which puts the head of the patient in a fixed position in reference to the coordinate system. CT, MRI or any other imaging technique can be used to identify the tumor with relation to the external frame [15, 16, 20]. The procedure for MRI imaging has been mentioned in the presented chapter. The procedural steps for any of these imaging techniques are of similar nature.

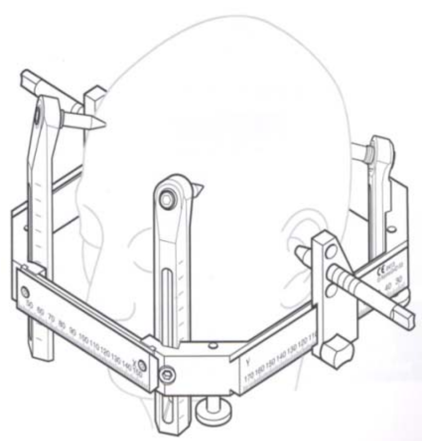

Figure 2.5: Stereotactic Coordinate Frame (SCF) [16]

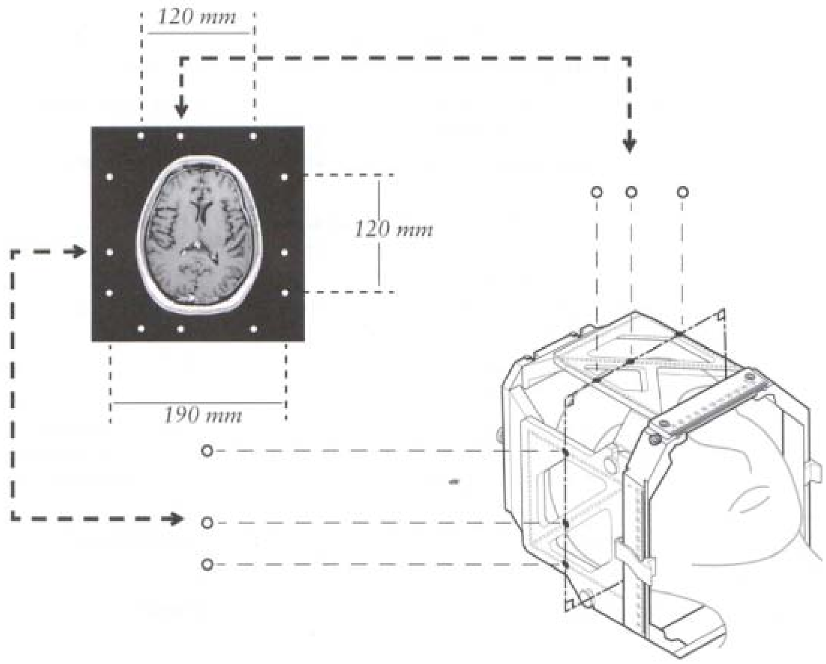

Figure 2.6: Localizing frame and the corresponding slice of the scanned image [16]

Frame based stereotaxy is a two stage procedure. The first stage is the pre-imaging state which is at the MRI imaging room. A light-weight Stereotactic Coordinate Frame (SCF), as illustrated in figure 2.5 is attached to the head of the patient using local anesthesia such that it forms a constant rigid reference with respect to the skull. The SCF serves in establishing references. A localizing attachment, as shown in figure 2.6 is connected to the SCF. The localizing attachment is designed to possess certain characteristics, like indicator holes all around the frame (see figure 2.6). The Magnetic Resonance (MR) indicator-which is seen as white dots in the scan vastly, improves the localization.

After the imaging process on the patient is completed, the patient is relieved of the localizing attachment but the SCF has to be kept intact. The image is analyzed; the localizing frame (white dots) and the tumor are visible in the scanned images, which lead to measuring the distance of the target (centre of the tumor) from the reference points on the frame's three dimensions. Further, from the measurements, the tumor relation with respect to the SCF is established. When the patient is moved to the surgical table, a stereotactic arc is connected on the SCF (refer figure 2.4). The stereotactic arc has three vernier scales, which can arbitrarily position and orient the arc with respect to the SCF. This is required to guide the surgical tool. Therefore a relationship between the tool frame on the surgical tool with respect to the SCF and further from the tool frame to the tumor inside the brain has to be obtained. The figure

2.4 illustrates the biopsy needle attached to the stereotactic arc used for performing biopsy on the patient. The entire assembly is accurately placed in such a manner so that the centre of the stereotactic arc exactly coincides with the tumor. This is called as the "arc-centered" principle. The settings of the coordinates depend on the desired orientation of the stereotactic arc. The coordinates may be determined by manual calculation on the MRI console.

The frame based stereotactic surgery became very popular and has been accepted for long, over three decades. For the last one decade, a campaign for **frameless stereotaxy** has been gaining momentum. In frame based stereotaxy, the patient has to wear the bulky frame for a long duration, from the time of imaging till the completion of the surgery. Sizing the frame to fit different head dimensions occurring across age groups and gender is difficult. The presence of the frame around the head causes hindrance in the surgical procedures and in the movement of the surgical tools. Any displacement or removal of the frame causes loss of reference. In such eventualities, the whole exercise from the first stage has to be repeated all over again. In the next section further evolution and newer direction known as frameless stereotaxy is discussed.

2.4 Frameless Stereotaxy

Research into frameless stereotaxy gathered momentum as the researchers wanted simpler solutions and circumvent the problems faced in frame based stereotaxy. The basic purpose of the frame was to develop a relation of the tumor with respect to the anatomical frame and the surgical tool base frame. The newer means to find a relation between the tumor and the surgical tool base frame without using a frame fixture continued. Presently there are two frameless stereotaxy technologies being preferred instead of frame based stereotaxy. One is the marker-based frameless stereotaxy system and another is the marker-less frameless stereotaxy. Research focus has also been directed towards another development known as neuronavigation or image guided surgery. As the name suggests, the image guided surgery basically means that during the surgery, the MRI image data of the patient along with the position of the surgical tool will be available on the computer screen to the surgeon [1]. During the surgery, the surgeon can visualize in real time the current position of the surgical tool along with the image of the patient on the computer workstation. This is similar to the

GPS system use to navigate while using the land route. The prerequisite of the neuro navigation is that the relationship of the tumor and the surgical tool should be established.

Frameless Stereotaxy Registration Techniques: The concept of frameless stereotaxy is to establish the relationship of the surgical tool with respect to the tumor without using a conventional frame of reference. An intermediary body frame is introduced, which relates the tumor to the surgical tool. Determination of the relation between the MRI data and the intermediary body frame is called the registration. In order to make a reliable and accurate registration, many registration ideas were explored, each with a different technical approach. The frameless registration techniques can be classified into three categories [21].

The first technique is the **marker-less pair point registration**. In this technique, a set of three or more MRI image data and the corresponding actual anatomical landmark positions are matched. The anatomical landmark positions are having a pre-determined relationship with the body frame of reference. The tracking device touches the chosen anatomical points in the actual physical space (say ***R1***) and co-registers the corresponding same point on the MRI image (as ***R1***). Similarly three or more points are registered (as ***R1, R2, R3,..)*** The points are chosen such that they are linearly independent. The least square method is used to determine a relation of points in the image space to the points in the physical space. The method is simple as no markers or frames have to be attached to the patient before the imaging process. This technique lacks the registration accuracy as the anatomical positions on the body are subject to shift or swell while the registration is taking place.

The second technique is called the **marker based pair-point registration**. In this, skin based or bone based markers or fiducials are fixed to the skull (refer figure 2.7) before the pre-operative imaging. As illustrated in figure 2.7, the blue points are fiducials (registered points) and form a body frame of reference. The position of the tumor (represented as red point) is established with respect to the body frame of reference from the MRI image data. The base frame of the surgical tool and the body frame of reference are related from the measured data. The fiducials and the tumor are visible and distinguishable in the imaging and hence a relation of the tumor with the body frame of reference can be established. The skin fiducials are placed in such a position that the mobility of the skin on the underlying tissues is minimal. Bone fiducial markers are fixed to the skull using a titanium screw. Fiducials are kept intact on the patient from pre-operative imaging to surgery. For the registration purpose, the tracking device touches the fiducials and co-registers it with the corresponding image data [21-24].

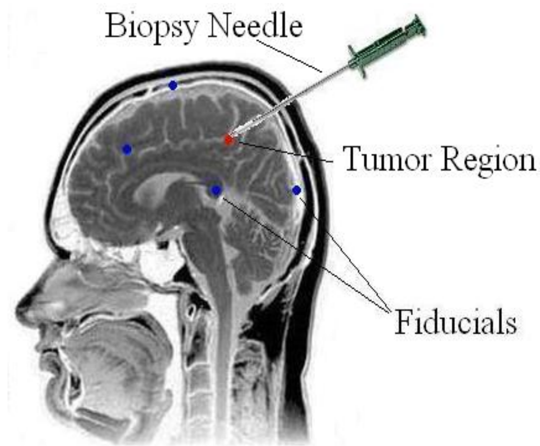

Figure 2.7: Representation of marker based pair-point registration.

The third technique is called **surface registration**, which consists of two large sets of points, which represent the same surface, but there are no point pairs. One set of data is generated from the preoperative imaging data and the other from the LASER pointing device which is traversed on the patient's skin. The transformation is determined, which matches and aligns the two sets of points generated for the surface using a surface matching algorithm. The calculated transformation is used by the neuronavigation system to relate the image data to the surgical tool. [21, 23]

2.5 Neuronavigation System or Image Guided Surgery

Rapid developments in computer based technologies and collaboration of researchers across disciplines led to the development of image guided surgery in the field of stereotaxy. In the image guided surgery, the MRI image data of the patient along with the position of the surgical tool can be available on the computer screen to the surgeon [1]. The tip of the pointing device is projected as crosshairs in the different projections of the image data. During the surgery, the surgeon can view in real time, the position of the surgical tool along with the image of the patient on the computer workstation. The prerequisite of the neuronavigation is the determination of the relationship of the tumor with the image data, which is obtained in the neuro-registration process. The surgical tool position has to be tracked with respect to the patient's image throughout the surgery. For the initial registration of the patient data and tracking of the surgical tool, various tracking mechanisms were developed. The various tracking mechanisms are discussed by Eggers [21].

Figure 2.8: Polaris position sensor [22]

Figure 2.9: Four marker probe [22]

Fig 2.10: Rigid body fixture [22]

Optical Tracking is well accepted for the use in neuronavigation systems. The Polaris [22] optical position sensor is one such kind of optical tracking mechanism. Optical motion-trackers typically use two or more imaging sensors (cameras) to detect passive retro-reflective *markers* affixed to the surgical tool or patient body. The markers consist of reflecting spheres that reflect the infra-red light emitted from the source. The information available on these cameras is merged to generate a spectroscopic image, similar to the human vision. Based on the information received from multiple cameras, the system is able to compute the location of every marker through geometric triangulation. When three or more markers are grouped to form a rigid-body target, it is possible to determine the target's orientation, thus obtaining all the six coordinates of the body. The figures 2.8, 2.9 and 2.10 show the main components of the Polaris [22] position sensor. Commercially available systems such as BrainLab, Philips Easyguide use the optical tracking method [23, 25]. The neurosurgeon is able to view the tool maneuvering inside the brain in MRI image during the surgery. Figure 2.11 shows the BrainLab system [23] with all its components. Frey [24], Doward [25], [26] exhibit the use of the frameless stereotaxy systems in neurosurgery.

Although optical tracking is well accepted, it has some inherent limitations. The limitations of optical based frameless stereotaxy procedures are: (1) the accuracy of optical based tracking is not as comparable to frame based stereotaxy (2) it suffers from ‘line of sight’ problem ([21], [26], [26A]). The ‘line of sight’ refers to the condition that the camera system cannot ‘see’ the marker (reflecting spheres); hence the tracking is not feasible.

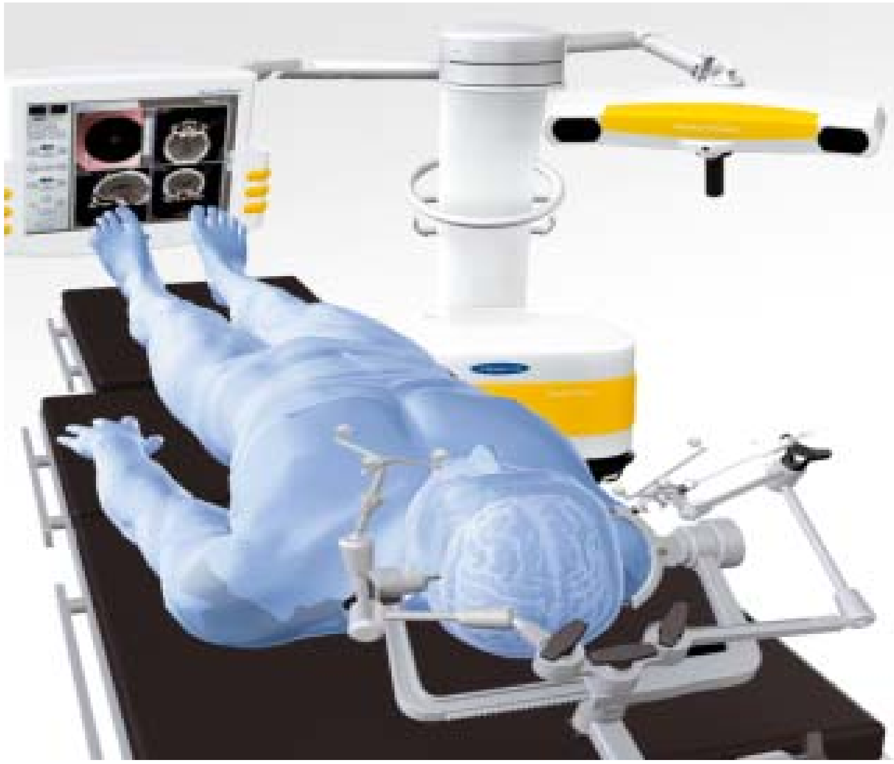

Figure 2.11: BrainLab frameless stereotactic system [23]

The frameless and frame-based stereotaxy systems have different characteristics. The difference lies in terms of the image information and the ergonomics. Image guided surgery or neuronavigation is possible only with the frameless stereotactic systems. The frameless technique may achieve application accuracy comparable to frame-based systems exploiting high quality images (1 mm slice thickness) and high precision bone marker registration. However, when skin mounted fiducials are used for the patient registration; the frameless stereotaxy is less accurate than the frame based systems. The frameless biopsy and surgery are unsuitable for the smaller lesions (less than 10 mm). Frame-based stereotaxy so far remains the gold standard for accurate targeting of the smaller lesions (less than 10 mm) and for the functional procedures.

Brain shift and Intra-operative Imaging System: Brain shift signifies the change in anatomical structure of the patient's brain during the surgery. This happens when a large amount of fluid is drained, like the cerebrospinal fluid from the ventricular system or the tumor fluid from a cyst/tumor. Thus, the pre-operative image data does not reflect the actual anatomy, once distortion has occurred during the surgical procedure. Since the stereotactic based procedure relies on the pre-operative imaging, the displacement of the tissue is not taken into consideration. Intra-operative MRI and ultrasound imaging are emerging practices to update the imaging data in on online manner. Imaging is carried out at intervals while surgery is being performed, which allows image-guided surgery based on current updated patient data.

2.6 Robotic Surgery

Robotic surgery or robotic-assisted surgery is the technological development that aids the surgeon to perform the surgical procedure with the assistance of robots. Robot assisted surgery is performed to aid the surgeon performing the surgery and achieve minimal invasion in surgery. The advantages of robotic surgery over conventional surgery are automation, higher accuracy, smaller incisions, decreased blood loss, less pain, and rapid healing time. All the mentioned advantages lead to the faster recovery of the patient. In the case of robotic-assisted minimally invasive surgery, the surgeon uses a joystick to command a tele-manipulator or computer control to maneuver the surgical tool. A tele-manipulator is a device that extends a person’s manipulating ability to a remote location. A tele-manipulator equipped with a surgical tool based on telepresence and the master slave operation allows the surgeon to perform the movements associated with the surgery on the patient. In computer-controlled systems, the surgeon uses a computer input to control the surgical robot. [27].

Dr. James McEwen, a biomedical engineer, Geof Auchinleck, a engineering physics graduate, and Dr. Brian Day as well as a team of engineering students developed the first surgical robot called as “Heartthrob”. It was used first time in Vancouver, Canada in 1983. The first orthopedic robotic surgery was performed on 12 March 1984, at the UBC Hospital in Vancouver [28, 29, 30]. In 1985, the Unimation Puma 200 robot was used to place a needle for a brain biopsy using a CT imaging guidance. In 1992, the PROBOT robot developed by the Imperial College, London, was used to perform prostatic surgery at Guy's and St Thomas' Hospital, London. The ROBODOC from the Integrated Surgical Systems was introduced in 1992 to mill out precise fittings in the femur for hip replacement. That same year the ROBODOC development team was awarded the prestigious Computerworld Smithsonian Award for Innovation in the Arts and Sciences for Medicine [28, 29, 30].

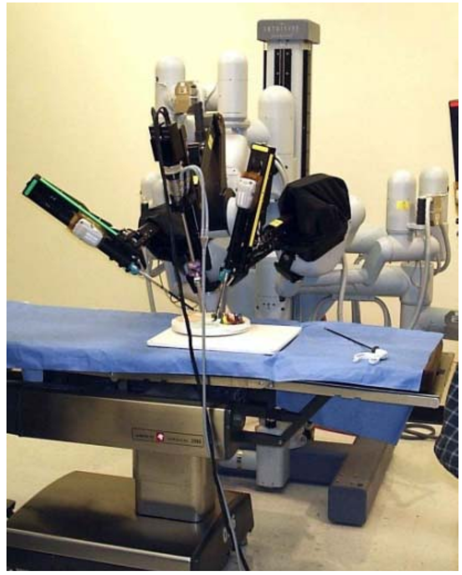

Figure 2.12: da Vinci Surgical System [31]

Figure 2.13: da Vinci Surgical System in operation [32]

SRI International and Intuitive Surgical developed the da Vinci Surgical System (figure 2.12, 2.13). Intuitive Surgical, Inc. is the global technology leader in minimally invasive robotic-assisted surgery. The Company's ‘da Vinci® Surgical System’ enables minimally invasive surgery through a few small incisions or the belly button from a nearby ergonomic console. The da Vinci system has a magnified 3D High Definition (HD) vision system and tiny wristed instruments that have more dexterity in comparison to the human hand. The da Vinci senses the surgeon’s hand movements and translates them electronically into scaled-down micro-movements to manipulate the tiny proprietary instruments. It also detects and filters out any tremors in the surgeon's hand movements, so that they are not duplicated robotically. As a result of this technology, da Vinci enables surgeons to operate with vision and high precision. The first prototype for the da Vinci System was developed in the late 1980s at the former Stanford Research Institute under contract to the U.S. Army. The initial work was funded in the interest of developing a system for remotely performing battlefield surgery. In

1995, Intuitive Surgical was founded to test this theory to a broader range of procedures. Intuitive launched the da Vinci System in January 1999 and became the first robotic surgical system approved by the Food and Drug Administration (FDA) for general laparoscopic surgery in 2000. Consecutively da Vinci System received FDA approval for chest surgery, cardiac surgery, urologic, gynecologic, pediatric, and transoral otolaryngology procedures. The da Vinci Surgical System relies on a human operator for all input and is not designed as an autonomous system. All operations (including vision and motor functions) are performed through remote human-computer interaction [27, 31-38].

Figure 2.14: ZEUS Robotic Surgical System for coronary bypass surgeries [39]

Automated Endoscopic System for Optimal Positioning (AESOP), a medical robot developed by Computer Motion, got FDA approval in 1994 to assist surgeons in performing minimally invasive surgery. AESOP's function was to maneuver an endoscope inside the patient's body during the surgery. The camera moves were guided on the basis of voice commands of the surgeon. Later, the ZEUS Robotic Surgical System (ZRSS) (figure 2.14) was developed by Computer Motion as a successor to AESOP. ZRSS got FDA approval in 2001. ZEUS had three robotic arms which were remotely controlled by the surgeon. The first arm allowed the surgeon to visualize inside the patient’s body. The other two robotic arms imitated the surgeon’s movements in order to make precise incisions and extractions [39-44].

In May 2006, the first unassisted robotic surgery by an artificial intelligence doctor was performed on a 34 year old male to treat heart arrhythmia. The results were rated as better than average in comparison to a surgery performed in a conventional manner by a human surgeon. The machine had a database of 10,000 similar operations. In August 2007, Dr. Sijo Parekattil of the Robotics Institute and Center for Urology, Florida, performed the first robotic assisted microsurgery procedure of the spermatic cord for chronic testicular pain. In February 2008, Dr. Mohan S. Gundeti of the University of Chicago Comer Children's Hospital performed the first robotic pediatric neurogenic bladder reconstruction using the da Vinci Surgical System. [27, 45, 46]

Research on robotic based neurosurgery also kept pace with other specialties. Neuromate was the first image-guided, computer controlled robotic system for stereotactic functional brain surgeries developed by Benabid in 1987. Integrated Surgical Systems developed the same for commercial use and was available in 1997. It became the first device which was approved by FDA for neurosurgery. NeuroMate includes a five degree of freedom robotic system and a pre-surgical planning workstation which includes kinematic positioning software. The NeuroMate system positions, orients and manipulates the surgical tools within the surgical field as planned by the surgeon on the image planning workstation. The first generation NeuroMate System required the use of cumbersome frame based stereotactic systems. The latter versions used frameless techniques for neurosurgery. NeuroMate is currently owned by Renishaw [47-52]. Figures 2.15, 2.16 illustrate the application of the NeuroMate robotic system.

Figure 2.15: Renishaw NeuroMate surgical robot [50]

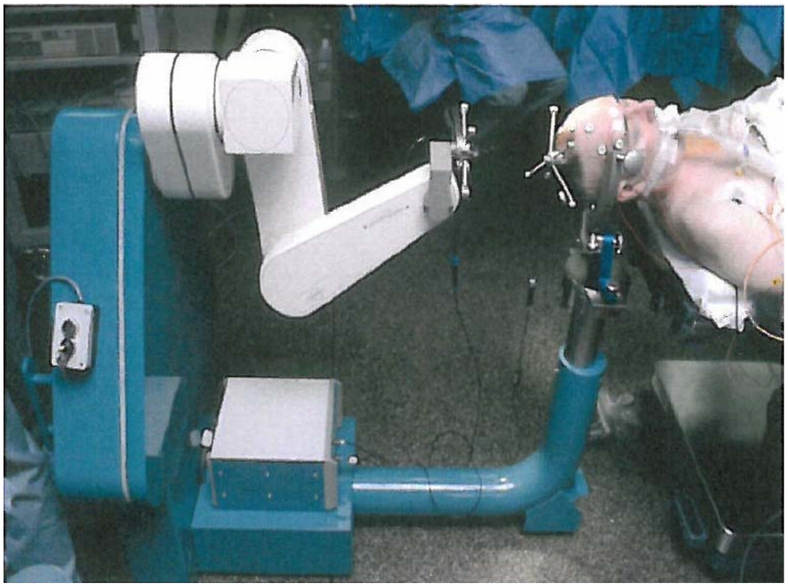

Figure 2.16: NeuroMate robotic system intra-operative registration [49]

Figure 2.17: PathFinder surgical robot from Prosurgics [53]

In 2004, FDA approved another robotic system called PathFinder (figure 2.17) from Prosurgics (formerly Armstrong Healthcare Ltd.) for neurosurgery. In this system, the surgeon specifies a target and trajectory on pre-operative medical images of the patient, and the robot guides the instrument to the specific position with high accuracy. PathFinder was used for guiding needles for biopsy and guiding drills to make burr holes. The PathFinder system consists of a planning workstation and a positioning robot. The use of PathFinder involves two stages: pre-operative planning and surgical implementation. The PathFinder robot is a 6-degree of freedom serial manipulator of roughly human arm dimensions, mounted on a wheeled trolley [53-56].

On May 12, 2008, a team from the Foothills Medical Centre completed the first surgical removal of a brain lesion with the help of an image-guided neurosurgical robot, NeuroArm. It is an engineering research surgical robot specifically designed for neurosurgery. It is the first image-guided, MR-compatible surgical robot that has the capability to perform both microsurgery and stereotaxy (figure 2.18 and 2.19). IMRIS, Inc. acquired NeuroArm assets in 2010, and the company is working to develop a next generation of the technology for worldwide commercialization. It will be integrated with the VISIUS(TM) Surgical Theatre under the name SYMBIS(TM) Surgical System [57-65].

Figure 2.18: Dr. Sutherland with the NeuroArm surgical robot [64]

The system is based on the master-slave control in which the commanded hand-controller movements are replicated by the robot arms. NeuroArm includes two remote detachable manipulators on a mobile base. For stereotactic biopsy, one of the arms is transferred to a stereotactic platform that attaches to the MRI bore. The procedure is performed with image-guidance, as MRI images are acquired in near real-time. The end-effectors interface with the surgical tools which are based on standard neurosurgical instruments. As NeuroArm is MRI-compatible, stereotaxy can be performed inside the bore of the magnet with near real-time image guidance [57-65].

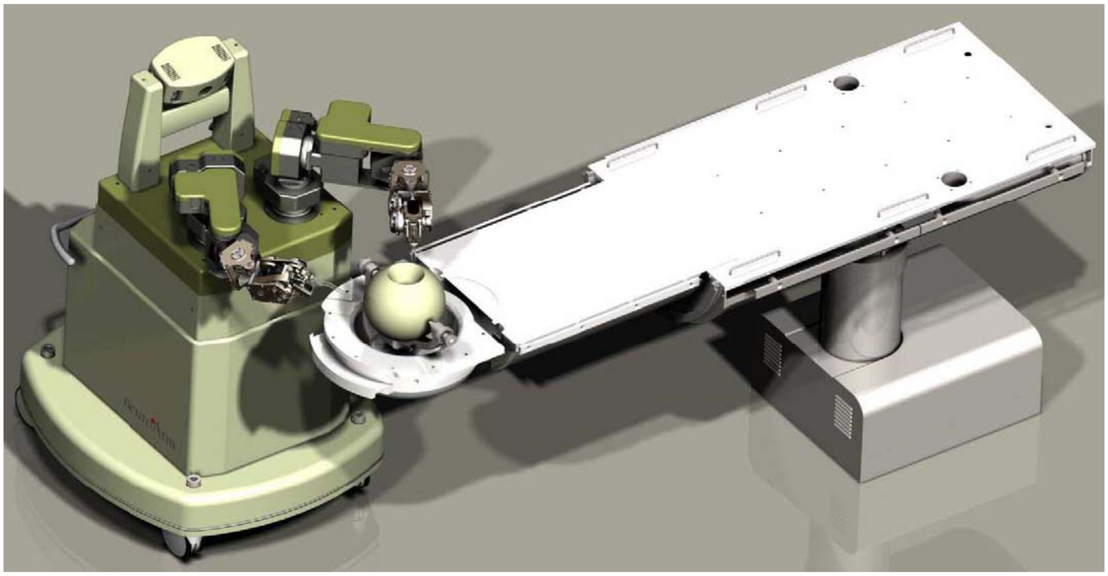

Figure 2.19: NeuroArm in position of surgery [65]

Literature reveals that the robot assisted surgery is gaining momentum since a couple of decades. Most of the surgical robots available are based on the master slave technology. There are a couple of fully automated robotic systems designed for surgical applications. The next significant aspect seen in the literature is that most of the surgical robots use serial link based architecture.

The other architecture, which could improve certain performance characteristics to the manipulating properties, is the parallel architecture, classified as a closed loop mechanism. Because of the reciprocal form of the structure to that of a serial manipulator, the properties of parallel mechanisms are also quite reciprocal to that of the serial mechanism employed for robots. It has high load capacity because the end effector wrench is sustained by its in-parallel linkages in a distributive manner. Therefore it can offer stiff surgical tooling. The other characteristic is its high positional accuracy and repeatability, high precision trajectory following characteristics, which result from the fact that the joint errors are not cumulative as in serial manipulators. The aspect of compact design with six degrees of freedom along with the above mentioned properties prompts one to consider the mechanism for demanding applications like neurosurgery. Hence, parallel architecture based robots can make better options for neurosurgical applications if the robot meets the neurosurgical workspace requirements. The research is being carried out in few laboratories in the area of application of parallel robots in stereotactic neurosurgery. Fraunhofer Institute for Manufacturing Engineering and Automation approached Physicinstrumente (PI), which is a manufacturer of hexapod robots, with the idea of surgical robots [65A, 65B]. The PI M-850 hexapod served as a modular platform for surgical instruments like endoscope. Later, the system was modified further to use a Nanopad (a hexapod with three additional legs with position sensors). To the best of the knowledge, there is no commercially available hexapod based robot available for stereotactic neurosurgery till date. Keeping this preview, the subsequent sections discuss various aspects of parallel robotic systems.

2.7 Grounds for Parallel Mechanisms

As the inception of robotics was with a humanoid flavor, initial developments were centered on attempts to simulate the emotion capabilities of a human arm which apparently consists of a serial open-chain structure. Subsequently, industrial robotics extensively used serial kinematic structures marking a paradigm shift from the traditional industrial arena of mechanisms which is rich in the theory of closed-loop mechanisms. It was quite apparent that the main thrust was towards using open-loop chains as robot manipulators. Such robot manipulators have the advantage of sweeping workspaces and dexterous maneuverability like the human arm. The main constraint is that their load carrying capacity is rather poor due to the cantilever structures. Consequently, from strength considerations, the links become bulky on one hand, while on the other hand they tend to bend under heavy load and vibrate at high speed. Though possessing a large workspace, their precision positioning capability is quite poor. In a nutshell, open-loop serial manipulators have pros and cons of the human arm [66, 67].

Hence, for applications where high load carrying capacity, good dynamic performance and precise positing are of paramount importance, it is desirable to have an alternate to the conventional serial manipulators. For possible solutions, biological world is real inspiration and it can be observed that (1) the bodies of load-carrying animals are more stably supported on multiple in parallel legs compared to the biped human, (2) human beings also use both the arms in cooperation to handle heavy loads and (3) for precise work like writing, three fingers actuated in parallel are used. In general, it is expected that robot manipulators having the end-effector connected to the ground via several chains having actuations in parallel will have greater rigidity and superior positioning capability. This makes the parallel manipulators appealing for certain applications and the last two decades have witnessed considerable research in this direction [66-67].

Parallel robots or Parallel Kinematic Mechanisms (PKM) are closed-loop mechanisms presenting high performance characteristics in terms of accuracy, rigidity and ability to manipulate high loads. They are being used in a large number of applications ranging from astronomy to flight simulators, and are becoming increasingly popular in the machine-tool industry [67]. A **generalized parallel manipulator** is identified as a closed-loop mechanism whose end-effector is linked to the base by several independent kinematic chains [68]. The fundamentals of parallel robots have been discussed in detail by Merlet [68] and introduction to kinematics and first order kinematics is given by Duffy [69].

2.8 Evolution of Parallel Manipulators

The evolution of the parallel manipulators goes back to 1928, where James E. Gwinnett built a motion platform (commonly known under the oxymoron "motion base") for the entertainment industry. The device was designed by James E. Gwinnett who got the same patented in 1931. The device, which was based on a spherical parallel robot, is exhibited in the figure 2.20 [68, 70, 71, 72].

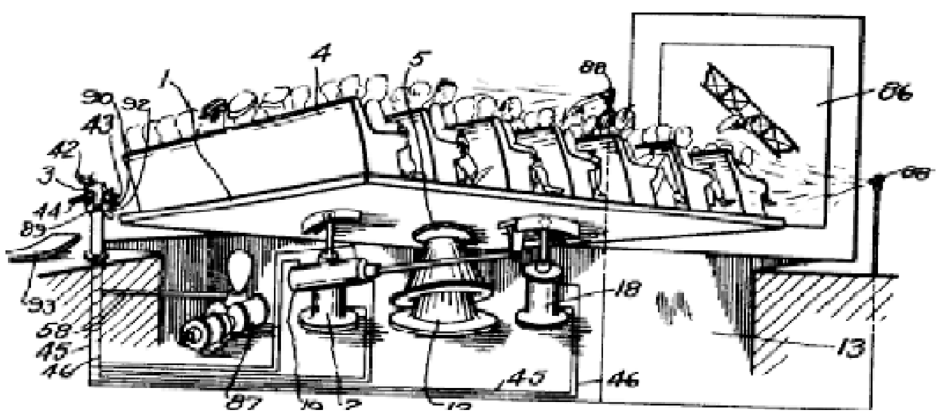

Figure 2.20: The spherical mechanism proposed in 1928 by J.E. Gwinnet, patented in 1931 (US Patent No. 1,789,680) [68, 70, 71, 72]

In the parallel kinematics community, Pollard's parallel robot is well known as the first industrial parallel robot design. This ingenious invention represented a five-DOF three-branched parallel robot (refer figure 2.21). Pollard's parallel robot was intended for spray painting but, unfortunately, never accomplished this goal. The engineer who co-designed the first industrial robot was Willard L.V. Pollard's son; Willard L.G. Pollard Jr. Pollard Jr.'s was issued a patent for the mechanism on June 16, 1942 [68, 70, 71, 73].

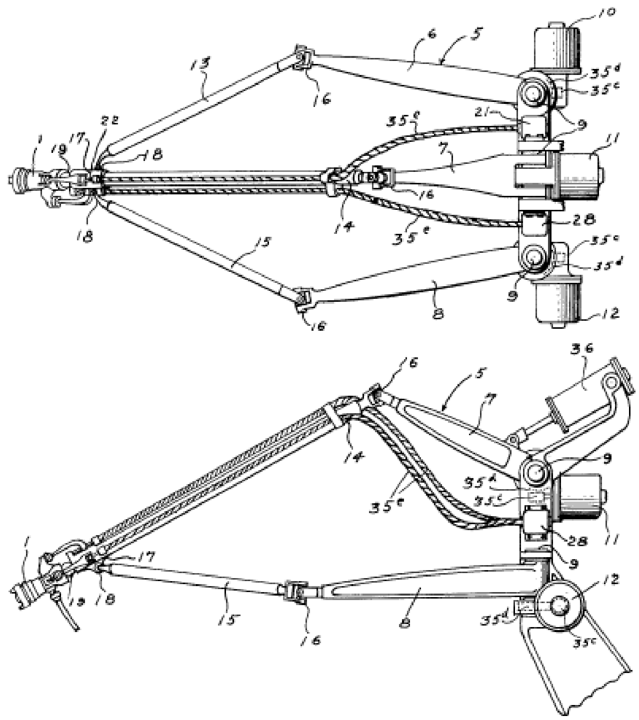

Figure 2.21: First spatial industrial parallel robot, patented in 1942, by L.G. Pollard Jr (US Patent No. 2,286,571) [68, 70, 71, 73]

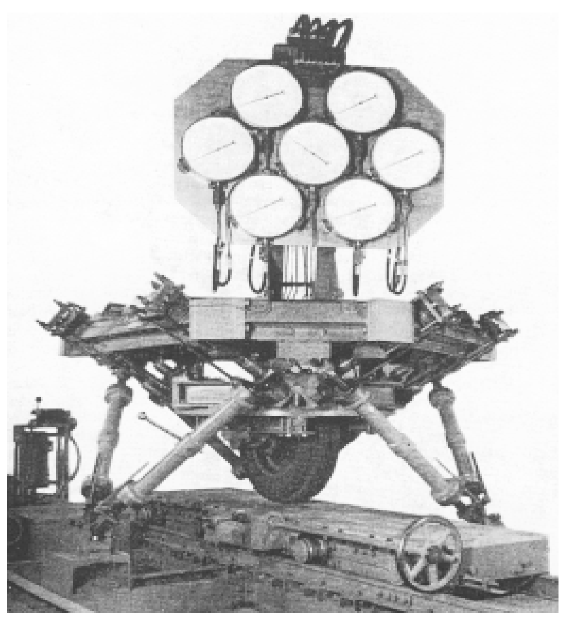

Figure 2.22: Gough mechanism [68, 70, 71, 74, 75]

In 1947, Gough [74] established the basic principles of a mechanism with a closed-loop kinematic structure (figure 2.22), which allows the positioning and the orientation of a moving platform so as to test tire wear and tear. He built a prototype of this machine in 1955 [75]. This device was in use till 2000, the year when it was antiquated. [68, 70, 71, 74, 75]. In 1965, Stewart [68, 70, 76] suggested that motion simulators should be fitted with the mechanism as shown in figure 2.23. The Stewart's paper [76] was instrumental in the development off-light simulator [68, 70, 71, 76].

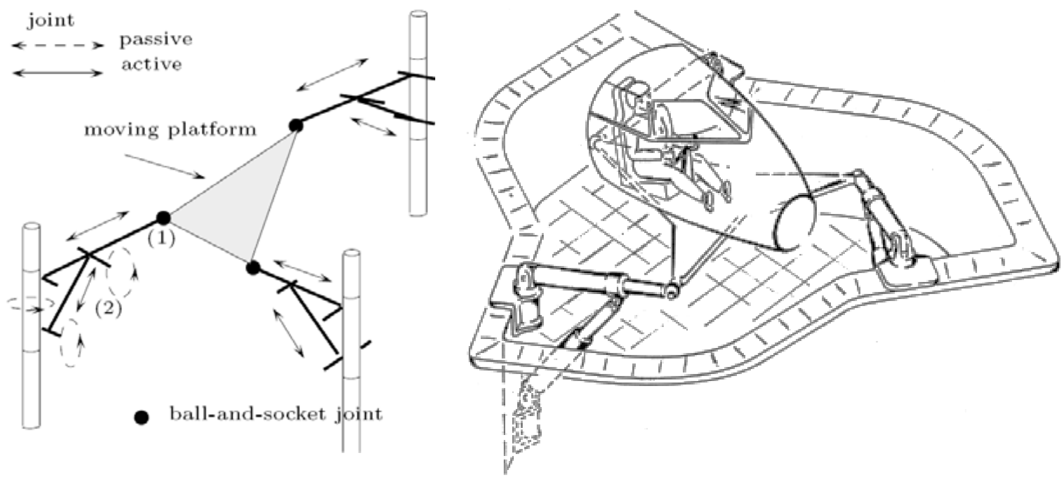

(a) (b)

Figure 2.23: Stewart platform [68, 70, 71, 76]

Ilian Bonev [70] reported that in 1962, an engineer from the Franklin Institute, Klaus Cappel, was given the task of improving an existing Multi Axis Shake Table. He came up with the same octahedral arrangement as Gough. This device was patented in 1967 (figure 2.24) [68, 70, 71, 77].

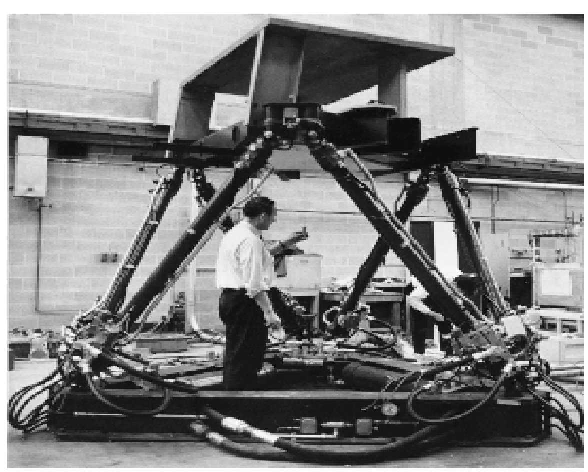

Figure 2.24: The parallel mechanism designed in the mid 1960's by Klaus Cappel [68, 70, 71, 77]

Later, Hunt [78] suggested the use of Stewart's parallel-actuated mechanism based flight simulator as a robot manipulator. He emphasized that such parallel manipulators deserve detailed study in the context of robotic applications in view of their specific advantages (e.g. better stiffness and precise positioning capability) over conventional serial robots. This was the starting point of research on parallel manipulators in general and the Stewart platform in particular in robotic applications. In due course of time, the popular architecture underwent generalizing modifications. The generalized Stewart platform, as it is understood today, consists of two rigid bodies (referred to as the base and the platform) connected through six extensible legs, each with spherical joints at both ends or with a spherical joint at one end and with a universal joint at the other end [66, 67].

Though the above description somewhat varies from Stewart's original design [76], the mechanism of Gough and Whitehall [75] is older and closer to this description, this manipulating structure has gained recognition among researchers as generalized Stewart platform or simply as `the Stewart platform'. In recent years, some authors have referred to the mechanism as `Stewart-Gough Platform'. In particular, the kinematic structure with spherical joints at both ends of each leg will be referred to as a 6-SPS (spherical-prismatic-spherical) Stewart platform. Similarly, the structure with a universal joint at the base and spherical joint at the top (platform-end) of each leg will be referred to as a 6-UPS (universal-prismatic-spherical) Stewart platform. Both the manipulating structures are actuated at the six prismatic joints of the legs and are identical to each other regarding all input-output relationships with an exception that the 6-SPS structure possesses six passive DOF corresponding to the rotation of each leg about its axis [66, 67].

Earl and Rooney [79] analyzed the kinematic structures for robotic applications and their inter connections including both serial and parallel mechanisms and presented methods for synthesis of new kinematic structures. Hunt [80] studied the structural kinematics of parallel manipulators on the basis of screw theory and enumerated promising kinematic structures. He also analyzed the singularities in geometrical terms classifying them into `stationary configurations' and `uncertainty configurations', and discussed the assembly modes of parallel manipulators. Fichter and McDowell [81] applied the conventional method of serial manipulators to the solution of inverse position kinematics (including passive joint variables) of the individual limbs of parallel manipulators and implemented the method on the Stewart platform. Mohamed et. al. [82] and Mohamed and Duffy [83] studied the instantaneous kinematics of parallel manipulators on the basis of the screw theory and presented the inverse and forward kinematics solutions. Yang and Lee [84] performed a kinematic feasibility study of the Stewart platform manipulator and made the first attempt towards its workspace analysis including the physical restrictions on the spherical joints. They developed an algorithm for finding the section of the reachable workspace on a particular plane and provided numerical evidence to the fact that the workspace and maneuverability of parallel manipulators (and the Stewart platform in particular) is rather poor [66, 67].

During the period of 1980’s, various kinematic arrangements of legs in parallel mechanisms were proposed. The first kinematic design is that the base and the platform are triangles with legs meeting in pairs at both ends (3-3 design); and the second kinematic design is having a triangular platform with pair wise meeting of the legs but with six distinct base points in a plane (6-3 design). The third kinematic design that became popular is the one having the semi-regular hexagonal arrangement of the connection points at both the base and the platform. This was perhaps the second choice from the viewpoint of symmetry because the most symmetrical structure, i.e., one having both the base and the platform as regular hexagons, would be uncontrollable [66, 67]. The initial phase of development of the Stewart platform as a research ended through the comprehensive contributions of Fichter [85] and Merlet [86]. Fichter derived the kinematic equations of the general Stewart platform, formulated the dynamic equations in a rudimentary form (by assuming mass less legs and frictionless joints) and stated the condition of singularity along with the enumeration of a few singular configurations. In addition, he made some recommendations for practical construction of a Stewart platform manipulator and explained a construction developed at Oregon State University, which used, incidentally, an equilateral triangular platform and a semi-regular hexagonal base. Merlet considered the design aspects of the Stewart platform and dealt with the special architectures discussed above. He presented some description of the prototype of the Stewart platform built at INRIA, Sophia-Antipolis, France and addressed the solution of the kinematic equations, development of the Jacobian, derivation of dynamic equations with slightly more general conditions than those used by Fichter. He also mentioned the potential of the Stewart platform as a force sensor and passive compliance device. These two works [85, 86] put together embody all the basic concepts of kinematics and dynamics of the Stewart platform manipulator [66, 67].

The challenge of finding all the solutions of the direct kinematics problem has gained a lot of attention. It was proved by Raghavan [87] and Ronga [88] that the maximum possible solutions for 6-6 parallel mechanism would be 40. After numerous unsuccessful attempts for establishing a univariate polynomial formulation, of degree 40, the solution was obtained by Husty [89] in 1994. Husty used a method based on dual quaternions [68].

The static force transformation and singularities have direct significance to the use of the Parallel Kinematic Mechanism as a force-torque sensor. The structure (zero degree of freedom mechanism) has good stiffness and the reconstruction of the wrench applied at the platform from the measured leg forces is quite straight forward. A parallel mechanism with instrumented elastic legs can be used as a wrist force sensor. The first of this kind of sensor was developed by Gaillet and Reboulet [90] based on the octahedral structure of the Stewart platform. The concept of a passive in-parallel mechanism with spring-loaded legs was used by Griffis and Duffy [91] for theoretical modeling of a compliant coupling. Theoretical and experimental investigations of the behavior of the Stewart platform sensors have been carried out by various authors. Dasgupta et. al. [92] presented a design methodology for the Stewart platform sensor structure based on the optimal conditioning of the force transformation matrix [66]. Dwarakanath et. al. [93] presented the design and development of a Stewart platform based force-torque sensor. Dwarakanath and Venkatesh [94] presented the simply supported, joint-less parallel mechanism based force–torque sensor. Dwarakanath and Bhutani [95] brought major simplification in the transduction and thus enabled building miniature sensors. Ghosal's [96] work exhibited isotropic and singular configurations of the force-torque sensor based on Stewart-Gough parallel mechanism. Ranganath et. al. [97] worked on a force-torque sensor based on the Stewart platform in a near-singular configuration.

Singularity in parallel mechanisms is the configuration where the force transformation matrix is rank deficient. At such configuration, the mechanism gains a degree of freedom (loses degree of constraint) and becomes uncontrollable. An analytical study of such singularity has been discussed by Gosselin and Angeles [98]. Choudhury and Ghosal [99] worked in the singularities of parallel mechanisms and their relationship to the controllability of parallel mechanisms. Ghosal and Ravani [100] presented a geometrical approach to analyze the singularities of two and three degree of freedom serial and parallel mechanisms. Bandyopadhyay and Ghosal [101, 102] worked on the analysis of the configuration space of parallel mechanisms and parametric representation of the singularity manifold of the Stewart platform.

The subsequent sections in this chapter present the literature survey on specific unresolved issues in parallel mechanisms on which research is carried out and presented in subsequent chapters.

2.9 Parallel Kinematic Mechanism (PKM) Mobility and Workspace Analysis

The term 'mobility' refers to motion or movement in general. In the presented thesis, the term 'mobility' is referred to as the range of rotation or translation of the joints or the platform (end-effector) of the mechanism. The mobility of the passive composite joints (also referred as passive mobility) refers to the extent to which the passive composite joint can rotate about its axis. The mobility of the platform of PKM (also referred as mobility of PKM) refers to the range of motions along and about its degree of freedom.

The parallel mechanism based systems are developing steadily and possibilities of its use in wide ranging applications is encouraging research and development in the mentioned area. The enhanced interest is because the mechanism is useful in the jointed structure form, in the jointed compliant structure form and in the jointed manipulator form. The structural architectures of parallel manipulators consist of a large number of universal (U) and spherical (S) passive composite joints. The 3-DOF pure translational parallel manipulator is an assemblage of 3-UPU (Universal-Prismatic-Universal) connectors, consisting of 6 U-joints. The 3-DOF, spherical parallel manipulator is made up of 4 S-joints and 3 U-joints. The high speed 4-DOF, Delta parallel robot consists of 12 S-joints. The six-DOF Stewart-Gough mechanism consists of 6-U and 6-S joints, the theory and the construction of this mechanism is given in Fichter E. F. [85]. The structural kinematics and the best kinematic postures which are beneficial for synthesis of the mechanisms are given in Hunt K. H. [80] and Lee J. et. al. [103].

The synthesis and design of passive composite joints is very vital in the parallel mechanism based constructions. Unlike in open loop mechanisms, the numbers of passive composite joints largely outnumber the active joints in closed loop mechanisms. The passive joints can have composite joints to constrain the intersecting axes. The other challenge is that the best forms of geometry of parallel manipulators result in co-incident passive joints and in spatial systems, co-incident passive composite joints. This poses significant complexity in manufacturing passive composite joints for high precision parallel mechanisms. In parallel manipulators, the main limitation is of small workspaces [104]. Apart from the kinematic arrangement, the limited angular mobility of the passive composite joints (universal and spherical joints) is the major constraint. Hence, the orientation of the passive composite joints has to be such that the angular mobility is completely utilized. The optimal positioning and orientation of the legs of the mechanism should be such that there is no interference between them throughout the desired workspace.

Di Gregorio R. et. al. [105] dealt with the mobility and singularity analysis of the 3-UPU translational parallel mechanism. Static analysis and singularity loci of the 3-UPU wrist are presented by Gregorio R. D. [106]. Gosselin C. [107] presented an algorithm to determine the workspace of 6 DOF parallel manipulators for a given orientation. Wang Z. et. al. [108] presented the boundary search algorithm to determine the workspace for parallel machine tools. The orientation plots method was used by Pernkopf F. and Husty [109] for calculation of the workspace taking into account limitations of active and passive joints. A numerical approach was used to determine the workspace of a 6-DOF UPS (Universal-Prismatic-Spherical) parallel robot by Ciprian L. et. al. [110]. The orientation workspace of the parallel manipulators was discussed by Merlet J. P. [111]. Workspace, kinematics and dynamics of a 3-DOF parallel machine tool were discussed by Cai G. Q. et. al. [112]. Gosselin C. M. et. al. [113] presented an algorithm for determining the workspace of planar parallel manipulators with joint limits. Merlet J. P. et. al. [114] presented an algorithm to determine workspaces of planar parallel manipulators. The inverse problem of determining the mobility of passive composite joints for a given workspace of a manipulator has not been found in the literature.

2.10 Three DOF Spatial Parallel Kinematic Mechanism (3D-SPKM)

Spatial three degree of freedom pure translational mechanisms are mostly employed in the industry. Most of them are serial based mechanisms and widely applied in 3-axis cranes, machining centers, coordinate measuring machines, etc. 3-axis parallel mechanisms are in the emerging stage of entry in the industry through Delta Robots for high speed pick and place applications. Tsai et. al. [115] first proposed a 3-DOF based Universal-Prismatic-Universal (UPU) kinematic chain. The fully parallel mechanism can exhibit high stiffness in most of the mechanism workspace. The geometric conditions for a pure translational motion for a 3-UPU mechanism and the workspace analysis are presented in [116] and [117]. Mobility analysis was well analyzed by Di Gregario and Parenti-Castelli [105]. The work on stiffness and deformation of a 3-UPU mechanism has been carried out by Hu and Lu [118]. All the above mentioned theoretical analysis endorses feasibility of the simple and practical 3-DOF, fully parallel mechanism which is known as the 3-UPU parallel mechanism. The 3-UPU mechanism is the particular mechanism of the most generalized 3-RRPRR (Revolute-Revolute-Prismatic-Revolute-Revolute) mechanism, wherein in the first two and last two RR (Revolute-Revolute) joints are replaced with universal joints. Very few research reports based on experimental results for a 3-UPU mechanism are available till date.

The observations and negative results presented in Han et. al. [119] and a reference to this in a survey by Merlet [120] raises concerns regarding the feasibility of 3-UPU parallel mechanisms. Later it was observed that the geometry of a 3-UPU mechanism developed by Han et. al. [119] is in singularity by Walter et. al. [121]. The theoretical models of Venanzi and Parenti-Castelli [122] and Meng et. al. [123] presented the results showing that the end effector position is very highly sensitive to the joint clearances. They have reported very high positional errors acknowledging the results of Han et. al. [119] even in a non-singular geometry. These results largely shifted the focus away from 3-UPU based parallel mechanisms despite sound theoretical assertions [105, 106, 115, 116, 117, 118, 121, 124, 125, 126]. In an accuracy analysis with the joint clearance model given in Venanzi and Parenti-Castelli [122], the total error of the mechanism is stated as the absolute sum of maximum of clearance of all the individual joint pairs constituting the mechanism; which is a highly unlikely scenario. The model does not consider the effect of geometry of the mechanism to arrive at the error at the output link. Adding the absolute values of the maximum errors in all the joints of the mechanism is an erroneous estimate and results in an exaggerated error value in closed loop mechanisms.

2.11 Scope of Work

Medical robotics is an emerging field; high initial cost is associated with the research and technological development. Hence the current robot based neurosurgeries are very expensive. The scope of the work in the presented thesis includes the research and technology development of a robot based neurosurgery with economic considerations without any compromise on the neurosurgical requirements.

Many studies have been conducted on frame and frameless stereotaxy which list the advantages and limitations of the procedures. Literature study states that the accuracy achieved by frame based stereotaxy is much better than frameless stereotaxy. The scope of work includes development of a prototype of a robot and the associated setup which aid the neurosurgeons for frameless stereotactic neurosurgery. The developed system shall have an accuracy comparable to frame based stereotaxy system and at the same time patient comfort levels equivalent to frameless stereotaxy. The research work seeks to eliminate the line of sight problem observed in optical based frameless stereotaxy. The scope of the research includes formulating the structure of the various associated devices, localization and detailed analysis and development of robotic systems necessary for frameless stereotaxy.

The research includes:

- Detailed analysis of the parallel mechanisms in order to find the influence of choice of design parameters on the performance characteristics of the mechanism.
- To examine various design options to provide the practical design solutions to determine relation of the tumor with respect to the robot frame of reference.
- To ascertain that there is no extreme kinematic sensitivity due to torsional clearances in case of 3 DOF UPU spatial parallel mechanisms as projected in [119], [122] and [123]. It would be exhibited that with the precise constraints and accurate mechanism design, the prototype behaves as per the theoretical observations.
- Demonstrating several experiments to establish the precision of the 3 DOF UPU (Universal-Prismatic-Universal) based 3 DOF Spatial Parallel Kinematic Mechanism (3D-SPKM) in conducting neurosurgical procedures.

2.12 Problem Formulation

The objective of the research is to achieve frameless stereotaxy in robot assisted neurosurgery. The research objectives are addressed in two parts. The first part of the proposed problem deals with eliminating the physical frames. It details development of a methodology and a mechanism to determine the relation of the tumor with respect to the surgical tool. The second part of the proposed problem deals with the mechanism synthesis, analysis, modeling, simulation and prototype development of the robot which will be used for neurosurgery. The synthesis of the robot would be carried out to meet the workspace and manipulability requirements of the neurosurgery.

In the first part, the localization of the tumor/target point with respect to an anatomical reference frame is obtained. The localization is obtained at the instant when a MRI scan is performed. In order to eliminate wearing the physical frame, a frameless referencing is obtained. In the frameless stereotaxy, fiducial markers are affixed on the scalp or fixed to the bones which would be used as an Anatomical Reference (AR) frame (body frame of reference). A localization of the anatomical Target Point (TP) with respect to the AR frame is obtained from the group of MRI images. Further, a relationship between the AR frame and the Robot Reference (RR) frame is formulated. A methodology for frameless stereotaxy that localizes an anatomical TP with respect to the RR frame has been developed. The scope of the methodology includes the design and development of a prototype of a metrology system. The metrological measurements would be incorporated to develop a relationship of the AR frame with respect to the RR frame. The relationship between the coordinate frames will aid in the transfer of a group of MRI images data to the RR frame.

The second part of the proposed problem deals with the mechanism synthesis, analysis, modeling, simulation and prototype development of the robot for frameless stereotaxy neurosurgery. The neurosurgical requirement demands high precision, therefore the robots based on the parallel mechanism architecture is chosen for neurosurgery. The 3 DOF UPU based spatial parallel kinematic mechanism and the 6 DOF parallel kinematic mechanism are the two parallel mechanisms taken into consideration. The synthesis of these mechanisms would be carried out to meet the workspace and manipulability requirements. An algorithm would be developed to arrive at the mobility and optimum orientation of the passive composite joints for a desired workspace of the robot. The sensitivity analysis would be conducted to establish a region in the workspace about which the best performance of the mechanism can be obtained. An algorithm for error analysis would be developed. The algorithm determines the posture error at the platform due to the inaccuracies in passive composite joints for a desired posture in the workspace of the robot. This is significant from the design point of view as the aim of the presented research is to develop a system having high positional accuracy and repeatability. A kinematic analysis would be performed to ensure that the kinematic arrangement of the mechanism is singularity free in the entire workspace. The 3D geometrical modeling of the different components of the robot would be developed. The simulation of the robot would be carried out to visualize the interference free motion trajectory. The motion simulation would be extended to visualize the frameless stereotaxy procedure. It is proposed to develop a prototype of a robot considering the above synthesis which can be used for the frameless stereotactic neurosurgery.

Finally, the first part, the registration using a metrology system and the second part, the design and prototype of the parallel mechanisms are combined to demonstrate a high precision frameless stereotaxy in the robot assisted, lab simulated neurosurgery.

Chapter III

Analysis of Robot for Stereotactic Neurosurgery

3.1 Introduction

The idea of using robots for surgery has been reported thirty years ago. The evolution of engineering and technology in neurosurgery since then is presented in chapter 2. The use of robots for stereotactic neurosurgery is a recent development, and research is being conducted actively in the field. The general task is to provide solutions to access miniscule or deep rooted affected regions inside the brain. The use of robots for surgery would be helpful as the tumor point can be accessed with utmost precision and accuracy. The objective of this research is to develop a highly accurate, cost effective frameless stereotactic system using a fiducial based point-to-point registration technique. It consists of development of a 6 DOF robot which would maneuver the surgical tool with utmost precision to a tumor point; development of a surgical coordinate measuring mechanism to localize an anatomical reference plane with respect to the robot reference coordinate system; and the software development for a stereotactic navigation system.

This chapter presents a detailed analysis and synthesis of the robotic system based on the attributes required for a robot in a frameless stereotactic neurosurgery. The essential requirements of the robotic system are that it should be portable and have high precision and accuracy. It should also possess a good reach for the desired neurosurgical workspace. A **6 DOF Parallel Kinematic Mechanism (6D-PKM)** would be used for the stereotactic neurosurgery. The 6D-PKM, presented in the thesis, is a well known semi-regular Stewart platform manipulator. The feasibility analysis, which includes sizing, manipulator fixture, foot print studies and synthesis of workspace, has been conducted. They are verified again by developing a prototype **3 DOF Spatial Parallel Kinematic Mechanism (3D-SPKM)** of similar size and positional workspace. The 3D-SPKM, which is presented in the thesis, is a 3-UPU (Universal-Prismatic-Universal) based pure translational mechanism. The kinematic arrangement shows that the mechanism based on parallel architecture can possess high accuracy and repeatability. This is because, the end effector motion is generated by actuated links directly connected to the base. However, the kinematic arrangement does not reveal the design challenges because of the high number of passive composite joints present in the mechanism. Therefore, the influence of the passive joint selection or design has to be crucially considered in a manipulator design. Mobility, sensitivity, singularity and error analysis are carried out to synthesize the robotic system with the required properties. The best limiting positions for prismatic joint actuation range, resolution of controllability in the reachable workspace and singularity free workspace are demonstrated.

This chapter is organized as follows. Section 3.2 give details of the kinematic structure of both 6 and 3 DOF spatial parallel kinematic mechanisms. The details also include the inverse kinematic solutions of each mechanism. In section 3.3, the mobility analysis of passive composite joints is presented to arrive at the mobility and optimum orientation of passive composite joints of the 6D-PKM & 3D-SPKM. The rotational mobility of the platform for a given PKM at various locations is discussed. Sensitivity analysis is carried out in section 3.4 to determine the rate of change of motion of the platform of 3D-SPKM for the given rate of change of motion of each of its legs. Singularity analysis is performed in section 3.5 to position the boundaries of the workspace of the 3D-SPKM farthest from the singularities. Error analysis presented in section 3.6 deals with the posture error analysis at the platform of 3D-SPKM due to the inaccuracies in the passive composite joints. It helps in determining the magnitude of the error at the location of the surgical tool for the given torsional errors about each leg of the 3D-SPKM. The above analysis aids in the development of a high precision PKM robot for performing neurosurgery.

3.2 The 6D-PKM & 3D-SPKM Kinematic Model

3.2.1 Six DOF Parallel Kinematic Mechanism (6D-PKM) model

The 6D-PKM, presented in the thesis, is a well known semi-regular Stewart platform manipulator. The 6D-PKM consists of two rigid bodies and six legs. One end of each leg is connected to a rigid body through a universal joint and another end of each leg is connected to second rigid body through a spherical joint. In order to simplify modeling, design and manufacture, the six connecting points of the joints on each of the two rigid bodies are considered to lie in a plane. The planar rigid surface, which translates and rotates in 3 dimensions with respect to the other rigid planar surface, is termed as the platform and the reference fixed surface is termed as the base. To eliminate the interference of legs, the connecting points are suitably separated. Each of the six legs is a serial UPS (Universal-Prismatic-Spherical) chain and the six connection points form a semi-regular hexagon both at the platform and at the base.

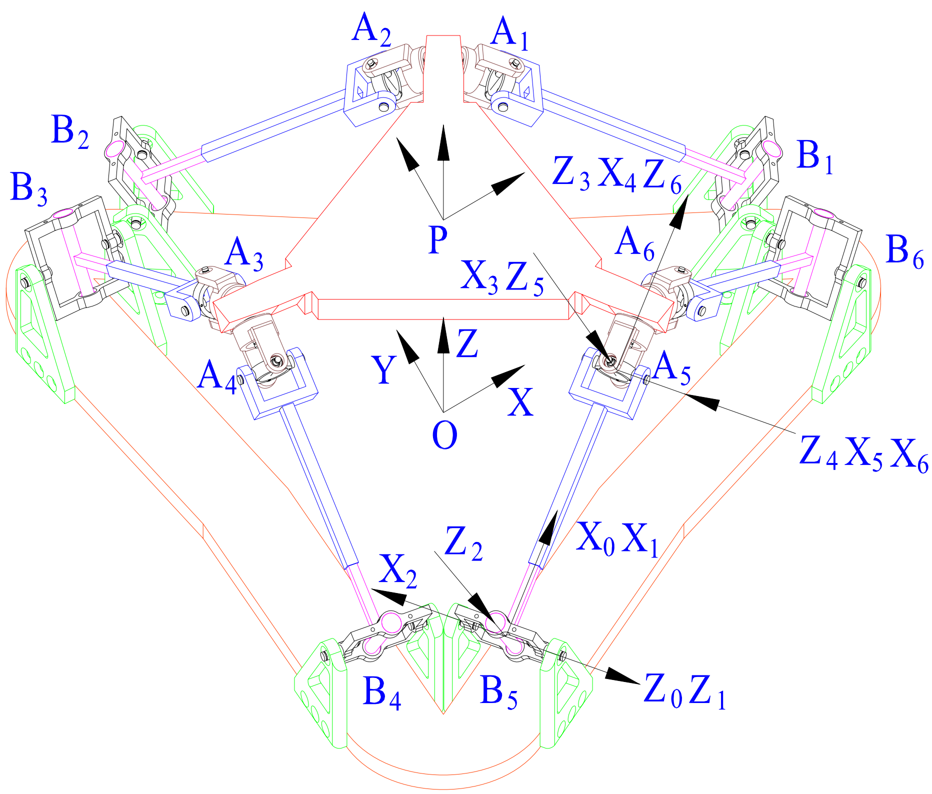

Figure 3.1: 6D-PKM isometric view

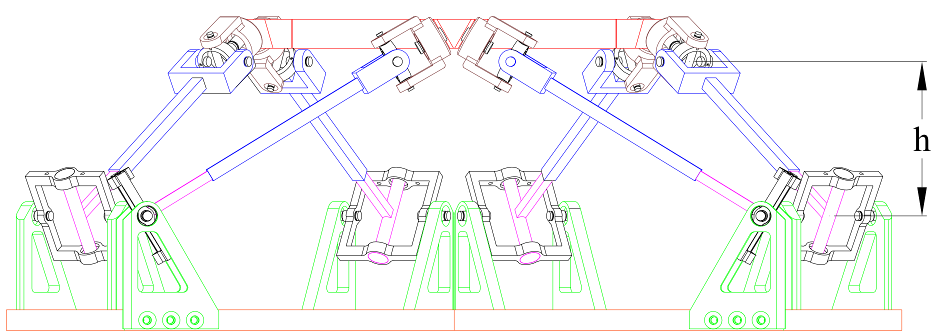

Figure 3.2: 6D-PKM front view

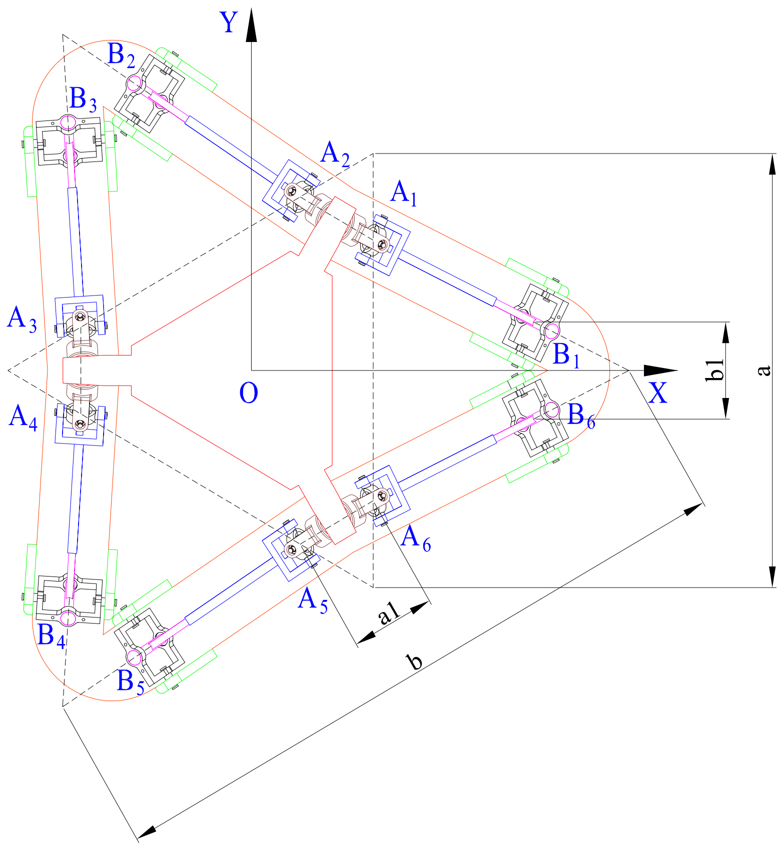

Figure 3.3: Top view of the 6D-PKM

The schematic sketch of the 6D-PKM is shown in the figure 3.1. The front view and the top view are shown in figure 3.2 & 3.3 respectively. The spherical and the universal joints are passive composite joints whereas the prismatic joint is integrated with the actuator and is referred to as the active joint. The coordinates of all the points are defined with respect to a global coordinate system fixed at the geometrical centre of the base ***O***(XYZ) as shown in figure 3.1 & 3.3. The height of the manipulator is described as the distance from the geometrical centre of the base to the geometrical centre of the platform. Both the base and the platform are designed as equilateral triangular plates. The design parameters denoted as 'b' is the side of the base equilateral triangle, and 'a' is the side of the platform equilateral triangle. B_i and A_i (i=1,..,6) are the six connection points at the base and at the platform respectively. Let 'b_1' be the offset of the base connection points from its nearest vertex (equal to smaller semi-hexagonal side at the base), and 'a_1' be the offset of the platform connection points from its nearest vertex (equal to smaller semi-hexagonal side at the platform). l_i are the leg lengths connecting base connection point B_i to the corresponding platform connection point A_i, (i=1,…6). A coordinate system is fixed at the center (of the semi-regular hexagon) of the base plate formed by the 6 connection points (B_i, $i = 1, \dots, 6$). The X-Y axes are defined along the plane of the base plate. The X-axis is directed from the center of the base plate to the midpoint of line connecting B_1 & B_6 (figure 3.3), the Z-axis is perpendicular to the plane of the base plate, and the Y-axis completes the right-handed coordinate system. $\hat{\imath}, \hat{\jmath}, \hat{k}$ are the unit vectors along the **X, Y** and **Z** axes. At the minimum height of mechanism, 'h', the coordinates of the geometrical center of the platform with respect to the geometrical center of the base at zero translation is (0, 0, h). The translation of the platform from its minimum height is given by (tx, ty, tz) and hence $(tx, ty, tz + h)$ are the coordinates of the center of the platform from **O**(XYZ) after the translation. R_{3X3} is the rotation of the platform with respect to the platform coordinate frame. For better clarity, the Denavit-Hartenberg (DH) parameters of 6D-PKM are presented in table 3.1. The coordinate frames attached to the various points on the leg; which are used for determining the DH parameters are shown in figure 3.1.

Table 3.1: DH Parameters of single leg of 6D-PKM

i	$Link\ Twist\ (\alpha_{i-1})$	$Link\ Length\ (a_{i-1})$	$Joint\ offset\ (d_i)$	$Joint\ Angle\ (\theta_i)$
1	0	0	0	θ_1
2	$\pi/2$	0	0	θ_2
3	$-\pi/2$	0	$Leg\ length\ (l_i)$	$-\pi/2$
4	$-\pi/2$	0	0	θ_4
5	$-\pi/2$	0	0	θ_5
6	$-\pi/2$	0	0	θ_6

The homogeneous coordinates of the leg connection points at the base with respect to **O**(XYZ) are given by

$$B_1 = \left[\frac{b}{\sqrt{3}} - \frac{b_1\sqrt{3}}{2}, \quad \frac{b_1}{2}, 0, 1\right]^T, B_2 = \left[-\frac{b}{2\sqrt{3}} + \frac{b_1\sqrt{3}}{2}, \quad \frac{b}{2} - \frac{b_1}{2}, 0, 1\right]^T,$$

$$B_3 = \left[-\frac{b}{2\sqrt{3}}, \quad \frac{b}{2} - b_1, 0, 1\right]^T, B_4 = \left[-\frac{b}{2\sqrt{3}}, \quad -\frac{b}{2} + b_1, 0, 1\right]^T,$$

$$B_5 = \left[-\frac{b}{2\sqrt{3}} + \frac{b_1\sqrt{3}}{2}, \quad -\frac{b}{2} + \frac{b_1}{2}, 0, 1\right]^T, B_6 = \left[\frac{b}{\sqrt{3}} - \frac{b_1\sqrt{3}}{2}, \quad -\frac{b_1}{2}, 0, 1\right]^T \qquad (3.1)$$

The homogeneous coordinates of the leg connection points at the platform with respect to **O**(XYZ) after the translation (tx, ty, tz) and rotation R_{3X3} are given by

$$A_1 = \begin{bmatrix} & R_{3X3} & & \begin{matrix} tx \\ ty \\ tz+h \end{matrix} \\ 0 & 0 & 0 & 1 \end{bmatrix} \left[\frac{a}{2\sqrt{3}}, \quad \frac{a}{2} - a_1, \quad 0, \quad 1\right]^T,$$

$$A_2 = \begin{bmatrix} & R_{3X3} & & \begin{matrix} tx \\ ty \\ tz+h \end{matrix} \\ 0 & 0 & 0 & 1 \end{bmatrix} \left[\frac{a}{2\sqrt{3}} - \frac{a_1\sqrt{3}}{2}, \quad \frac{a}{2} - \frac{a_1}{2}, \quad 0, \quad 1\right]^T,$$

$$A_3 = \begin{bmatrix} & R_{3X3} & & \begin{matrix} tx \\ ty \\ tz+h \end{matrix} \\ 0 & 0 & 0 & 1 \end{bmatrix} \left[-\frac{a}{\sqrt{3}} + \frac{a_1\sqrt{3}}{2}, \quad \frac{a_1}{2}, \quad 0, \quad 1\right]^T,$$

$$A_4 = \begin{bmatrix} & R_{3X3} & & \begin{matrix} tx \\ ty \\ tz+h \end{matrix} \\ 0 & 0 & 0 & 1 \end{bmatrix} \left[-\frac{a}{\sqrt{3}} + \frac{a_1\sqrt{3}}{2}, \quad -\frac{a_1}{2}, \quad 0, \quad 1\right]^T,$$

$$A_5 = \begin{bmatrix} & R_{3X3} & & \begin{matrix} tx \\ ty \\ tz+h \end{matrix} \\ 0 & 0 & 0 & 1 \end{bmatrix} \left[\frac{a}{2\sqrt{3}} - \frac{a_1\sqrt{3}}{2}, \quad -\frac{a}{2} + \frac{a_1}{2}, \quad 0, \quad 1\right]^T,$$

$$A_6 = \begin{bmatrix} & R_{3X3} & & \begin{matrix} tx \\ ty \\ tz+h \end{matrix} \\ 0 & 0 & 0 & 1 \end{bmatrix} \left[\frac{a}{2\sqrt{3}}, \quad -\frac{a}{2} + a_1, \quad 0, \quad 1\right]^T \tag{3.2}$$

The inverse kinematics of the 6D-PKM can be written as:

$$\|\vec{l_i}\| = \|\vec{A_i} - \vec{B_i}\|, \ i = 1, \dots 5,6 \tag{3.3}$$

3.2.2 Three DOF Spatial Parallel Kinematic Mechanism (3D-SPKM) model

In general, the 3-UPU based mechanisms can have various operation modes based on its assembly, as discussed by Walter and Husty [126A]. It is shown that the 3-UPU parallel manipulator has five operation modes out of which one is pure translation motion mode. The necessary conditions for the pure translational mode are given in [115, 116, 117]. The 3D-SPKM, which is discussed in the thesis, is a 3-UPU (Universal-Prismatic-Universal) based pure translational mechanism. Each leg consists of universal joints on either side of an actuated prismatic joint. It is shown by Tsai [115, 116] that the 3-RRPRR, 3D-SPKM under some geometric conditions results in pure translational motion. Each of the three legs of the manipulator is connected to the base and the platform through two revolute joints. The three legs have to meet the following necessary conditions (but not sufficient) for 3D-SPKM to have pure translational freedoms.

$$q_{i2} = q_{i4} \ and \ q_{i1} = q_{i5}, (i = 1,2,3) \tag{3.4}$$

where, q_{i1} and q_{i2} are the unit vectors of passive revolute joint axes at the base and similarly q_{i4} and q_{i5} are the unit vectors of passive revolute joint axes at the platform. The figures 3.4 and 3.5 represent the kinematic sketch of 3D-SPKM and describe the manipulator parameters. The three base connection points are chosen to form an equilateral triangle and so are the connection points at the platform. The coordinates of all the points are defined with respect to a global coordinate system fixed at the geometrical centre of the base ***O***(XYZ) as shown in figures 3.4 and 3.5. The above choice is based on the symmetry. The plane formed by the connection points at the platform is parallel to the base. The height of the manipulator is referred to the distance from the base to the platform plane. Let 'a' be the side of the platform equilateral triangle and 'b' be the side of the base equilateral triangle. l_1, l_2, l_3 are the leg lengths connecting base connector point B_i to the corresponding platform point A_i, i=1, 2, 3. $\hat{\imath}, \hat{\jmath}, \hat{k}$ are the unit vectors along the **X, Y** and **Z** axes. $(x, y, z)^T$ are the coordinates of the centre of the platform from ***O***(XYZ). The Denavit-Hartenberg (DH) parameters of 3D-SPKM are presented in table 3.2 and it can be seen that the conditions stated in equation (3.4) for pure translation is confirmed. The coordinate frames attached to the various points on the leg; which are used for determining the DH parameters are shown in figure 3.4.

Table 3.2: DH Parameters of single leg of 3D-SPKM

i	$Link\ Twist\ (\alpha_{i-1})$	$Link\ Length\ (a_{i-1})$	$Joint\ offset\ (d_i)$	$Joint\ Angle\ (\theta_i)$
1	0	0	0	θ_1
2	$\pi/2$	0	0	θ_2
3	$-\pi/2$	0	$Leg\ length\ (l_i)$	0
4	$\pi/2$	0	0	θ_4
5	$-\pi/2$	0	0	θ_5

The coordinates of the leg connection points at the base and the platform with respect to ***O***(XYZ) are given by

$$B_1 = \left[\frac{b}{\sqrt{3}}, 0, 0\right]^T B_2 = \left[\frac{-b}{2\sqrt{3}}, \frac{b}{2}, 0\right]^T \quad B_3 = \left[\frac{-b}{2\sqrt{3}}, \frac{-b}{2}, 0\right]^T \tag{3.5}$$

$$A_1 = \left[\frac{a}{\sqrt{3}} + x, y, z\right]^T A_2 = \left[\frac{-a}{2\sqrt{3}} + x, \frac{a}{2} + y, z\right]^T A_3 = \left[\frac{-a}{2\sqrt{3}} + x, \frac{-a}{2} + y, z\right]^T \tag{3.6}$$

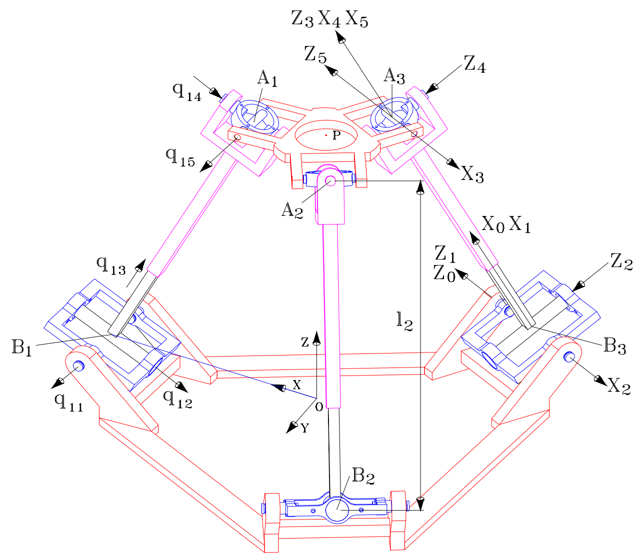

Figure 3.4: 3D-SPKM

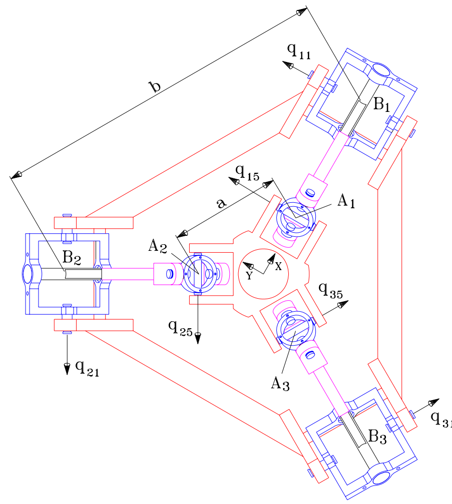

Figure 3.5: Top view of 3D-SPKM to describe kinematic parameters

The three leg vectors from the base connection points to the platform connection points are

$$\vec{l_1} = \vec{A_1} - \vec{B_1}; \qquad \vec{l_2} = \vec{A_2} - \vec{B_2}; \qquad \vec{l_3} = \vec{A_3} - \vec{B_3}; \tag{3.7}$$

The inverse kinematics solution can be written as

$$\left(\frac{a}{\sqrt{3}} - \frac{b}{\sqrt{3}} + x\right)^2 + y^2 + z^2 = l_1^2 \tag{3.8}$$

$$\left(\frac{b}{2\sqrt{3}} - \frac{a}{2\sqrt{3}} + x\right)^2 + \left(\frac{a}{2} - \frac{b}{2} + y\right)^2 + z^2 = l_2^2 \tag{3.9}$$

$$\left(\frac{b}{2\sqrt{3}} - \frac{a}{2\sqrt{3}} + x\right)^2 + \left(\frac{b}{2} - \frac{a}{2} + y\right)^2 + z^2 = l_3^2 \tag{3.10}$$

3.3 Mobility Analysis

3.3.1 Introduction to mobility analysis

The term 'Mobility' refers to motion or movement in general. In this thesis, the term 'mobility' is referred to as the range of rotation or translation of a body of the mechanism. The mobility of passive composite joints (also referred as passive mobility) refers to the extent by which the passive joint can rotate about its axis. The translational mobility of the platform of the parallel mechanism refers to the range of translation motion of the platform. The rotational mobility of the platform of the parallel mechanism refers to the range of rotational motion of the platform. Literature survey related to mobility analysis of PKM's has been discussed in previous chapter. Literature survey reveals that limited work has been carried out to determine the workspace of the PKM, considering the constraints of passive mobility at the composite joints. The inverse problem of determining the mobility of passive joints for a given workspace of a manipulator is not found in the literature. This section deals with the development of an algorithm to arrive at the mobility and the optimum orientation of passive composite joints of the PKM. The numbers of the passive joints largely outnumber the active joints in closed loop mechanisms. The performance of the PKM based constructions highly depend on the appropriate synthesis and design of passive composite joints.

The mobility about each axis of the passive joints should accommodate multi-dimensional translation and rotation range of the platform (end effector). The effect of restricted passive joint mobility on the platform workspace has been studied. An inverse mobility problem of determining the required passive mobility at the joints for the given platform workspace has been solved. Given the desired mobility of the platform frame P in the form of translations and rotations (based on neurosurgical requirements), a problem is solved to find

(1) Mobility required at passive joints at the platform and at the base

(2) The optimum posture of the passive composite joints at the base with respect to the base frame O and the passive composite joints at the platform with respect to the platform frame P are determined. It is done with an objective that the passive composite joints mobility is best served to achieve the desired platform mobility.

The mobility and posture of the passive composite joints are analyzed and the optimal posture for the best utility of the passive mobility is recommended. The results of the mobility analysis illustrates that the passive joints angular mobility requirement is high and the commercially available composite joints do not provide such an angular mobility. The novel options for the design of passive composite joints which give the required mobility have been explored in the subsequent chapters.

This section also addresses the issue of maximum possible rotational mobility of the platform for given PKM parameters at various locations in workspace. This provides an insight about how the rotational mobility of platform varies throughout the translational workspace of the PKM. The mobility required at the passive joints for the corresponding rotational mobility of the platform has been determined.

3.3.2 Methodology for calculation of mobility of passive composite joints

The mobility required at the passive composite joints of a kinematic chain constituting a leg is determined considering one leg of the PKM. Either ends of each of the legs are connected to the base and to the platform. It is known that the leg is a kinematic chain; and each leg constitutes of an active joint and a set of passive joints at the platform end and at the base end. Each leg in the PKM has to have same mobility characteristics. This is in contrast to a serial based mechanism.

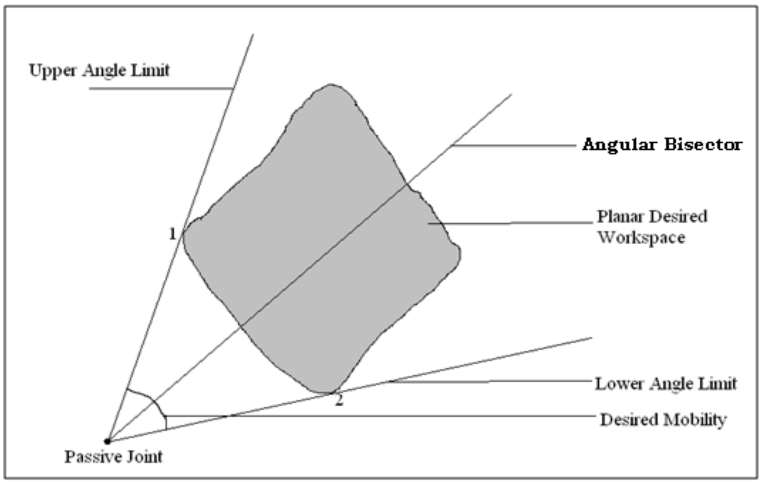

Figure 3.6: Mobility required for a 1 DOF passive joint

Given the translation and rotation ranges of the PKM, the passive mobility requirement and optimal orientation of passive joints is to be determined. The translational workspace of the connection point of the leg at the platform is same as that of the translational workspace at any other point on the platform. The rotational workspace is superimposed on the translational workspace at the connection point.

Before explaining the calculation for multi-DOF passive composite joints used in PKM, the terms and procedural steps for calculation of the passive mobility is illustrated considering a one DOF passive joint. Figure 3.6 illustrates the mobility requirement for the one DOF passive joint case.

An algorithm explaining the methodology is given below:

1. The desired workspace for the mechanism is generated taking into consideration all the likely translations and rotations. In Figure 3.6, the desired workspace is shown as a shaded area.

2. All the extreme end points of the workspace with respect to the passive joints are calculated. In a planar case, there are two extreme points 1 and 2. Figure 3.6 illustrates that “Lower Angle Limit” line and “Upper Angle Limit” lines form an angular segment with the passive joint position on a plane normal to the passive joint axis (angular segment with respect to intersecting point of passive joint axes).
3. The ray originating from the joint and the angular bisector of the angular limits is defined as the central axis. The angle at the passive joint made by the ray passing through extreme points and the central axis is called as extreme angle.
4. In the generalized case, the central axis of the cone is determined such that the maxima of all the extreme angles would be minimized. This is done to achieve the optimal position for placement of the mobility segment of the passive joint. The maxima of the extreme angle would give the value of the mobility required at the passive joint.

Using this methodology, the mobility analysis of the passive composite joints in PKM can be established. The subsequent subsection explains the procedural steps to determine the mobility of passive composite joints for PKMs.

3.3.3 Synthesis of mobility of passive composite joints

This section deals with the details of obtaining the mobility of passive joints in a 6D-PKM. The methodology remains same for a 3D-SPKM. The top view of the 6D-PKM is shown in the figure 3.3. The universal joints positioned at all six connection points at the base, and the spherical joints positioned at all six connections points at the platform are identical. Therefore, the analysis on any single leg arrangement is valid for the rest of the five legs. The desired translations and rotation parameters of the platform are set to suit the application requirements. For the given parameters like the size of the base, size of the platform, offset between the legs, and the initial height of the mechanism, the mobility analysis of the passive composite joints are carried out.

In the analysis, the translations along X-Y plane are assumed to be axis symmetric about Z-axis and the rotations of the platform are also assumed to be axis symmetric about X and Y axes (passing through centre of the platform, P). Considering pure translations $[tx, ty, tz]$, each point on the platform traces a cylinder, including the leg connecting point, $A_{1.}$. The maximum translation in the plane of the platform when parallel to X-Y plane is the radius of the cylinder and translation through the range along Z axis is the height of the cylinder. Figure 3.7 shows the top and front view of the workspace traced by the connection point A_1 at the platform due to pure translation.

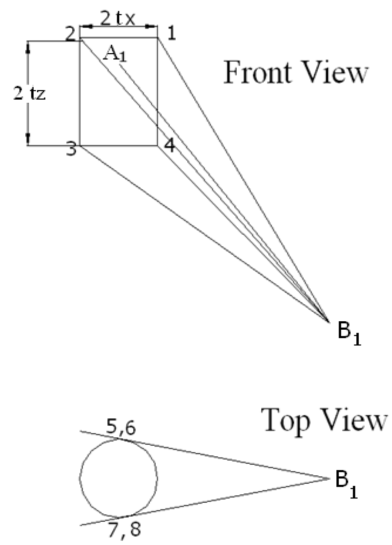

Figure 3.7: Views of translation workspace

The extreme points, which result in maximum angular displacement of the leg during the course of the trace of the workspace due to pure translations, are identified. The same are represented in Figure 3.7. Points 1, 2, 3, 4 (shown in front view in Figure 3.7) correspond to situations when leg line vector (defined as a vector from leg connection point at base B_j to leg connection point at platform A_j) lies in the diametrical plane of the cylinder which goes through point B_j and passes through the end points of the generator of the cylinder. Points 5, 6, 7, 8 (shown in top view in Figure 3.7) correspond to situations when leg line vector lies in the tangent plane of the cylinder which goes through point B_j and passes through the end points of the generator of the cylinder. The maximum angular displacements correspond to the extreme lines originating from the connecting point at the base. In figure 3.7, eight lines can be seen, out of which six are extreme lines which depend on the location of the cylinder with respect to the leg connection point at the base. To account for the rotational motion of the platform, the cylinder due to translations at the leg connection point is superimposed by the rotations of the platform about Z, Y, X sequentially. The sweep of the cylinder about the Z axis through its range results in a segment of a cylindrical shell with semi-cylindrical surfaces at the ends as shown in the figure 3.8. The top view of the workspace of a leg connection point at the platform after undergoing translations and a rotation is shown in figure 3.9. The rotation about X and Y axis is superimposed over the workspace resulting due to the translations and the rotation about the Z axis. After the rotations about X and Y are superimposed on the above workspace (as shown in figure 3.8), the top and bottom surfaces of the workspace would form a torus surface. The geometry of the workspace is simplified by circumscribing it in a cylindrical segment. Workspace thus generated encapsulates the toroidal workspace formed by the rotation and cylindrical workspace formed by the translation. It is observed that though this results in increase in workspace but will not generate any additional extreme points. As discussed earlier with respect to figure 3.7, there will be eight extreme points on one end cylinder (1-8) and eight extreme points at the other end cylinder (9-16). The points are shown in the figure 3.8. Four extreme points 17,18,19,20 correspond to situations when leg line vector lies in the tangent plane of the segment of the cylindrical shell which goes through point B_j and passes through the end points of the generator of the cylindrical shell (see figure 3.9). The points 21, 22, 23, 24 correspond to situations when leg line vector lies in the diametrical plane of the segment of the cylindrical shell which passes through point B_j and passes through the end points of the generator of the cylindrical shell. In this case, the angle is maximum in a plane containing the Z-axis, leg connection point at the platform and the center of the base. In all, there are 24 points and hence 24 angles. To find the mobility at the passive composite joints, all the extreme points on the workspace of a leg point, at the platform are identified. The angles formed by the line vector of the leg at these extreme points are found with respect to the coordinate system defined at the joint connection point at the base. The extreme angular positions of the leg with respect to the joint coordinate system X_j Y_j Z_j (defined at the connection point) to reach a given workspace are determined.

For the passive joint mobility synthesis, the central axis of the cone formed by the joint mobility is determined optimally with respect to the base coordinate system. The mobility (cone angle) of the joint should be such that all the extreme angular positions should lie on or inside the cone. The optimum orientation of the central axis of the cone is one that minimizes angular mobility of the joint to embed all extreme leg positions.

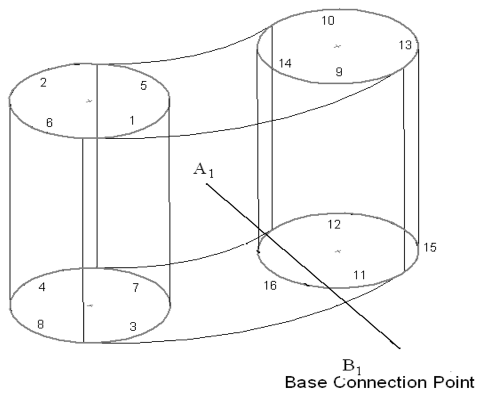

Figure 3.8: A segment of a workspace

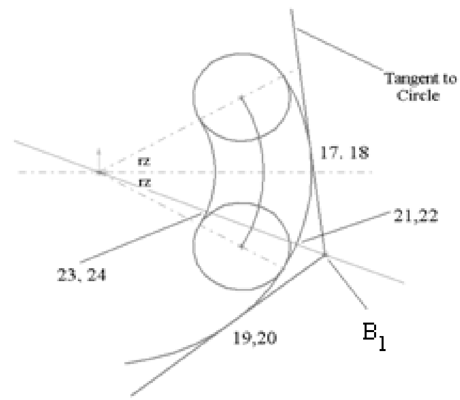

Figure 3.9: Top view of a segment of a workspace

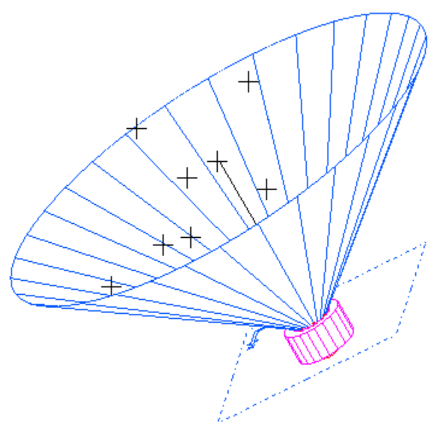

Figure 3.10 (a): Joint mobility cone embedding the extreme points

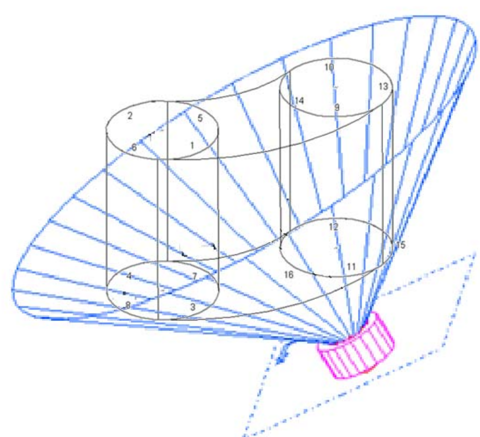

Figure 3.10 (b): Joint mobility cone encapsulating segment of workspace

Figure 3.10: Joint mobility cone

Figure 3.10 (a) shows the joint mobility cone of a spherical joint and the spread of extreme connecting points at the platform and figure 3.10 (b) shows the mobility cone encapsulating segment of the workspace. The above problem is equivalent to finding the minimum-angle bounding cone for the given three-dimensional vectors generated by extreme connection points. There are many numerical methods that exist ([126B], [126C], [126D]) to solve bounding cone problem. Instead of using iterative solutions, a simple method to compute the minimum-angle bounding cone and hence to determine the central joint axis is presented in this section. The steps to determine the optimal locations of the central joint axis of all the joints with respect to the base coordinate system are stated. The optimum location of the central joint axis gives the best utility posture in terms of mobility of the joints.

The steps are given as follows:

Step 1: Define a joint coordinate system with origin coinciding with the central point of the joint (center of the sphere in case of spherical joint or point of intersection in case of universal joint). The X_j, Y_j plane is defined on the surface of the jth joint, parallel to the top cylindrical surface. The origin of the joint coordinate system is defined at the center of the joint and Z_j - axis completes the right-handed coordinate system (refer Figure 3.11). The position of the center of the joint with respect to the base coordinate system is known. The extreme lines emerge from the origin of the joint coordinate system.

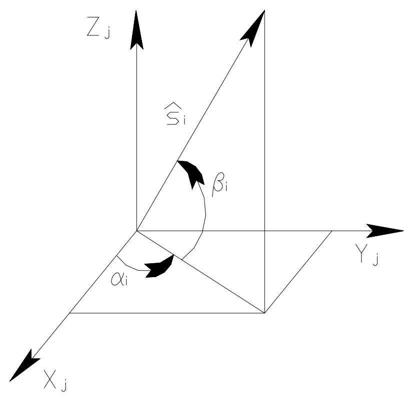

Figure 3.11: Spherical components of unit vector

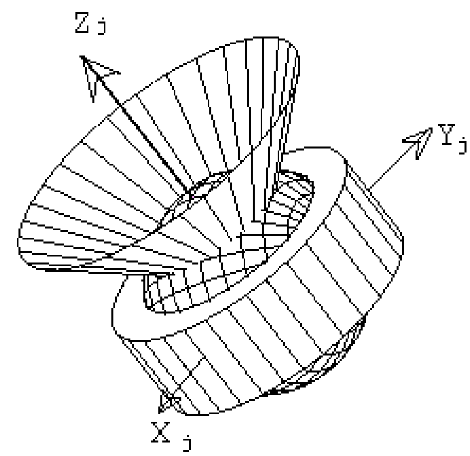

Figure 3.12: Optimum orientation of mobility cone

Step 2: The intersection of all the extreme lines (24 lines) with the unit sphere defined at the origin of X_j, Y_j, Z_j is determined. The schematic sketch of the typical line and its components is shown in figure 3.12. The unit vectors $\hat{l}_i$, i=1, 2…24 of all the extreme lines and angular components in the spherical coordinates are given as follows.

$$\alpha_i = tan^{-1}\left[\frac{l_{yi}}{l_{xi}}\right]; \quad \beta_i = tan^{-1}\left[\frac{l_{zi}}{\sqrt{(l_{xi}^2 + l_{yi}^2)}}\right] \qquad (3.11)$$

The angular measurement of α_i and β_i is based on $0^0 \;\; to \; 360^0$, the quadrant can be identified by the ordered pair of the signs of cosine and sine of an angle (cos(angle), sin(angle)).

$$l_{xi} = cos\,\alpha_i\,cos\,\beta_i\,; \qquad l_{yi} = sin\,\alpha_i\,cos\,\beta_i\,; \qquad l_{zi} = sin\,\beta_i \qquad (3.12)$$

Step 3: $(\alpha_{mean}, \beta_{mean})$ and $(\alpha_{range}, \beta_{range})$ are determined as follows

$$\alpha_{min} = (\alpha_{i,i=1,\dots,24})_{min}\,; \qquad \beta_{min} = (\beta_{i,i=1,\dots,24})_{min}\,; \qquad (3.13)$$

$$\alpha_{max} = (\alpha_{i,i=1,\dots,24})_{max}\,; \qquad \beta_{max} = (\beta_{i,i=1,\dots,24})_{max}\,; \qquad (3.14)$$

$$\alpha_{range} = \alpha_{max} - \alpha_{min}\ ; \qquad \beta_{range} = \beta_{max} - \beta_{min}\ ; \tag{3.15}$$

$$\alpha_{mean} = \frac{\alpha_{min} + \alpha_{max}}{2}\ ; \qquad \beta_{mean} = \frac{\beta_{min} + \beta_{max}}{2}\ ; \tag{3.16}$$

The two angular mean positions and angular ranges are based on the extreme angular positions. It is important to identify and keep track that all the angular positions that lie on or inside the range. The choice of angular measurement of α_i and β_i is based on 0^o to 360^o or -180^o to 180^o whichever results in a smaller angular range and corresponding following relationship should hold well.

$$\left(\alpha_{mean} - \frac{\alpha_{range}}{2}\right) \leq (\alpha_{i,i=1,\dots,24}) \leq \left(\alpha_{mean} + \frac{\alpha_{range}}{2}\right) \tag{3.17}$$

$$\left(\beta_{mean} - \frac{\beta_{range}}{2}\right) \leq (\beta_{i,i=1,\dots,24}) \leq \left(\beta_{mean} + \frac{\beta_{range}}{2}\right) \tag{3.18}$$

Step 4: The joint coordinate system is rotated about Z_j through α_{mean} , $R\left(Z_j,\ \alpha_{mean}\right)$ the rotated joint frame is again rotated about rotated Y_j, through β_{mean} , $R\left(Y_j,\ \beta_{mean}\right)$.

The resulting coordinate system gives an optimum joint coordinate system with Z_j pointing to the joint's central axis.

Step 5: The solid angle, $2 \times \gamma$ is computed as follows

$$2\gamma = cos^{-1}\left(\hat{R}_1 \,.\, \hat{R}_2\right) \tag{3.19}$$

$\hat{R}_1$ and $\hat{R}_2$ are unit radius vectors given by

$$\hat{R}_1 = cos\,\alpha_{min}\,cos\,\beta_{min}\,\hat{I}_j + sin\,\alpha_{min}\,cos\,\beta_{min}\,\hat{J}_j + sin\,\beta_{min}\,\hat{K}_j \tag{3.20}$$

$$\hat{R}_2 = cos\,\alpha_{max}\,cos\,\beta_{max}\,\hat{I}_j + sin\,\alpha_{max}\,cos\,\beta_{max}\,\hat{J}_j + sin\,\beta_{max}\,\hat{K}_j \tag{3.21}$$

where, $\hat{I}_j, \hat{J}_j, \hat{K}_j$ are unit vectors along $\hat{X}_j, \hat{Y}_j, \hat{Z}_j$ respectively.

Step 6: The central joint axis is oriented at (α_{mean} , β_{mean}) with a mobility solid angle range (full cone angle) of $2 \times \gamma$.

3.3.4 Numerical example of mobility analysis of passive composite joints of 3D-SPKM

In this subsection, the results for the mobility analysis of passive joints of a 3D-SPKM are presented. A numerical example considering the realistic values of the manipulator required for typical stereotactic neurosurgery parameters is explained. The figures 3.4 and 3.5 show the kinematic sketch and describe the manipulator parameters. The synthesis of passive joints for a given platform size and workspace ranges is detailed out. The optimum mobility ranges of passive joints for a given platform translation is as follows:

3D-SPKM Dimensions:

Base side (b)	329	Length of a side of a base equilateral triangle
Platform side (a)	78	Length of a side of a platform equilateral triangle
Height of Platform (h)	132	Distance between center of base to center of platform

Platform Mobility:

Translations, *tx* & *ty* 50

Translation, *tz* $\pm$ 50

Result:

Because of the symmetry, the required mobility at the base and the platform side is same. The passive joints selected/ designed should have the required mobility.

Mobility desired at the base joints: 39.62° (full cone angle)

Mobility desired at the platform joints: 39.62° (full cone angle)

The optimal locations of the central joint axes of all the joints with respect to the base coordinate system are given. Base and platform connecting points of the legs with respect to base coordinates are as follows

B_1 = (189.97, 0.0, 0.0) A_1 = (45.37, 0.0, 132.54)

B_2 = (-94.98, 164.52, 0.0) A_2 = (-22.68, 39.29, 132.54)

B_3 = (-94.98, -164.52, 0.0) A_3 = (-22.68, -39.29, 132.54)

The optimum orientation of the mobility cone is computed. The unit vectors of the central axis of the cones of the passive joint mobility are tabulated as follows.

	Unit vectors at base joint mobility cone	Unit vectors at platform joint mobility cone
Joint 1	{-0.73, 0.0, 0.68}	{0.73, 0.0, -0.68}
Joint 2	{0.37, -0.63, 0.68}	{-0.37, 0.63, -0.68}
Joint 3	{0.37, 0.63, 0.68}	{-0.37, -0.63, -0.68}

3.3.5 Numerical example of mobility analysis of passive composite joints of 6D-PKM

The second example is a 6D-PKM. The figures 3.1, 3.2 & 3.3 show the kinematic sketch of 6D-PKM. The synthesis of the passive composite joints for a given platform size and workspace ranges is worked out. The kinematic parameters chosen for the 6D-PKM are in concurrence with the neurosurgical requirements. The optimum mobility ranges of the passive joints for a given platform translation and orientation ranges is presented in this subsection. The synthesis was carried out for various sets of dimensions of base and platform. The results for a particular set are given as follows:

6D-PKM Dimensions:

Base side	553.90	Length of a side of a base equilateral triangle
Platform side	369.90	Length of a side of a platform equilateral triangle
Base Offset	81.30	Offset of the base connection point from the nearest vertex
Platform Offset	73.90	Offset of the base connection point from the nearest vertex
Height of Platform	125	Distance between the center of the base to the center of the platform

Platform Mobility

Translations, *tx* & *ty*	± 40
Translation, *tz*	± 35
Rotation about X & Y-axes	$\pm 20°$
Rotation about Z-axes	$\pm 20°$

Result:

Mobility desired at the base joints: 69.86° (full cone angle)

Mobility desired at the platform joints: 101.44° (full cone angle)

Optimal locations of the central joint axes of all the joints with respect to the base coordinate system are given. Base and platform connecting points of the legs with respect to the base coordinates are as follows:

B_1 = (248.94, 40.63, 0.0)	A_1 = (106.79, 111.04, 125.0)
B_2 = (-89.28, 235.91, 0.0)	A_2 = (42.76, 148.00, 125.0)
B_3 = (-159.66, 195.27, 0.0)	A_3 = (-149.55, 36.96, 125.0)
B_4 = (-159.66, -195.27, 0.0)	A_4 = (-149.56, -36.96, 125.0)
B_5 = (-89.28, -235.91, 0.0)	A_5 = (42.77, -148.00, 125.0)
B_6 = (248.94, -40.63, 0.0)	A_6 = (106.79, -111.04, 125.0)

The optimum orientation of the mobility cone is computed. The unit vectors of central axes of the cones of the passive joint mobility are tabulated as follows:

	Unit vectors base joint Mobility cone	Unit vectors platform joint Mobility cone
Joint 1	{-0.74, 0.28, 0.6}	{0.88, -0.24, -0.42}
Joint 2	{0.62, -0.5, 0.6}	{-0.64, 0.64, -0.42}
Joint 3	{0.13, -0.79, 0.6}	{-0.23, 0.88, -0.42}

Joint 4	{0.13, 0.78, 0.6}	{-0.23, -0.88, -0.42}
Joint 5	{0.62, 0.5, 0.6}	{-0.64, -0.64, -0.42}
Joint 6	{-0.74, -0.28, 0.6}	{0.88, 0.24, -0.42}

The commercially available passive composite joints do not satisfy the passive mobility requirement of the 6D-PKM. Hence formulation of the design options of the passive composite joints would be carried out to suit the mobility requirement. The same would be presented in next chapter.

3.3.6 Analysis of rotational mobility of the 6D-PKM platform through the workspace

The previous subsections dealt with the mobility of the passive composite joints for a given workspace of the mechanism. This subsection deals with determining the rotational mobility of the platform of the 6D-PKM at various locations inside the workspace. For a given set of parameters of PKM, the rotational mobility of the platform depends on the prismatic ranges of each leg, mobility at the passive composite joints and interference constraints between the legs. This subsection determines the rotational mobility of the platform for the given the prismatic ranges of the legs. A base side of 553.9 units, platform side of 369.9 units, offsets at base 81.3 units, offset at platform 73.9 units, minimum leg length 168 units and maximum length 253.5 units is taken for analysis of rotational mobility. A global coordinate system (refer figure 3.1 & 3.3) is fixed at the geometrical centre of the base **O**(XYZ). The X-Y axes are defined along the plane of the base plate, and the Z-axis completes the right-handed coordinate system. Figure 3.13 shows the variation of the rotational mobility of the platform about Z axis at incremental translations of the platform along the Z axis.

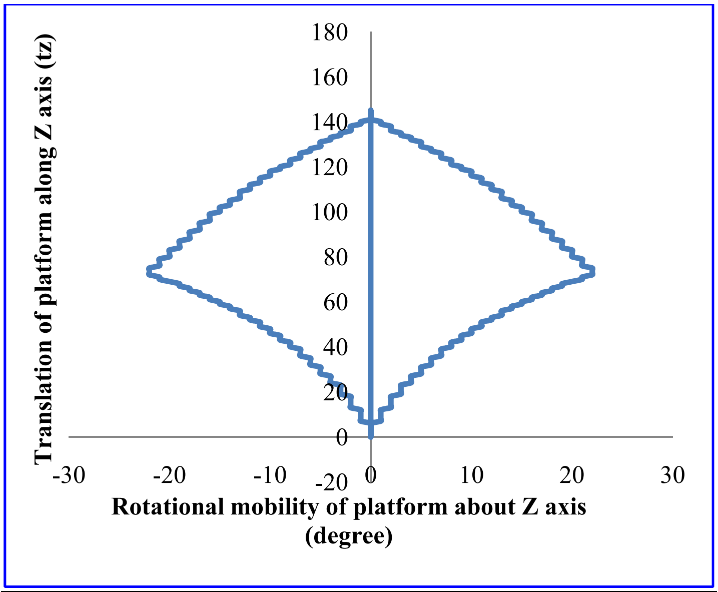

Figure 3.13: Variation of rotational mobility of platform about Z axis at incremental translations of 6D-PKM platform along Z axis

Figure 3.14 illustrates the rotational mobility of the platform about an axis which passes through the centre of the platform and is in the plane of the platform (parallel to XY plane). In figure 3.14, '*tz*' represents the translation of the platform along Z axis from its lowest position and it can be seen that the rotational mobility increases with *tz* up to a limit and then it decreases. The maximum rotational mobility of the platform occurs close to the midpoint of the Z axis translational range. The rotational mobility of the platform is maxima or minima at specific locations of the axis about which the platform is rotated. The cyclical variation of the rotational mobility about different angular position of the axis of rotation in the plane of the platform is interesting. The higher range rotational mobility benefit can be obtained by coinciding the axis of rotation corresponding to the peak values. It can be noticed that the difference between the maxima and minima is significantly less at elevated '*tz*' values. The rotational mobility pattern is symmetrical and the maxima or minima occur when the axis about which the platform rotates is at 30^o, 90^o, 150^o, 210^o, 270^o, 330^o with the X axis. The symmetrical pattern of the rotational mobility is attributed to the symmetrical placement of the legs in 6D-PKM.

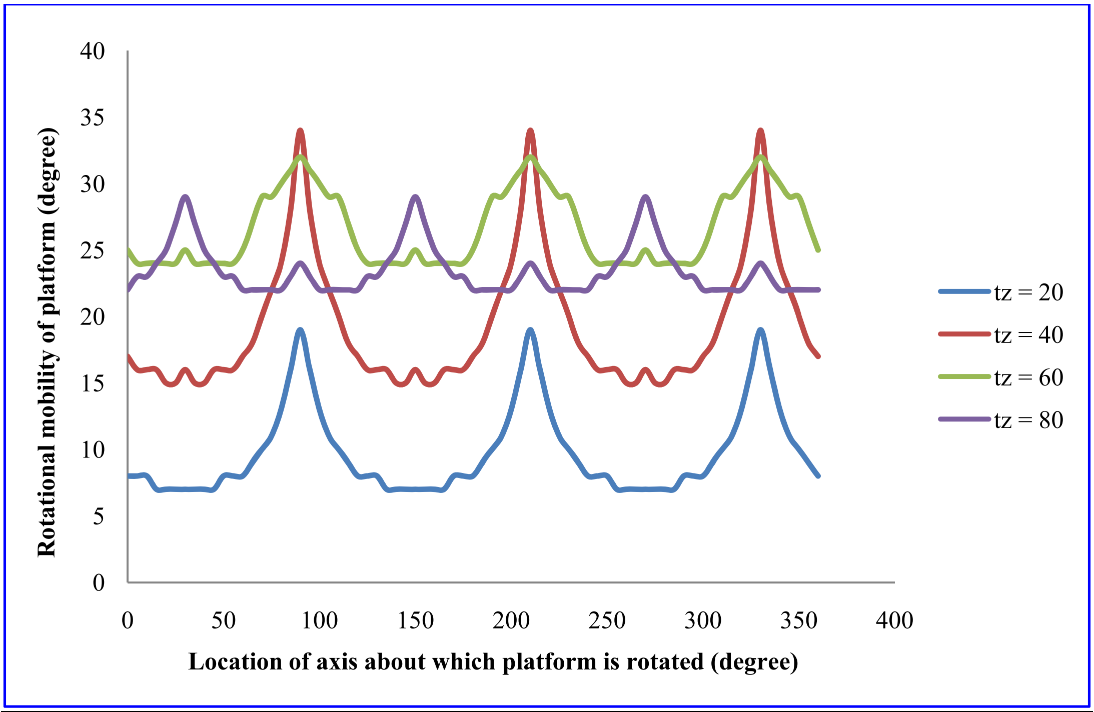

Figure 3.14: Variation of rotational mobility of platform about an axis which passes through the centre of platform and is in the plane of platform (parallel to X-Y plane) at various Z translations.

3.3.7 Analysis of mobility of passive composite joints required for a given translation and rotation of the 6D-PKM

In the previous subsection, the rotational mobility of the platform is analyzed. In this subsection, the mobility of the passive composite joints of the platform for the given translation and rotation of the platform is determined with a different perspective. This section is different from the earlier sections 3.3.2 - 3.3.5, where the mobility of passive joints is determined for the given workspace of the PKM. In this section, the mobility of passive joints is determined for a particular translation and rotation of the platform. As described earlier, each leg of the 6D-PKM consists of a universal joint at base connection point, a prismatic joint and a spherical joint at the platform connection point. The passive universal joint at the base being a 2 DOF joint can be represented by two rotations; about the axis 1 and 2 respectively. Axis 1 is the stationary axis connecting the base and the axis 2 is the axis connecting the leg. The corresponding angles are referred as U joint base angle 1 & 2 respectively. The passive spherical joint at the platform being a 3 DOF joint shall be represented by three rotations and termed as S joint platform angle 1, 2, 3 sequentially from leg to the platform. Given the rotational mobility of the platform of the PKM from the previous subsection, the two passive rotations required of the universal joint at the base side and the three passive rotations required of the spherical joint at the platform side are determined. The results shown in figure 3.15 are for translated motion of the platform at tz = 45.

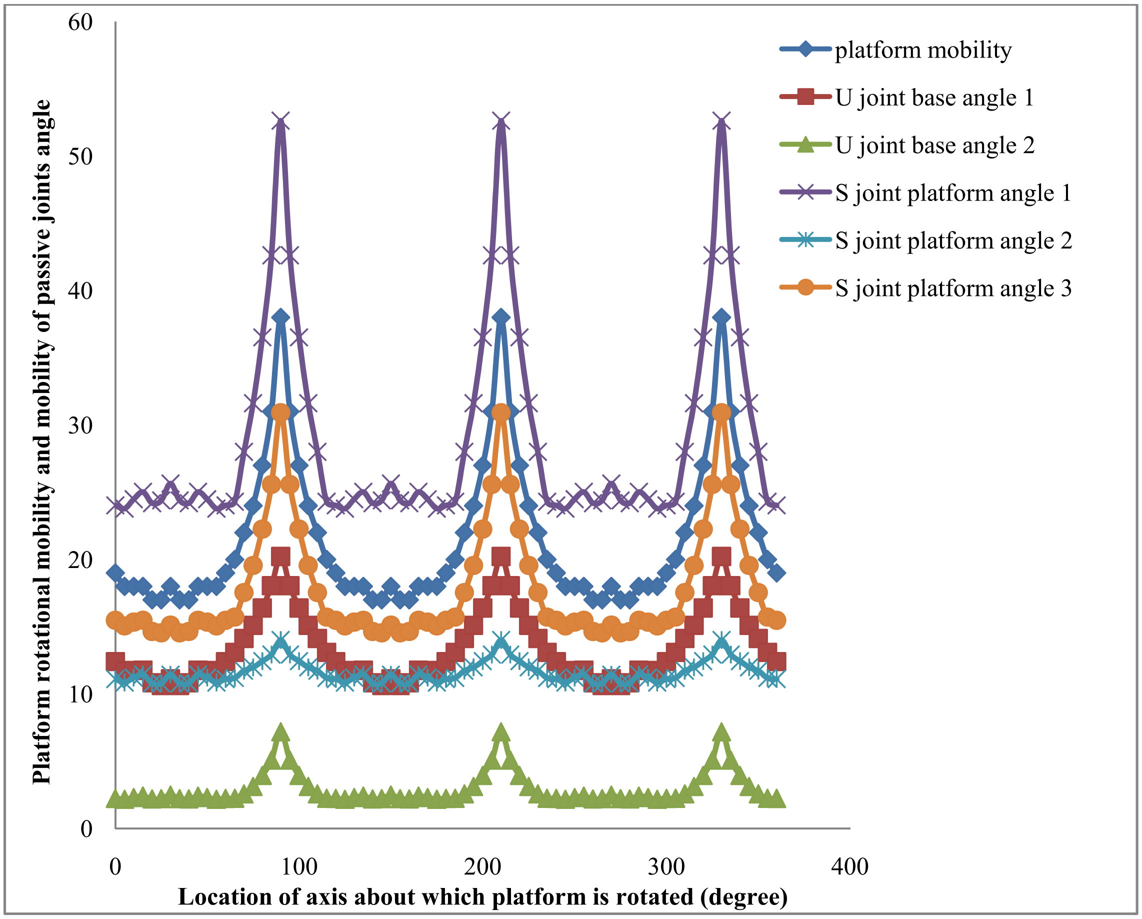

Figure 3.15: Variation of mobility of the passive composite joints required for the given translation and rotation of platform (tz = 45)

It can be interpreted from figure 3.15 that the rotation of the platform and mobility of the passive composite joints have a direct correlation; higher the rotation of the platform, higher will be the mobility requirement of the passive joints. The mobility pattern of the passive composite joints is similar to the rotational mobility of the platform. For a given translation and rotation of the platform, the passive mobility required at the universal joints at the base is generally lower as compared to the passive mobility required at the platform spherical joints.

3.4 Sensitivity Analysis

3.4.1 Reciprocal sensitivity parameters

There can be a point and a region around it in the workspace where the performance of the robot manipulator can be classified as the best and is the preferred region for the manipulator based surgical operations. The preferred region for working of manipulator depends on several kinematic, dynamic and control parameters. The sensitivity analysis presented in the section deals with one such kinematic parameter, on the basis of which the choice of preferred region for the manipulator can be made. The sensitivity analysis is performed to identify such regions and in general to understand how the sensitivity varies from point to point within the workspace of a manipulator. The sensitivity analysis is used to establish the best performing region in the workspace. Also, it determines the location (based on sensitivity analysis) where the surgical tool would have the utmost precision in performing a neurosurgery. The sensitivity is defined as the ratio of the rate of change of the position of the platform to the rate of change of the leg lengths. The equation (3.22) gives the transmission ratio of the velocities of the legs and the platform using combined Jacobian, J [127]. It is modified to reveal the transmission sensitivity.

$$\dot{l} = \mathrm{J}v_p \quad \Rightarrow \quad dl = \mathrm{J}\,dr \tag{3.22}$$

where, $\dot{l} = [\dot{l}_1, \dot{l}_2, \dot{l}_3]^T$ and $v_p = [\dot{x}, \dot{y}, \dot{z}]^T$ are the active leg velocities and the platform velocity respectively. $dl = [dl_1, dl_2, dl_3]^T$ and $dr = [dx, dy, dz]^T$ are the infinitesimal change in the active leg lengths and the corresponding change in the platform position. The elements of J can be obtained by differentiating the inverse kinematic equations 3.8, 3.9 and 3.10. The relation in the matrix form is given as

$$\begin{bmatrix} dl_1 \\ dl_2 \\ dl_3 \end{bmatrix} = \begin{bmatrix} \frac{1}{l_1}\left(\frac{a}{\sqrt{3}} - \frac{b}{\sqrt{3}} + x\right) & \frac{1}{l_1}y & \frac{1}{l_1}z \\ \frac{1}{l_2}\left(\frac{b}{2\sqrt{3}} - \frac{a}{2\sqrt{3}} + x\right) & \frac{1}{l_2}\left(\frac{a}{2} - \frac{b}{2} + y\right) & \frac{1}{l_2}z \\ \frac{1}{l_3}\left(\frac{b}{2\sqrt{3}} - \frac{a}{2\sqrt{3}} + x\right) & \frac{1}{l_3}\left(\frac{b}{2} - \frac{a}{2} + y\right) & \frac{1}{l_3}z \end{bmatrix} \begin{bmatrix} dx \\ dy \\ dz \end{bmatrix} \tag{3.23}$$

The reciprocal sensitivity indices are given by the members of the 3×3 Jacobian matrix. As it can be seen, the Jacobian matrix stated in equation (3.23) is the transpose of the commonly known force transformation matrix used in the static analysis of PKM's. The nine reciprocal sensitivity indices are $\frac{dl_1}{dx}, \frac{dl_1}{dy}, \frac{dl_1}{dz}, \frac{dl_2}{dx}, \frac{dl_2}{dy}, \frac{dl_2}{dz}, \frac{dl_3}{dx}, \frac{dl_3}{dy}, \frac{dl_3}{dz}$. The absolute range of the reciprocal sensitivity of the leg varies from zero to one. When there is no participation of the leg in the direction of the translation of the platform at the point, the reciprocal sensitivity is zero and when there is maximum participation of the leg in the concerned motion of the platform, it is one. Also for non singular motion, not all the three legs can have the sensitivity of either zero or one at the same point for a particular direction of motion of the platform. Isotropic sensitivity (or equal participation of all the legs) is a most desired quality but the sensitivity is not isotropic at all points in the workspace. The sensitivity analysis determines the sensitivity variations in the workspace to perform the input range synthesis. The sensitivity is a function of the manipulator parameters. The size of the base, the size of the platform and the spatial location of the platform constitutes the parameter set. The sensitivity indices are obtained as a function of the manipulator parameters and the best sensitivity indices for a set of points (workspace) can be known. Provided the design parameters, sensitivity analysis determines the best operating position for a given directional motion of the mechanism.

In this section, the mathematical model is developed for the sensitivity analysis of the 3D-SPKM. A numerical example is given, considering the realistic values of the manipulator parameters for the prototype. The next chapter details the prototype development based on the numerical values given in the present example, and presents the experimental results.

3.4.2 Sensitivity with respect to an arbitrary displacement vector

The reciprocal sensitivity index of a leg with respect to an arbitrary displacement vector $d\vec{r}$ is computed. The position vector of the platform with respect to **O**(XYZ) is given by

$$\vec{r} = x\hat{\imath} + y\hat{\jmath} + z\hat{k} \tag{3.24}$$

Differentiating the above, the displacement vector of the platform is written as

$$d\vec{r} = dx\hat{\imath} + dy\hat{\jmath} + dz\hat{k} \tag{3.25}$$

From the equation 3.7, the arbitrary leg vector is of the form

$$\vec{l}_i = (x + c_{i1})\hat{\imath} + (y + c_{i2})\hat{\jmath} + (z + c_{i3})\hat{k} \tag{3.26}$$

$$l_i^2 = (x + c_{i1})^2 + (y + c_{i2})^2 + (z + c_{i3})^2 \tag{3.27}$$

where, c_{i1}, c_{i2}, c_{i3} , $i=1,2,3$. are constants for a manipulator. Differentiating,

$$l_i dl_i = (x + c_{i1})dx + (y + c_{i2})dy + (z + c_{i3})dz = \vec{l}_i \cdot d\vec{r} \tag{3.28}$$

The reciprocal sensitivity index with arbitrary displacement vector, $d\vec{r}$ is given by

$$\frac{dl_i}{dr} = \frac{\vec{l}_i \cdot d\vec{r}}{l_i dr} = \hat{l}_i \cdot d\hat{r} = \cos\theta \tag{3.29}$$

Where $\hat{l}_i$ is a unit vector along $\vec{l}_i$, $d\hat{r}$ is a unit vector along $d\vec{r}$, and θ the angle between $\vec{l}_i$ and $d\vec{r}$. The reciprocal sensitivity index is given by the dot product of the unit leg vector and the unit displacement vector and is equal to the cosine of the angle between them. For illustration, dl_1/dx is given by the cosine of the angle between $\vec{l}_1$and the X axis. For the motion of the platform along Z axis, the absolute value of the cosine of the angle between $\vec{l}_1$ and the X axis decreases and hence dl_1/dx decreases. The expression implies that the change in the leg length is always less than or equal the resultant distance traversed by the platform of the 3D-SPKM. Synthesis of the manipulator workspace based on dl/dr alone is a tradeoff between fine control resolution, and a high motion response.

3.4.3 Isotropic sensitivity for the three legs

The isotropic sensitivity of the three legs for a given displacement vector at a point in the workspace is significant. In other words, it is important to find a translation vector from a point in the workspace, wherein the reciprocal sensitivities of all the three legs are equal. The condition for isotropic sensitivity can be written as

$$\hat{l}_1.d\hat{r} = \hat{l}_2.d\hat{r} = \hat{l}_3.d\hat{r} \tag{3.30}$$

From equation 3.25, 3.26 and 3.29, the expressions for $\hat{l}_i.d\hat{r}$, *i=1, 2, 3* are obtained. Equating the three expressions we get,

$$\frac{1}{l_1}\left[\left(\frac{a}{\sqrt{3}} - \frac{b}{\sqrt{3}} + x\right)dx + ydy + zdz\right] = \frac{1}{l_2}\left[\left(\frac{b}{2\sqrt{3}} - \frac{a}{2\sqrt{3}} + x\right)dx + \left(\frac{a}{2} - \frac{b}{2} + y\right)dy + zdz\right]$$
$$= \frac{1}{l_3}\left[\left(\frac{b}{2\sqrt{3}} - \frac{a}{2\sqrt{3}} + x\right)dx + \left(\frac{b}{2} - \frac{a}{2} + y\right)dy + zdz\right] \tag{3.31}$$

The above equation can be solved in two ways. In the first case, the location of the centre of the platform with respect to **O** (XYZ) is taken to be known. That is, $\vec{r} = x\hat{\imath} + y\hat{\jmath} + z\hat{k}$ is known, and the unit displacement vector $\frac{\overrightarrow{dr}}{r} = \frac{dx\hat{\imath}+dy\hat{\jmath}+dz\hat{k}}{r}$ is calculated. The equations formed would be a set of linear equations giving a single solution.

In the second case, the unit displacement vector is given, $\frac{\overrightarrow{dr}}{r} = \frac{dx\hat{\imath}+dy\hat{\jmath}+dz\hat{k}}{r}$, and the position of the platform, $\vec{r} = x\hat{\imath} + y\hat{\jmath} + z\hat{k}$ in the workspace is determined. The equations formed would be a set of non linear equations giving multiple solutions for this problem. The set of equations for the first case are:

$$\left[\frac{1}{l_1}\left(\frac{a}{\sqrt{3}}-\frac{b}{\sqrt{3}}+x\right) - \frac{1}{l_2}\left(\frac{b}{2\sqrt{3}}-\frac{a}{2\sqrt{3}}+x\right)\right]\frac{dx}{dz} + \left[\frac{1}{l_1}y-\frac{1}{l_2}\left(\frac{a}{2}-\frac{b}{2}+y\right)\right]\frac{dy}{dz} + z\left(\frac{l_2-l_1}{l_2 l_1}\right) = 0 \tag{3.32}$$

$$\left[\frac{1}{l_1}\left(\frac{a}{\sqrt{3}}-\frac{b}{\sqrt{3}}+x\right) - \frac{1}{l_3}\left(\frac{b}{2\sqrt{3}}-\frac{a}{2\sqrt{3}}+x\right)\right]\frac{dx}{dz} + \left[\frac{1}{l_1}y-\frac{1}{l_3}\left(\frac{b}{2}-\frac{a}{2}+y\right)\right]\frac{dy}{dz} + z\left(\frac{l_3-l_1}{l_3 l_1}\right) = 0 \tag{3.33}$$

Numerical examples:

Considering the symmetry at *x = 0, y = 0,* and expressing the leg length in terms of manipulator parameters, the result is

$$l_1 = l_2 = l_3 = \sqrt{\left(\frac{a}{\sqrt{3}}-\frac{b}{\sqrt{3}}\right)^2 + z^2} \tag{3.34}$$

Substituting the above values and solving the equations (3.32) and (3.33), result is

$$\frac{dx}{dz} = \frac{dy}{dz} = 0, \qquad \frac{d\vec{r}}{r} = \frac{0\hat{\imath} + 0\hat{\jmath} + dz\hat{k}}{dz} = \hat{k} \tag{3.35}$$

The result illustrates that, if the translation is along Z axis (at *x = 0, y = 0)*, the sensitivity of the three legs are equal and therefore any point on the Z axis is isotropic. This result can be clearly visualized from the symmetry of the mechanism.

Considering a more general case to find isotropy in XZ (y = 0) plane, y = 0 is substituted in equation (3.9) and (3.10) to get $l_2 = l_3$ and further substituting and solving the equations (3.32) and (3.33), result is

$$\frac{dy}{dz} = 0;\ \left[\frac{1}{l_1}\left(\frac{a}{\sqrt{3}}-\frac{b}{\sqrt{3}}+x\right) - \frac{1}{l_2}\left(\frac{b}{2\sqrt{3}}-\frac{a}{2\sqrt{3}}+x\right)\right]\frac{dx}{dz} + z\left(\frac{l_2-l_1}{l_2 l_1}\right) = 0 \tag{3.36}$$

Solving equation (3.36), the value of dx/dz can be determined. The direction of isotropy (dx, dy, dz) varies at each point in the range of $77^0\ to\ 105^0$ measured from the positive X axis. In figure 3.16, the boundary corresponds to the reachable workspace in the XZ plane and the arrow head at each of the grid points shows the direction of motion of the platform for isotropic sensitivity.

In a similar procedure, the isotropic sensitivity vector can be determined for any position in the workspace. Trajectory planning of the 3D-SPKM is done such that deviation from isotropic sensitivity is minimal throughout the trajectory for improved dynamic characteristics. The isotropic sensitivity also aids in synthesis of the mechanism. In other words, if the position (x, y, z) and the direction vector (dx, dy, dz) of the platform of the 3D-SPKM is given for a particular preferential trajectory, the kinematic parameters (*b, a*) can be determined from the isotropic sensitivity equation (3.31). In many surgical applications it is important to approach and perform precise operations at a certain predefined point with high precision than the rest of the workspace points. Information of isotropic sensitivity enhances micro managing the workspace for high precision manipulation of the surgical tool.

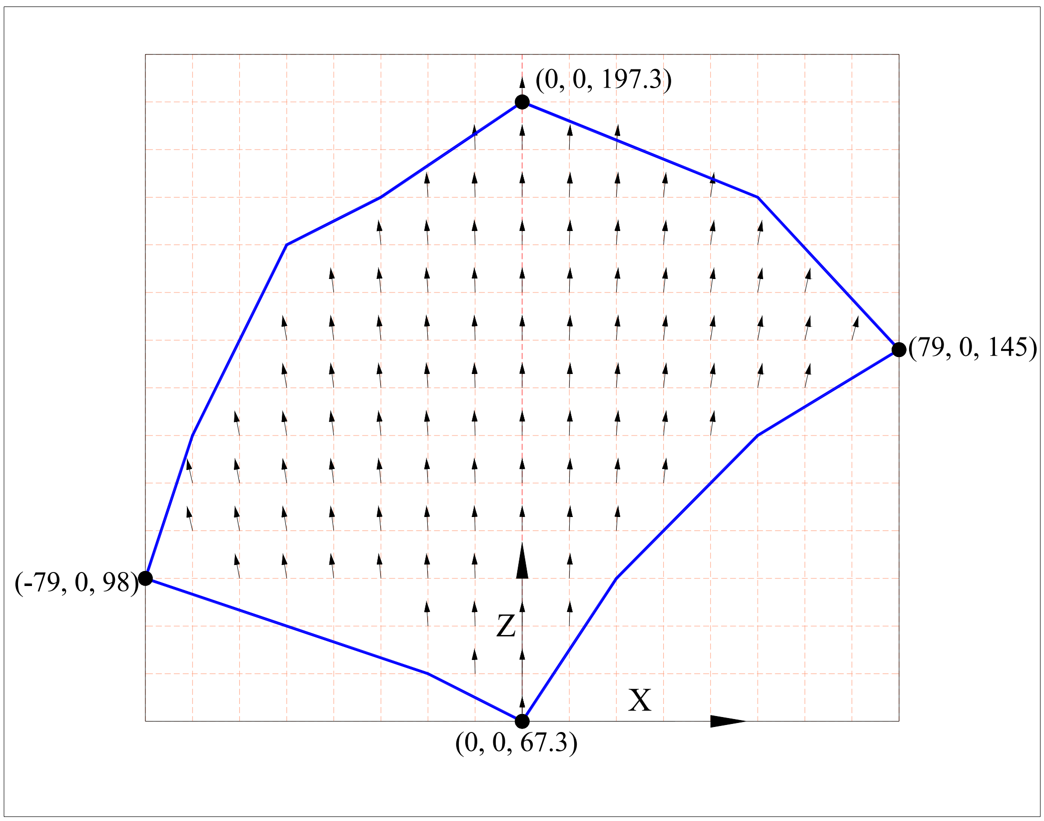

Figure 3.16: Direction of motion of platform for isotropic sensitivity in XZ plane

3.4.4 Variation of sensitivity indices at boundary of manipulator workspace

A 3D-SPKM having design parameters, $b=329$, $a=78$, $159 \leq l_i \leq 245$, based on which the prototype is developed is considered to characterize sensitivity at various points on the boundary of the workspace. Figure 3.17 shows distribution of the reciprocal leg sensitivity, $dl_1/dx, dl_1/dy, dl_1/dz$ on the workspace envelopes. It represents only the relative variation of the reciprocal sensitivity parameters. Because of the symmetry, the distribution of the reciprocal leg sensitivities of the other two legs is same as shown in figure 3.17. The color of the sphere represents the value of the reciprocal sensitivity parameter. The red spheres on the envelopes represent the high reciprocal sensitivity or high control resolution and the green represents the smaller sensitivity or higher motion response. The envelopes always exhibit extremities of the sensitivity range.

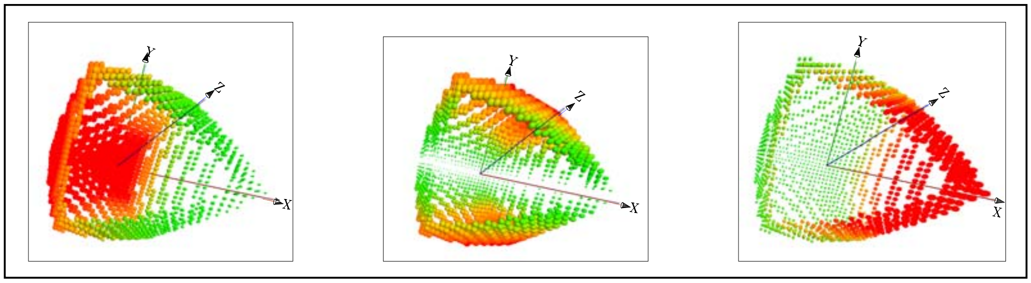

Figure 3.17: Reciprocal leg sensitivity distribution, dl_1/dx , dl_1/dy , dl_1/dz on workspace envelope due to positional change along X, Y and Z axes respectively.

The extreme sensitivities are at the envelopes of the workspace. The magnitude of the reciprocal leg sensitivity at a point and its distribution in the manipulator workspace provides a good insight in planning the fine control resolution trajectories in the task space. It provides a good handle to design a right balance between the control resolution and the motion response. The size of the spheres indicates the sensitivity, while the sparseness of the spheres indicates the motion response.

3.4.5 Variation of sensitivity indices in manipulator workspace

A 3D-SPKM having kinematic parameters, b = 329 mm; a = 78 mm is considered to characterize sensitivity at the various points inside the workspace. The reciprocal sensitivity parameters at the various points inside the workspace are computed. Translations $-50.0 \leq x \leq +50.0$; $y = 0.0$; $82.0 \leq z \leq 182.0$ are considered for the analysis and the sensitivity indices at various points inside the workspace.

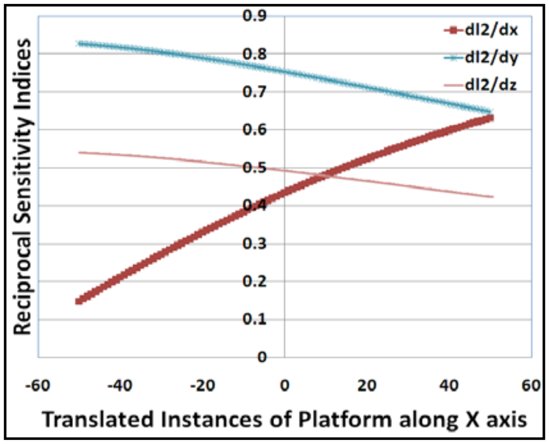

Figure 3.18: Reciprocal sensitivity indices verses X instances at $y = 0$ and $z = 82$

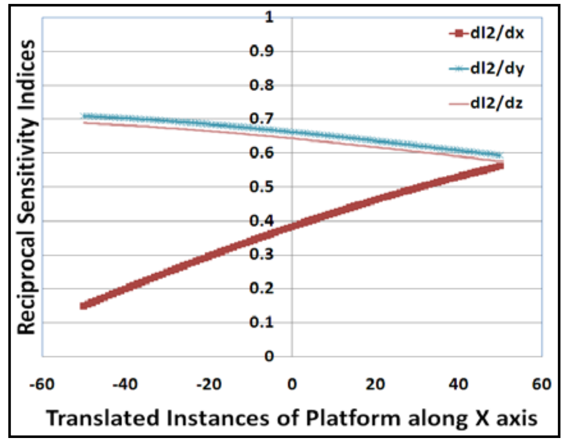

Figure 3.19: Reciprocal sensitivity indices verses X instances at $y = 0$ and $z = 132$

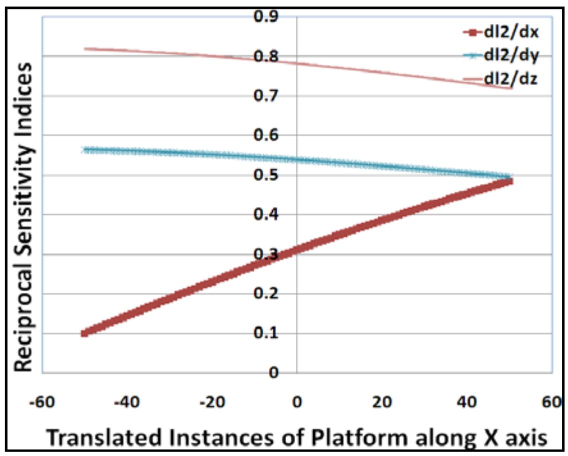

Figure 3.20: Reciprocal sensitivity indices verses X instances at $y = 0$ and $z = 182$

Figures 3.18, 3.19 and 3.20 show the variation of the three reciprocal sensitivity indices, at translated instances of the platform along X axis keeping (y, z) coordinates constant at (0, 82), (0, 132) and (0, 182) respectively. The distribution of the reciprocal leg sensitivities of other two legs is similar to the one described because of the symmetry. Some of the indices show a downward trend and the other illustrates an upward trend as the values of the translated instances of the platform along X and Z axes change. This can be attributed to the variation in the angle between the leg vector and the translation vector as mentioned earlier. At $x = 40$, $y = 0$, and $z = 132$, where many reciprocal sensitivity indices tend to approach a closer and higher value, would be close to isotropic point for the given workspace. The point and the region around this point can be a preferential region in the workspace for the surgical tool operation.

3.5 Singularity Analysis

The singularity free workspace and the kinematic synthesis are significant to set the boundaries of the workspace farthest from singularities. The mechanism will have an undesirable mobility at or near the singular positions due to poor stiffness along one or more directions. The singularity aspect of the 3-UPU based SPKM is well presented in the earlier work by Gregorio and Parenti-Castelli [105]. The singularity analysis pertaining to the numerical values of the design parameters, based on which the prototype is built is presented. As stated earlier, the 3D-SPKM has been assembled to have pure translation mode of operation only. The presented research work is not intended for any other modes of operation and hence the same are not explored. The singularity of 3D-SPKM in other operation modes and the translation possibilities into other operation modes has been verified by Prof. Husty's ([121], [126A]) lab, Austria and hence it is determined that the 3D-SPKM workspace is far away from any operation mode changing surface. As stated earlier, the numerical values of the kinematic parameters $b = 329$, $a = 78$, and prismatic stroke range of $159 \leq l_i \leq 245$ $(i=1, 2, 3)$ are taken for singularity analysis.

The singularity occurs under any of the following three conditions.

1) Rotational singularity, when $\hat{n}_1 \cdot (\hat{n}_2 \times \hat{n}_3) = 0$, where $\hat{n}_i = (\hat{q}_{i1} \times \hat{q}_{i2})$
2) Translation singularity, when the scalar triple product $\hat{l}_1 \cdot (\hat{l}_2 \times \hat{l}_3) = 0$
3) The other condition for translation singularity is when, $(n_i . \hat{l}_i) = 0$

The condition no. 1 results in a cylindrical singularity surface [105]; the diameter of the cylinder is 578.41 for the chosen numerical kinematic parameters. Conditions no. 2 and no. 3 occur when the platform is coplanar with the base. Even with the above three singularity constraints, the feasible design space is quite large. The design space is considerably reduced by the symmetric considerations: the kinematic arrangement is designed tri-symmetric with respect to the global Z axis, and the workspace boundary surfaces lie at equal distances from the singular surfaces. The synthesis of the proportion of design parameters and practical ranges for the active prismatic strokes are worked out in such a manner so as to stay farthest from the singular surfaces. The figures 3.21 & 3.22 show the secure separation of the workspace from the cylindrical singularity surface and the figure 3.23 shows the safe distance from the platform getting coplanar with the base (The distance of separation is represented by the vertical line). The mechanism would be in singularity if the reference point of the platform coincides with any point on the cylindrical singularity surface shown in figure 3.24. Out of the infinite singular configurations six positions of the platform are shown in figure 3.24. It is illustrated that these positions lie outside and far away from the actual reachable workspace of the platform (refer figure 3.21, 3.22 and 3.23).

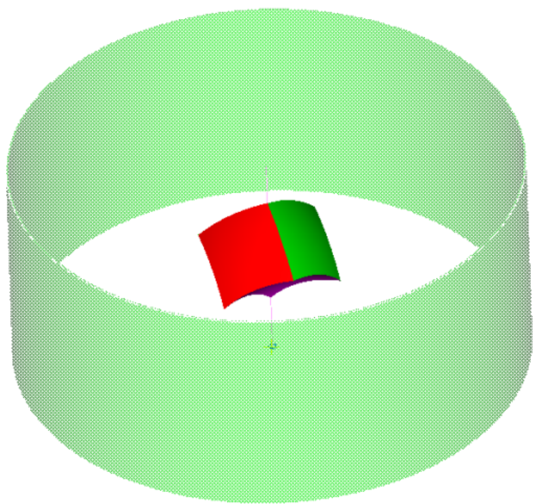

Figure 3.21: Positioning of workspace relative to singular surface.

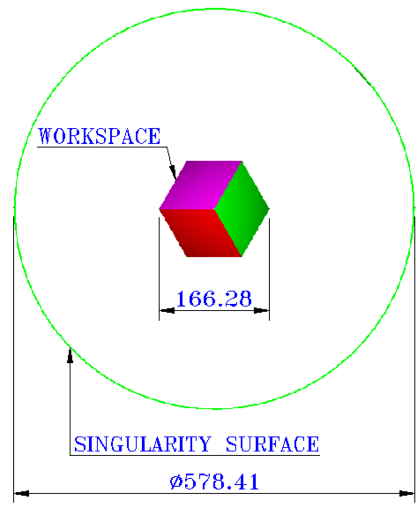

Figure 3.22: Sizing of workspace related to singular surface

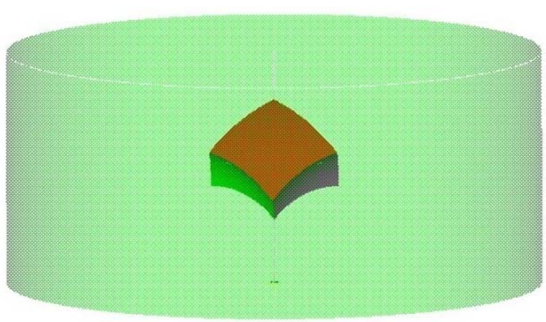

Figure 3.23: Separation of workspace relative to base surface of singularity

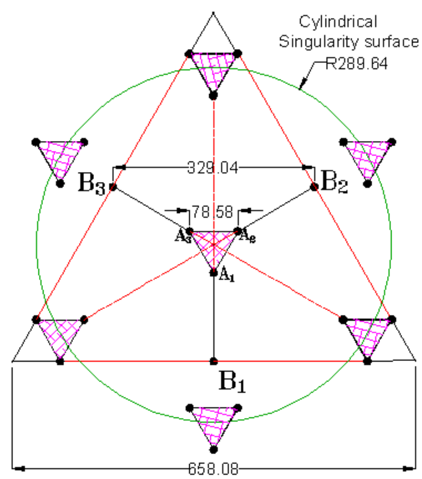

Figure 3.24: Position of platform at home position and six singular configurations

3.6 Error Analysis

This section deals with error analysis. It deals with determining the possible magnitude of the error at the location of surgical tool (attached with platform of 3D-SPKM) for the given torsional errors about each leg of the 3D-SPKM. It is done to ensure that the surgical tool maneuvers with the utmost precision throughout the neurosurgery. In this section, the torsional joint clearance errors are analyzed to determine their influence on the posture accuracy of the platform. The major source of error is the torsional rotation in the universal joints. An algorithm is developed to arrive at the posture error at the platform of the 3D-SPKM due to the inaccuracies in the passive composite joints for a specified workspace. The inaccuracies in the passive joints and the active prismatic joints lead to an uncontrolled torsion rotation about each of the prismatic axis of the leg of the 3D-SPKM. The mathematical model presented relates the posture of the platform and an uncontrolled torsional rotation (error) about each of the prismatic axis. The objective is to understand the torsional rotations for the given posture of the platform.

The design parameters of the 3D-SPKM are deduced from kinematic analysis. The geometrical arrangement of the leg as well as the platform is set to fulfill the geometric conditions given in equation (3.4). The home posture is defined when the platform (the plane formed by the three connection points at the platform) is parallel to the base and the prismatic joint axis of the each leg is normal to both the axis of the universal joints on either side.

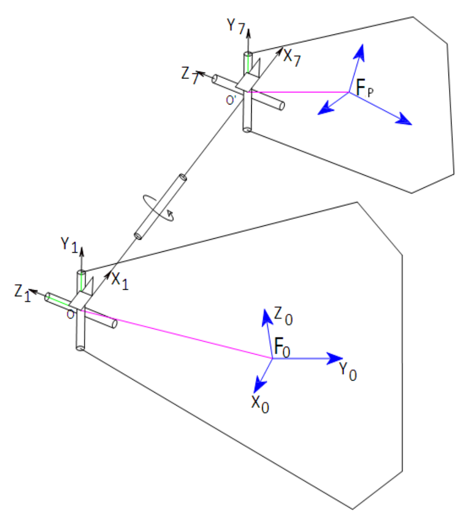

Figure 3.25: Description of joint frames of 3D-SPKM at home position for the purpose of error analysis.

The home posture is set, when the legs are at the minimum length and the x and y coordinates of the centre of the platform are zero. At the home posture, the passive rotations of the two universal joints as well as the torsional rotations are taken as zero. The home posture serves as the reference for all the passive rotations as well as the torsional rotation measurement.

The posture of the platform coordinate frame, F_P is assumed to be given with respect to the base coordinate frame, F_0. The inverse kinematic solution is easily obtained and the leg lengths $l_1,\ l_2,\ l_3$ can be calculated. A mathematical model is obtained to formulate a matrix equation relating the posture of the platform to the passive joint rotations of the 3D-SPKM and an additional torsional rotation about each of the prismatic axis. The 12 rotations (four for each leg) are solved pertaining to all the passive joints of 3D-SPKM as well as the 3 additional torsional rotations about the prismatic axis for a given posture of the platform using the transformations stated below. It is essential to know the torsional rotations of the passive joints for the given posture of the platform. Thereby, the extent of torsional mobility required to satisfy the posture can be determined. To establish a model, a coordinate frame is defined in each of the bodies separated by the joints. The frames are numbered from the base to the platform progressively and the frame *n* is termed as F_n. F_0 is the fixed frame attached to the geometrical centre of the base. F_1 is attached to the leg connection point at the base. The position and orientation of the frame, *n* with respect to the preceding frame, *m* is described by the DH parameters, the homogeneous transformation matrix is given by ${}^{m}_{n}T$. F_7 is attached to the leg connection point at platform and F_P is attached to the geometrical centre of the platform as illustrated in figure 3.25. Rest of the frames, F_2 …. F_6 are attached at the intermediate bodies of the leg.

${}^{0}_{1}T$ is the transformation of F_1 with respect to fixed F_0. ${}^{7}_{P}T$ is the transformation of F_P with respect to F_7. The connecting points at the base and at the platform are known as F_0 and F_P respectively. The other intermediate frames and its successive transformations are as given below:

1. ${}^{1}_{2}T$: Rotation θ_1 of F_2 with respect to F_1 about Y_1 (passive rotation due to universal joint).
2. ${}^{2}_{3}T$, Rotation θ_2 of F_3 with respect to F_2 about Z_2 (passive rotation due to universal joint).
3. ${}^{3}_{4}T$, Rotation θ_3 of F_4 with respect to F_3 about X_3 axes (torsional backlash error).
4. ${}^{4}_{5}T$, Translation of F_5 with respect to F_4 along X_4 axes (active prismatic joint).
5. ${}^{5}_{6}T$, Rotation θ_5 of F_6 with respect to F_5 about Z_5 axes (passive rotation due to universal joint).
6. ${}^{6}_{7}T$, Rotation θ_6 of F_7 with respect to F_6 about Y_6 axes (passive rotation due to universal joint).

For the given posture of the platform, all the passive joint rotations (θ_1, θ_2, θ_5, θ_6) and the torsional backlash errors (θ_3) for the three legs for a given platform posture are analytically solved using the above transformations. The solutions give insight into the required mobility of the passive joints and torsional backlash error for a given posture. The results are tabulated in tables 3.3 to 3.7. The tables 3.3 to 3.7 give the platform posture followed by the corresponding mobility of all the passive joints and torsional backlash error for one leg. Tables 3.3 to 3.7 show the passive and torsional rotations (θ_3) required for the given postures of the platform. It is evident from the tables given above that any rotation of the platform from being parallel to the base always results in a torsional rotation (θ_3) of the leg. For a pure translational 3D-SPKM, the combined torsional stiffness of the legs dictates the rotational stiffness of the manipulator.

Table 3.3: Platform at home posture

Rotation along X	Rotation along Y	Rotation along Z	Translation along X	Translation along Y	Translation along Z
0	0	0	0	0	100

Joint Space Vector

	θ_1(Passive)	θ_2(Passive)	θ_3(Error)	θ_5(Passive)	θ_6(Passive)
Leg1	0	0	0	0	0
Leg2	0	0	0	0	0
Leg3	0	0	0	0	0

Table 3.4: Parallel to base posture & translation along Z Axis

Rotation along X	Rotation along Y	Rotation along Z	Translation along X	Translation along Y	Translation along Z
0	0	0	0	0	150

Joint Space Vector

	θ_1(Passive)	θ_2(Passive)	θ_3(Error)	θ_5(Passive)	θ_6(Passive)
Leg1	8.95^0	0	0	0	-8.95^0
Leg2	8.95^0	0	0	0	-8.95^0
Leg3	8.95^0	0	0	0	-8.95^0

Table 3.5: Rotation about X axis

Rotation along X	Rotation along Y	Rotation along Z	Translation along X	Translation along Y	Translation along Z
5^0	0	0	0	0	100

Joint Space Vector

	θ_1(Passive)	θ_2(Passive)	θ_3(Error)	θ_5(Passive)	θ_6(Passive)
Leg1	0	0	-2.5^0	5^0	0
Leg2	-0.98^0	-0.04^0	1^0	2.2^0	5.2^0
Leg3	-1.19^0	-0.04^0	1.4^0	2.1^0	5.5^0

Table 3.6: Rotation about Y axis

Rotation along X	Rotation along Y	Rotation along Z	Translation along X	Translation along Y	Translation along Z
0	5^0	0	0	0	100

Joint Space Vector

	θ_1(Passive)	θ_2(Passive)	θ_3(Error)	θ_5(Passive)	θ_6(Passive)
Leg1	1.11^0	0^0	0^0	0^0	-6.1^0
Leg2	0.66^0	0.04^0	2.3^0	-3.7^0	-3.25^0
Leg3	0.66^0	0.04^0	-2.3^0	3.7^0	3.25^0

Table 3.7: Rotation about Z axis

Rotation along X	Rotation along Y	Rotation along Z	Translation along X	Translation along Y	Translation along Z
0	0^0	5^0	0	0	100

Joint Space Vector

	θ_1(Passive)	θ_2(Passive)	θ_3(Error)	θ_5(Passive)	θ_6(Passive)
Leg1	-0.09^0	2.49^0	4.34^0	-5^0	-0.25^0
Leg2	0.09^0	-2.49^0	4.34^0	5^0	0.25^0
Leg3	-0.09^0	2.49^0	4.34^0	-5^0	-0.25^0

The results in tables 3.3 to 3.7 give the required mobility range in Universal-Universal (U-U) joints for the desired workspace. Figure 3.26 shows the concurrent torsional rotations (θ_3) in all the three legs in relation to the rotation of the platform about the Z axis. The figure 3.26

illustrates the proportionality between the magnitude of the torsional rotation in each leg with respect to the rotational displacement in the platform.

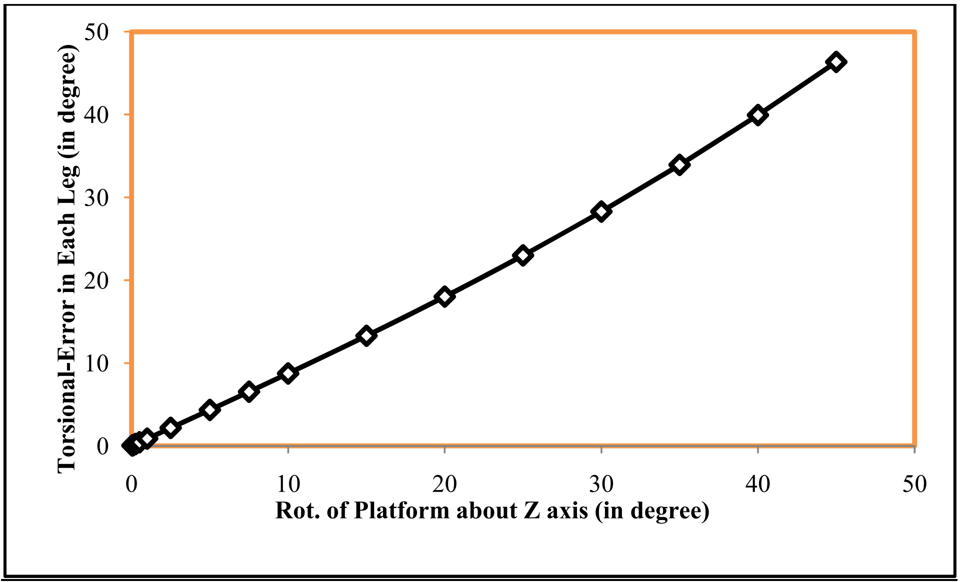

Figure 3.26: Proportionality in torsional error

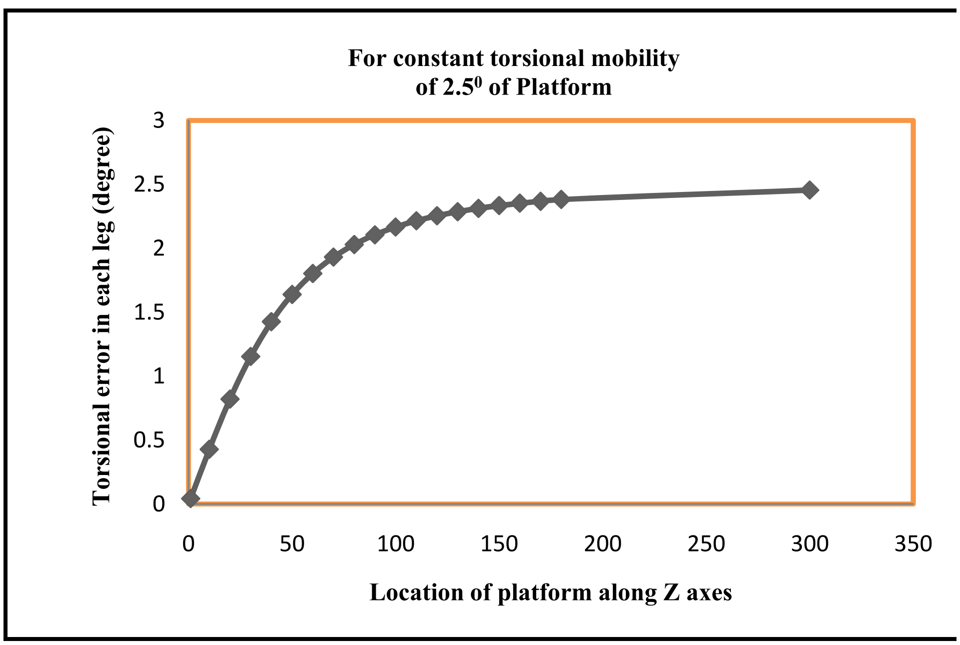

Figure 3.27: Concurrent torsional rotation (θ_3) of legs for increasing Z translations at constant torsional mobility of 2.5^0 of platform.

Further, for a constant torsional mobility of the platform, the required concurrent torsional rotation (θ_3) of the legs for various Z translations is studied. Figure 3.27 shows the required amount of concurrent torsional play/error (θ_3) of the legs for constant torsional play of 2.5^0 of the platform at increasing Z translations. It is observed that at smaller Z translations, the torsional mobility of the platform has higher sensitivity to θ_3 but flattens out after certain Z translation, the result serves to design the Z translation range. It can be concluded from the above analysis is that there is no extreme kinematic sensitivity to the torsional errors within a certain working range of the manipulator. The mechanism does not display disproportionate sensitivities with respect to the clearances in the passive joints. The above analysis serves to plan the working range of the manipulator. The presence of torsional clearances concurrently in more than one leg will result in unwanted proportional rotational mobility on the platform.

3.7 Summary

Based on the attributes required for the robot for stereotactic neurosurgery, analysis and synthesis of the robotic system were presented. A detailed methodology was developed to determine the mobility requirement of the passive composite joints for a given set of parameters of the PKM. The locations of the central axis of the solid angle (cone angle) of the passive composite joints were optimized. The optimum orientations of the central-axis of the joints are the one that minimize angular mobility of the passive composite joints to embed all extreme leg positions. This gives the best utility posture in terms of mobility of the passive joints. Two numerical examples were presented considering realistic dimensions to arrive at optimum mobility ranges of the passive joints at the platform and at the base. The design synthesis was presented with an objective of enhancing the utility of the passive joint mobility to improve the workspace of parallel mechanisms. The results of the mobility analysis illustrates that the angular mobility requirement is high and cannot be obtained from the commercially available composite joints. The novel options for the design of passive composite joints are explored in the next chapter. The rotational mobility of the platform at the various locations in workspace was determined. The corresponding mobility at the passive joints of the platform was determined. Based on the design analysis, a prototype 3D-SPKM and 6D-PKM is developed and the same is presented in subsequent chapters.

In this chapter, a detailed account of sensitivity analysis for the 3D-SPKM was presented. The sensitivity analysis determines the location where the surgical tool would have utmost precision in performing a neurosurgery. The analysis determined the best operating position for a given directional motion of the mechanism. The results obtained from the sensitivity analysis are significant in the synthesis of leg ranges. The sensitivity analysis determined the variations of the sensitivity in the workspace with respect to the input range parameters. The error analysis illustrated that the Tsai 3-UPU based 3D-SPKM does not go through disproportionate sensitivity in its workspace due to torsional errors. The singularity analysis ensured that the workspace boundary is farthest from the singularity surfaces. The results presented were in contrast to the results presented in [119] for the similar 3 axis translational parallel manipulator. The uncontrolled gross motion was attributed to the improper kinematic design considerations instead of the extreme sensitivities of the mechanism to the clearance. The analysis confirmed that the mechanism preserves the in-parallel property and it benefits the positional error reduction at the platform. The error analysis results evidently conclude that the absolute of the sum of maximum individual errors at each joint pairs of all the legs do not accumulate to reflect large position error at the platform. This result was in contrast to the results reported by Venanzi and Castelli [122] and Meng et. al. [123], which presented a highly exaggerated figure that cannot be taken as a good estimate.

The above analysis is an essential requirement for the development of a 6D-PKM based robot which would maneuver the surgical tool with utmost precision to the tumor point.

Chapter IV

Synthesis, Prototype Development and Experimental Results of 3D-SPKM

4.1 Introduction

A detailed analysis pertaining to the aspects of passive mobility, optimum location of joints' axes, sensitivity, singularity and error analysis of the 3D-SPKM were presented in the previous chapter.

This chapter presents the engineering design considerations, workspace analysis, motion simulation, prototype development and experiments undertaken for the performance evaluation of the 3D-SPKM. The experiments also validate the capability of the 3D-SPKM in performing frameless stereotactic neurosurgery procedures. The design considerations which ensure negligible torsional backlash for the prototype designed are presented. The design initiatives necessary to develop a high precision robotic system, the workspace analysis and 3D motion simulation of the 3D-SPKM for successful robotic based stereotactic surgery are presented. The visual 3D motion simulation facilitates interference free mobility and trajectory planning of the 3D-SPKM throughout its workspace. The workspace analysis ensures the reach-ability requirements of the surgical tool. A software model is developed and the same is used to run the mock up of the stereotactic surgery to confirm the feasibility of the various trajectories in the specified work-zone. The development of the 3D-SPKM incorporating the design considerations mentioned above and accounting for mechanical constraints is given. The experimental results for the repeatability and trajectory following accuracy for various payloads are also presented. It is demonstrated that the prototype behaves as per the theoretical and simulated observations.

4.2 Engineering Design Considerations

In this section, the engineering design considerations are presented to achieve the theoretical kinematic design conditions. The engineering design steps which establish and maintain the geometric conditions are very important as discussed by Blanding [128]. These design considerations ensure development of a high precision robotic system for neurosurgery. Two universal joints of which, each is built with a common cube block and with a pair of orthogonal hinges located closely together is not a good solution. Such joints are not free of torsional backlash. As described in the previous chapter, the presence of torsional backlash influences the rotational mobility of the manipulator platform. The commercially available universal joints are meant to transmit high torque with minimal direction reversals and not meant for establishing high precision geometric constraints. A small clearance along the radial direction and close hinge supports would ill define a hinge axis, whereas with the same clearance and a longer bearing support, the angular play is considerably reduced. The figures 4.1 and 4.2 show these joints demonstrating the advantage of one support over the other.

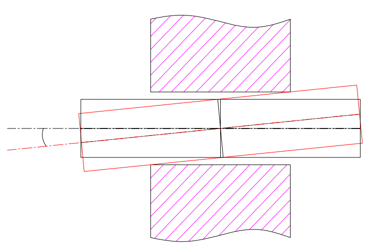

Figure 4.1: Shorter bearing support, higher angular play

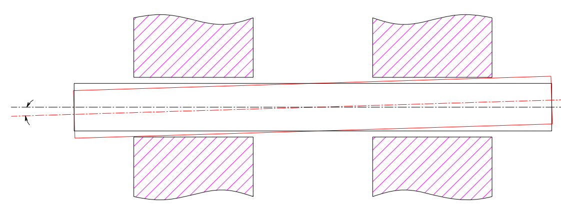

Figure 4.2: Longer bearing support, smaller angular play

Figure 4.3: 3-UU system using single block universal joints

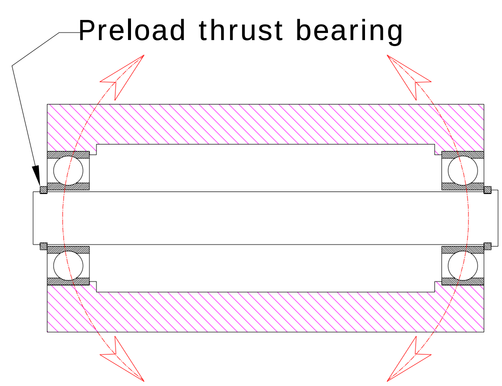

Figure 4.4: Long bearing support with end thrust bearing preloaded to eliminate torsional backlash

As discussed earlier in chapter 2 & 3, the observations and negative results presented in Han et. al. [119] and a reference to this in a survey by Merlet [120] raised the questions regarding the feasibility of the 3-UPU parallel mechanisms. The theoretical models of Venanzi and Parenti-Castelli [122] and Meng et. al. [123] came out with the results showing that the end effector position is very highly sensitive to the joint clearances. They have reported very high positional errors acknowledging the results of Han et. al. [119] even in a non-singular geometry. Going by the conflicting results in theory and very fewer observations based on practical models, the 3-UPU mechanism has been revisited and a theoretical model has been built and validated with stage wise prototype models and experiments. This aspect was further studied by building a 3-Universal-Universal (UU) structure based on single block universal joints. The prototype is shown in the figure 4.3. The sizing of the 3-UU structure is chosen in accordance with the design of the 3D-SPKM. The design parameters of the 3D-SPKM are chosen to suit the neurosurgical requirements. The base side 'b' of the 3-UU system is 300 mm, platform side 'a' is 70 mm and the shortest distance of the platform from the base is 150 mm. The platform motions due to joints' clearance are measured and it is found to be much less than the maximum predicted using theoretical model by Venanzi and Parenti-Castelli [122]. The absolute sum of the maximum individual errors at each joint pair of all the legs as reported by Venanzi [122] and Meng [123] gives a highly exaggerated figure and cannot be taken as a good estimate. Clearly, no disproportionate motion of the platform is observed as indicated by Han et. al. [119]. The disproportionate motion of the 3D-SPKM reported in [119] is because of the geometrical singularity and this is also confirmed in the model given by Walter et. al. [121]. It is clear from the inspection and assessment of the prototype model that the imprecision is due to the torsional backlash at the joints. Also, it was observed that when the partial play on the joints is externally arrested on one of the legs, the stiffness of the 3–UU platform significantly improved confirming the joint error analysis made in chapter 3.

The observations made in the 3-UU structure suggest that building a high precision 3-UPU SPKM has a practical feasibility. The feasibility of a high precision manipulator is practicable if the design solution accounts for precise constraint axis definition and elimination of torsional backlash apart from optimum design of the manipulator components. The essential design solution required for elimination of torsional backlash has been proposed. Instead of closely held pin hinges, distantly separated hinges can considerably reduce the torsional backlash. Also instead of a pin and a bush, a high precision, wide needle bearing assists in reduction of torsional backlash. In order to reduce the backlash due to clearance, further, pre-loaded outside thrust bearing retainers are accommodated in place as shown in the figure 4.4. The mechanical design of each revolute axis of a universal joint shown in the figure 4.5 is evolved after cautious assessment of the theoretical model and the observations made on the 3-UU prototype. In the design, two block gimbal joint is used, which provides longer bearing support instead of the commercially available universal joints. The prototype provided negligible torsional backlash. The two support gimbal joints reduce the errors in axis definition, besides improving the torsional rigidity of the leg.

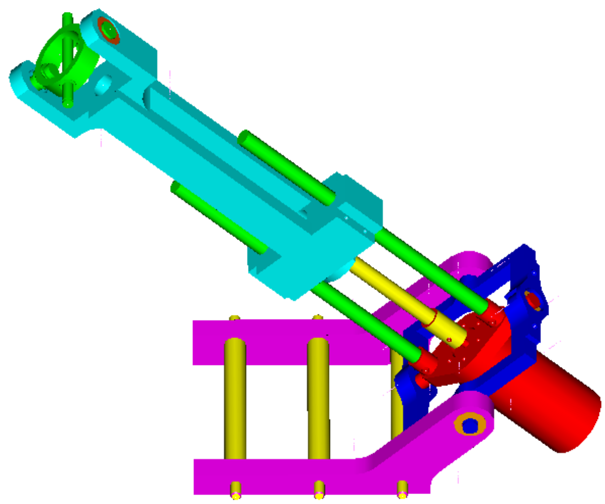

Figure 4.5: A UPU kinematic chain used in 3D-SPKM

The single block universal joints that are available commercially do not meet the angular mobility requirement of the 3D-SPKM. The proposed design shown in figure 4.5 adequately addresses the mobility requirement of the passive universal joints. Due to the improved design and optimal positioning of the passive joints, mobility of the passive universal joints is not a constraint throughout the workspace of the 3D-SPKM. The leg assembly consists of a serial chain formed by UPU (Universal-Prismatic-Universal) joints. Prismatic joints are another source for undesired torsional mobility. The prismatic joints (ball screw arrangement in the presented case) act as a cylindrical joint unless proper design constraints are incorporated. The critical aspect is to build a reference for pure prismatic motion. The seat of the universal joint designed as per the design considerations discussed above serves as the reference plane, free of torsional mobility. Two parallel pre-loaded ball splines housed in the reference seat serve as guides for pure prismatic motion. The two pre-loaded ball splines are arranged in such a manner that they increase the torsional rigidity and eliminate angular backlash. The figure 4.5 shows the near zero backlash UPU chain used in the 3D-SPKM which incorporates all the design considerations. These design considerations are an essential requirement for the development of a high precision robot for stereotactic neurosurgery.

4.3 Workspace Analysis and Motion Simulation of 3D-SPKM

The kinematic model of the 3D-SPKM has been described in the previous chapter. Prior to the prototype development, workspace analysis and 3D motion simulation of the 3D-SPKM is carried out to ensure its interference free mobility and trajectory planning throughout its motion. A software module has been developed with the desired translations as an input which displays an OpenGL software model showing the sequence of all the translations. The software model is used for checking the feasibility of the trajectories in the workspace. The design and selection of the various components of the 3D-SPKM have been carried out in accordance with the theoretical results. Figure 4.6 shows the software simulation snapshot and figure 4.7 illustrates the workspace of the manipulator obtained by the intersection of six spheres. The workspace of 3D-SPKM is determined analytically using the equations (4.1), (4.2) and (4.3).

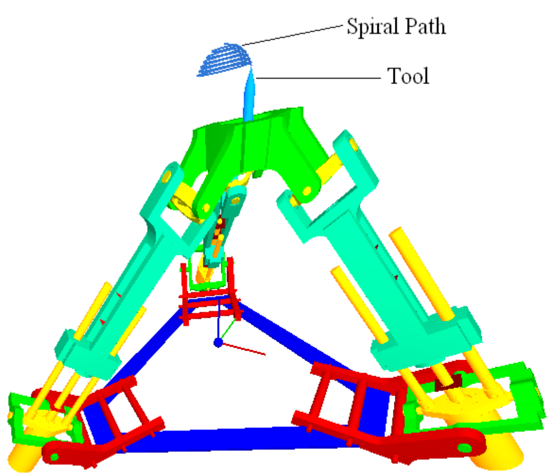

Figure 4.6: 3D motion simulation of 3D-SPKM

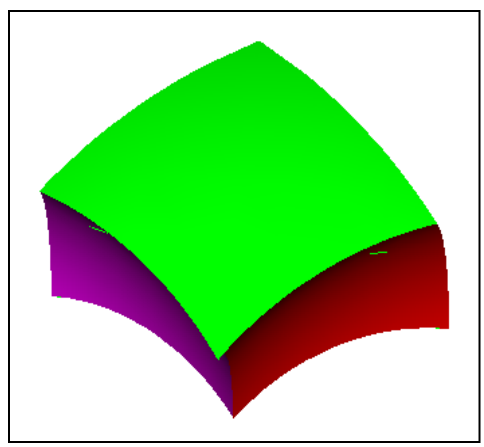

Figure 4.7: Workspace of 3D-SPKM

Based on the design solution, the 3D-SPKM having design parameters, *b* (base side) $=329$, *a* (platform side) $=78$, $159 \leq l_i$ (leg length) ≤ 245, has been developed. Each kinematic chain (see figure 4.5) consists of a DC motor integrated with an encoder of resolution 4000 counts per revolution, coupled to a ball screw having a lead of 1 mm. This arrangement provides high control resolution along the prismatic motion to the legs of the 3D-SPKM. Based on the manipulator parameters and selection of the prismatic joints, the translation workspace of the manipulator has been determined. The translation range of the mechanism along the Z axis is $0 \leq z \leq 130$ mm. The translation range along the X and Y axis is $-52 \leq x \leq 79$ mm and $-69 \leq y \leq 69$ mm at different values of z. The realizable workspace is determined from the constraint of leg ranges. The workspace points (shown in figure 4.7) satisfy the constraints given by equations (4.1), (4.2) and (4.3).

$$l_{min}^2 \leq \left(\frac{a}{\sqrt{3}} - \frac{b}{\sqrt{3}} + x\right)^2 + y^2 + z^2 \leq l_{max}^2 \tag{4.1}$$

$$l_{min}^2 \leq \left(\frac{b}{2\sqrt{3}} - \frac{a}{2\sqrt{3}} + x\right)^2 + \left(\frac{a}{2} - \frac{b}{2} + y\right)^2 + z^2 \leq l_{max}^2 \tag{4.2}$$

$$l_{min}^2 \leq \left(\frac{b}{2\sqrt{3}} - \frac{a}{2\sqrt{3}} + x\right)^2 + \left(\frac{b}{2} - \frac{a}{2} + y\right)^2 + z^2 \leq l_{max}^2 \tag{4.3}$$

Where l_{min} and l_{max} are the minimum and maximum leg lengths of each leg of 3D-SPKM.

4.4 Accuracy and Repeatability Analysis

Experiments were carried out to measure the repeatability and trajectory following accuracy for various payloads. The repeatability in achieving a position along X, Y and Z axis is measured individually using a high precision millitron gauge arrangement. The manipulator is fed with an input along each axis to achieve a pre-defined position several times. The variation of the readings is recorded by using millitron gauge arrangement. Figure 4.8 shows a distribution graph for the number of tests of the prototype manipulator. The experiments illustrate high precision. Most of the test results demonstrate repeatability better than 10 µm.

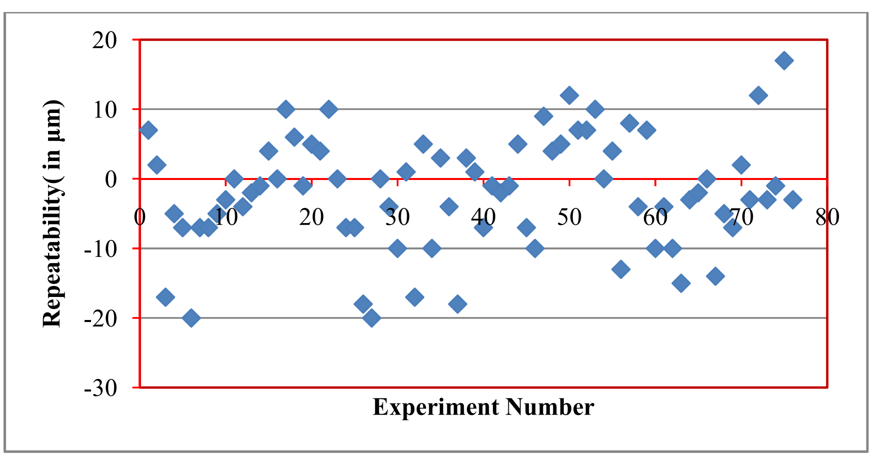

Figure 4.8: Precision test of the 3D-SPKM

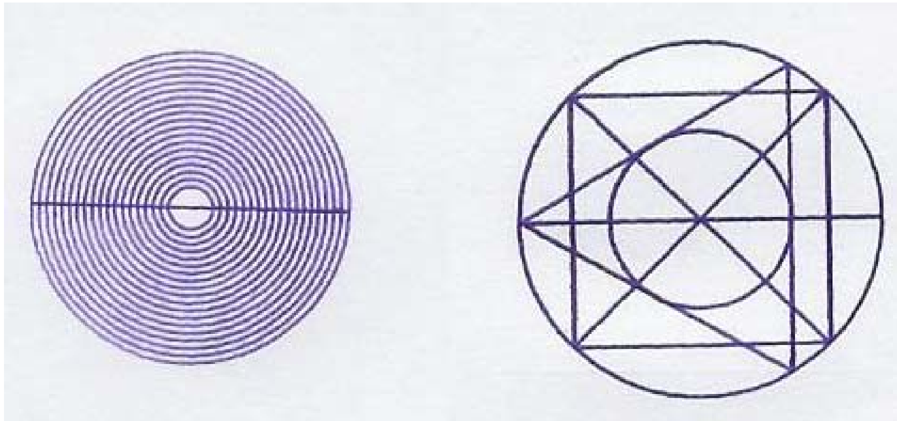

Figure 4.9: Geometric shapes drawn by 3D-SPKM

The experiments to measure the accuracy of the manipulator are performed by comparing the actual paths recorded on a plain paper. The paths included some standard geometrical shapes like a circle, square, rectangle, triangle and concentric circles, the actual pen trace is shown in figure 4.9. In order to determine the accuracy, the actual shape of the path has been compared with the values of the input path using a profile projector. The comparison of the input and output data shows that the trajectory following accuracy to be within 30 μm.

4.5 Accuracy Demonstration in Performing a High Precision Job

Experiments have been conducted to measure the repeatability, and trajectory following accuracy for various payloads. Figure 4.10 illustrates the prototype of the 3D-SPKM performing a high precision job of inserting a 0.8 mm thick needle in a 1.0 mm hole made in a glass flask. The glass flask is used to simulate the human skull. Figure 4.11 shows the 3D-SPKM inserting the 0.8 mm needle in 1.0 mm hole along the 15 mm diameter in a cylindrical block. These experiments are conducted several times in order to determine the trajectory tracking behavior. Experimental analysis demonstrates the accuracy of the manipulator to be within 30 μm. Figure 4.12 shows the trajectory tracking behavior of the 3D-SPKM during a needle insertion procedure. The experiment demonstrates the high accuracy trajectory following capability of the manipulator.

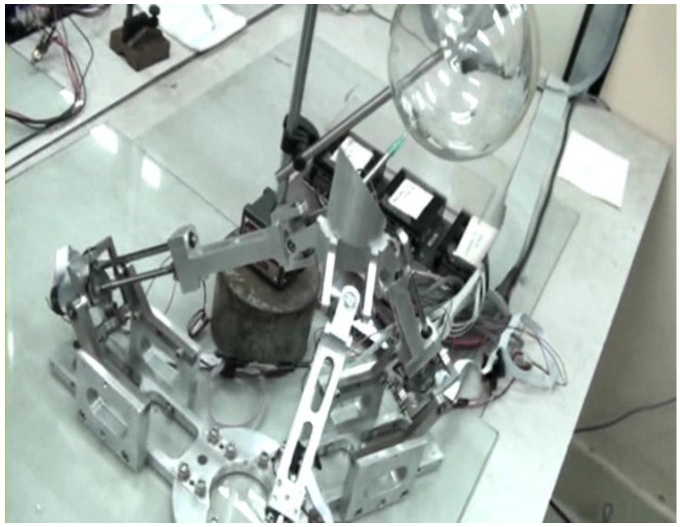

Figure 4.10: 3D-SPKM performing a high precision job of inserting 0.8 mm needle in a glass flask having 1.0 mm hole

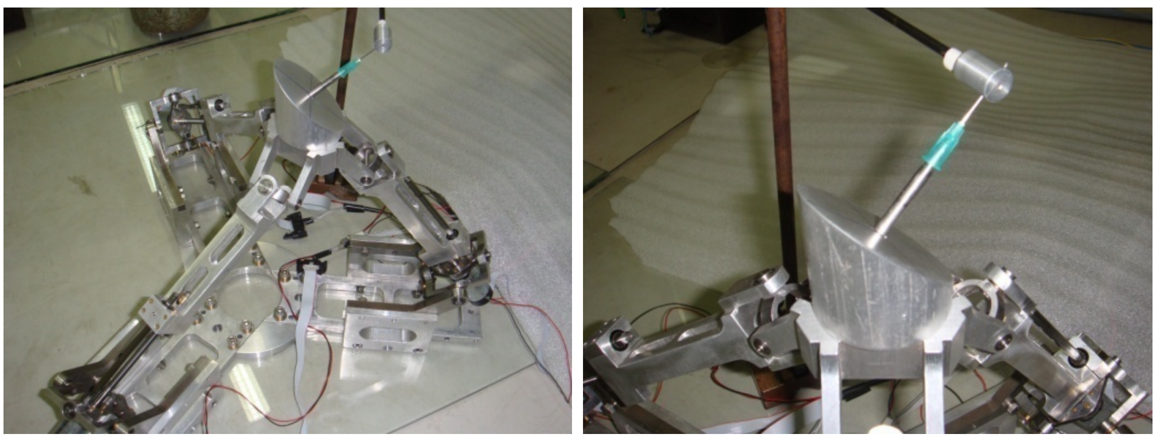

Figure 4.11: 3D-SPKM performing a high precision job of inserting a 0.8 mm needle in a cylindrical block having a 1.0 mm hole

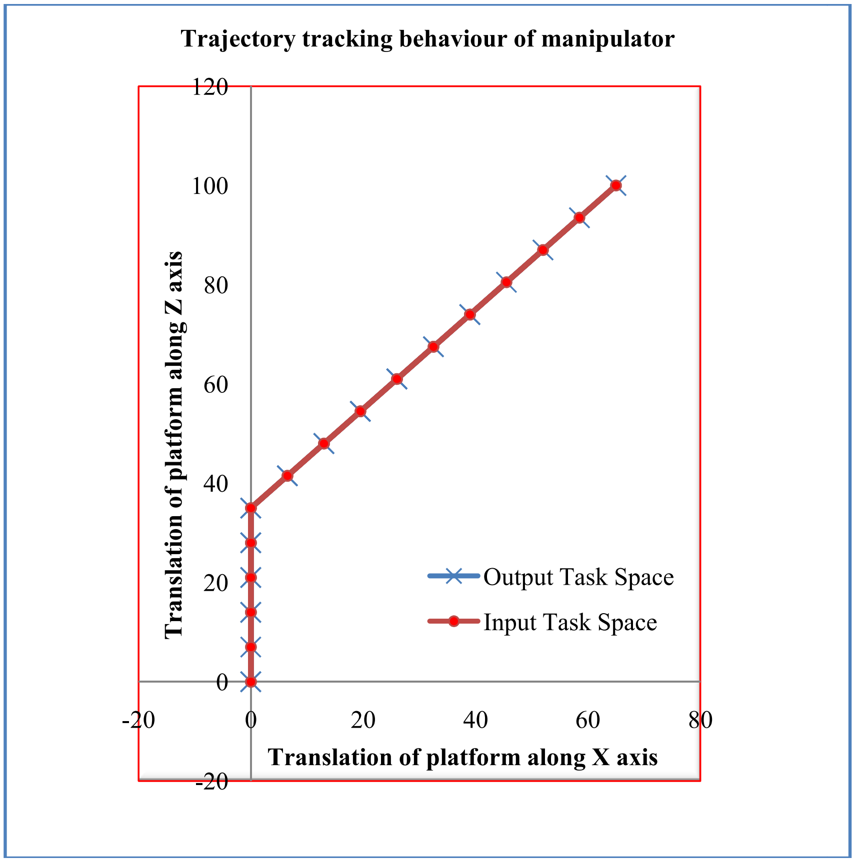

Figure 4.12: Trajectory tracking behavior of 3D-SPKM performing a high precision job

4.6 Repeatability and Trajectory following using Force-Torque Sensor

Several experiments have been conducted to measure the repeatability and trajectory following accuracy for various payloads. A very highly sensitive 6 axis Force-Torque (F-T) sensor has been used to conduct various repeatability tests. The full scale force range of the sensor is ±1.0 N and the force resolution is ± 2.5 mN. Figure 4.13 shows the 3D-SPKM traversing through a trajectory on the platform of the sensor. A test to check the repeatability of the 3D-SPKM has been conducted by repeatedly resting the tip of the end effector on the 6 axis F-T sensor. The 3D-SPKM is given an input to approach perpendicularly on the pre-defined positions of the F-T sensor platform, due to which force (normal to the platform surface) is applied. The deviation of the force experienced by the F-T sensor for repeatable motions of the 3D-SPKM gives a measure of its repeatability. For figure 4.14(a) and 4.14(b), the 3D-SPKM is moved to a point, one at a time at three radially equal distances from the center of the platform. The moment lines in response to the applied force are shown in figure 4.14(a). Even minute difference in positions (error in repeatability) of the resting points will largely shift the direction and the radial distance of the moment lines. This test has been repeated several times to observe the position and directional repeatability. It is evident from figure 4.14(b) that all the moment lines show an excellent directional accuracy and repeatability.

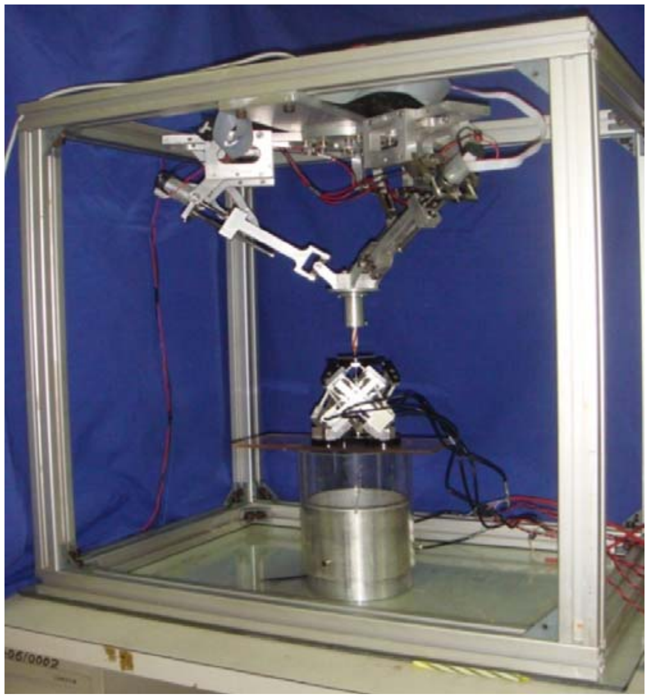

Figure 4.13: A prototype of the 3D-SPKM along with 6 axis Force-Torque sensor unit.

Further figures 4.14(c) and 4.14(d) show the force trace and repeatability, when the tip of the end effector is traversing in a radial trajectory to the six points on the platform of the sensor. Similarly, figures 4.14(e) and 4.14(f) represent force diagrams when a circular trajectory trace is conducted. The force diagram also records changes in the manipulator inertial force during the course of a change in direction (more evident in figure 4.14(e) and 4.14(f) which represents the course change from one concentric circle to the adjacent one). The sensitivity of the sensor is 5 mN/μm and the deviation of the force experienced by the sensor moving throughout the given trajectory is 0.1 N. Hence, the maximum variation of the trajectory from the mean trajectory is estimated to be in the order of 20 μm. The force-graph is drawn using only applied wrench data. It reflects the very high trajectory following performance of the manipulator.

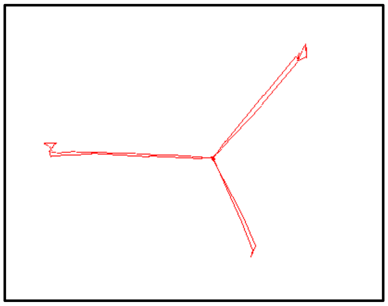

(a) Point forces at equal radial distances, separated by 120^0

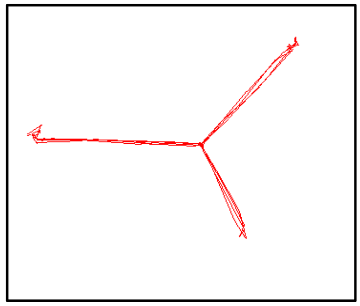

(b) Repeat of (a) to test the repeatability

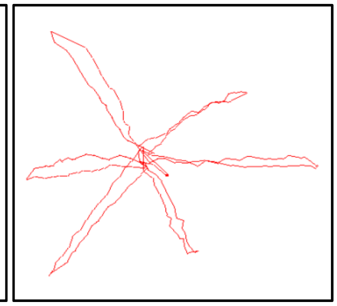

(c) Force trajectory to equal radial distances

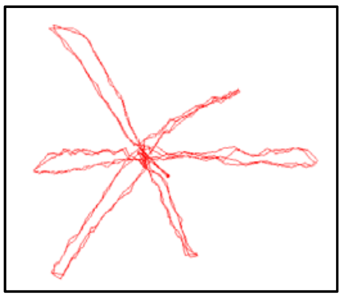

(d) Repeat of (c) to test the repeatability

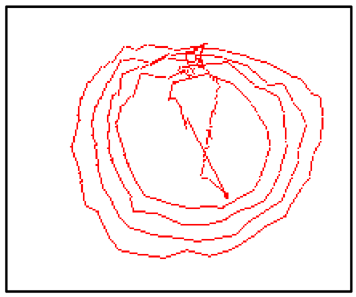

(e) Concentric circular force trajectory

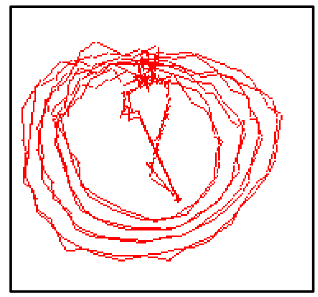

(f) Repeat of (d) to test the repeatability

Figure 4.14: Tests to check directional accuracy and repeatability of moments about orthogonal axes lying in the platform plane

4.7 Experiments of 3D-SPKM in a Master Slave Interface

These experiments were carried out to simulate the robot based frameless stereotactic neurosurgery procedures. In this application, a computer is taken as a master and the 3D-SPKM is used as a slave to generate a precise trajectory while the end effector is in contact with the environment. Figure 4.15 shows the snap shot of the master screen containing the computer commanded trajectory in window $\mathbf{W_m}$ and the feedback of the path followed by the 3D-SPKM in window $\mathbf{W_s}$. The commanded trajectory and the path following feedback were updated in real time, both in $\mathbf{W_m}$ and $\mathbf{W_s}$. A radial distance of 1 mm separates the concentric circles in figure 4.15.

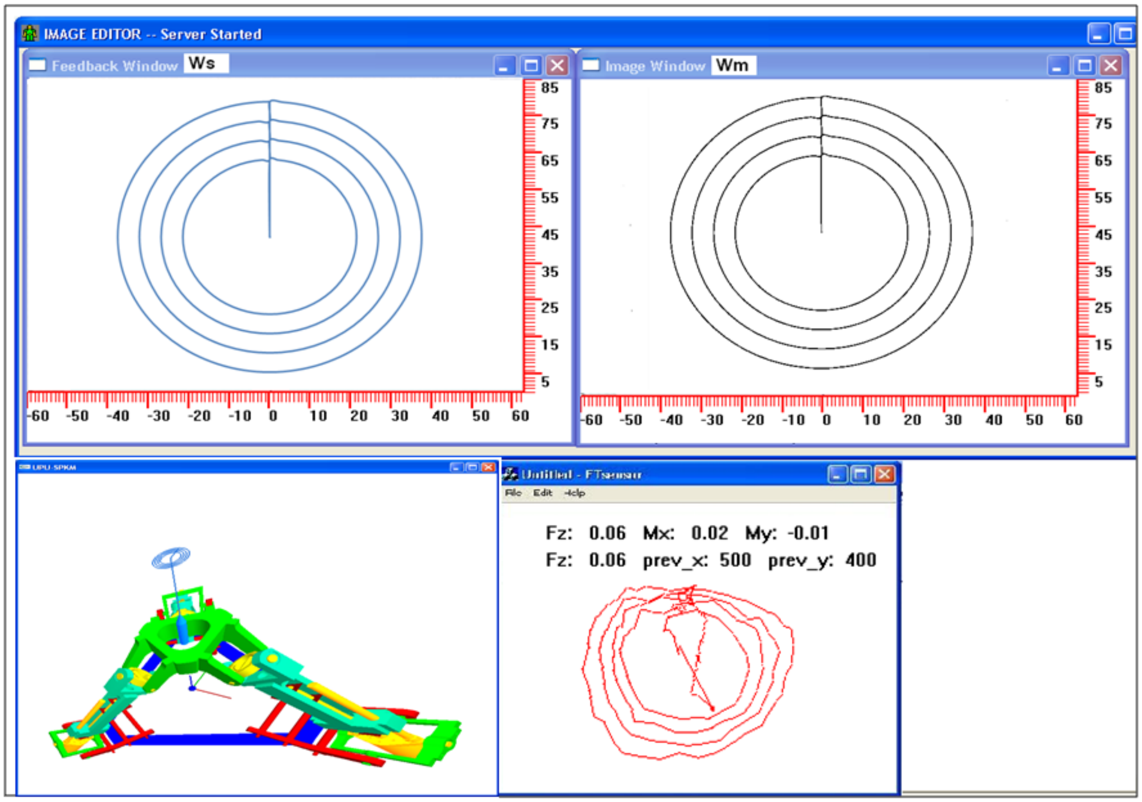

Figure 4.15: Master screen depicting the trajectory commanded at the master site and the path followed by the 3D-SPKM slave along with 3D visualization of the slave and force diagram in force feedback window

The precision in the trajectory following capability of the 3D-SPKM is reflected in two windows of the master screen. In addition to the task space trajectory, the graphic simulator duplicates the motion of the 3D-SPKM in real time. The operator at the master site can visualize the slave manipulator linkage motions through a real time graphic simulator visual display. In all the trajectory motions, no difference is visually noticed between the 3D-SPKM prototype and the graphic display, suggesting that the DOFs and constraints of the actual mechanism are well accounted in a theoretical model. Force feedback is important for contact motion assessment. The real time force field feedback at the bottom right is displayed on the master screen (refer figure 4.15). This enables the operator to monitor the force interaction between the tool tip and the environment. Any manipulator vibration or unexpected force disturbance on the job table at the slave site may go unnoticed in the trajectory feed back window, $\mathbf{W}_s$ and in the graphic simulator display but it would show a noticeable change in the force diagram drawn in the force feedback window. Any distortion in the force diagram can be considered as an indication of an unexpected force interaction. The undulations in the force diagram in figure 4.15 represent very small moment variations, the amplitude from the mean represents 0.1 N force or in length dimensions it is estimated to be less than +/- 20 μm. These experiments are carried out as a prerequisite to robot based frameless stereotactic neurosurgery procedures. In the neurosurgical procedures, the neurosurgeon would be able to determine the position and orientation of the robot with respect to the patient. The master screen similar to figure 4.15 would be available for the neurosurgeon. The details have been covered in the subsequent chapters.

4.8 Coordinate Measuring and Manipulation using 3D-SPKM

Coordinate registration and navigation is an application illustrated in the figure 4.16. Typically, in some neurosurgical procedures, certain spatial external points on the surface have a definite relationship with the inaccessible problem points. This forms the basis of frameless stereotactic neurosurgery procedures. The geometric relationship between accessible surface points and the inaccessible problem points is built using scanned images (MRI scan). The coordinates of the accessible external spatial points are to be registered accurately to create a local reference frame. The accuracy with which coordinates of the external points are measured largely determines the accuracy of the reference. In this application, the accurate measurement and navigation employing the 3D-SPKM has been demonstrated.

The skull is placed on the platform of the F-T sensor. The measuring probe (attached to the 3D-SPKM) is made to move till the threshold of the force magnitude experienced by the F-T sensor is less than 0.2 N. The stop command is triggered when the threshold is crossed. The manipulator stops effectively within a very small distance exhibiting fine motion control. The compliance corresponding to 0.2 N is estimated to be 40 μm. The encoder positions of the 3D-SPKM are recorded at the instant of contact. The Cartesian coordinates can be determined by solving direct kinematics at the rested point. The distance between the several specific points on the skull is repeatedly measured in order to evaluate the repeatability. It is observed that the repeatability is within 30 μm over a distance of up to 80 mm. The surface generated by the manipulator was found to be in close agreement with the actual surface. Figure 4.17 shows the surface generated by the manipulator based measurement.

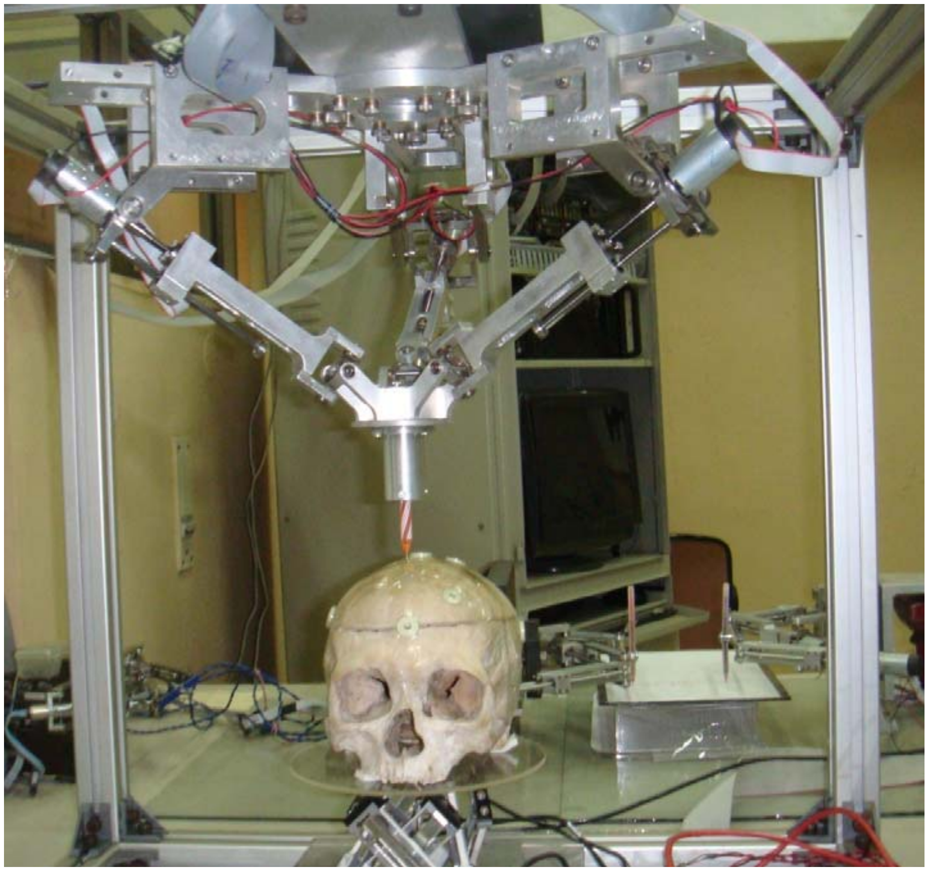

Figure 4.16: 3D-SPKM is being used as a coordinate measuring manipulator and tracing the surface for localization purpose

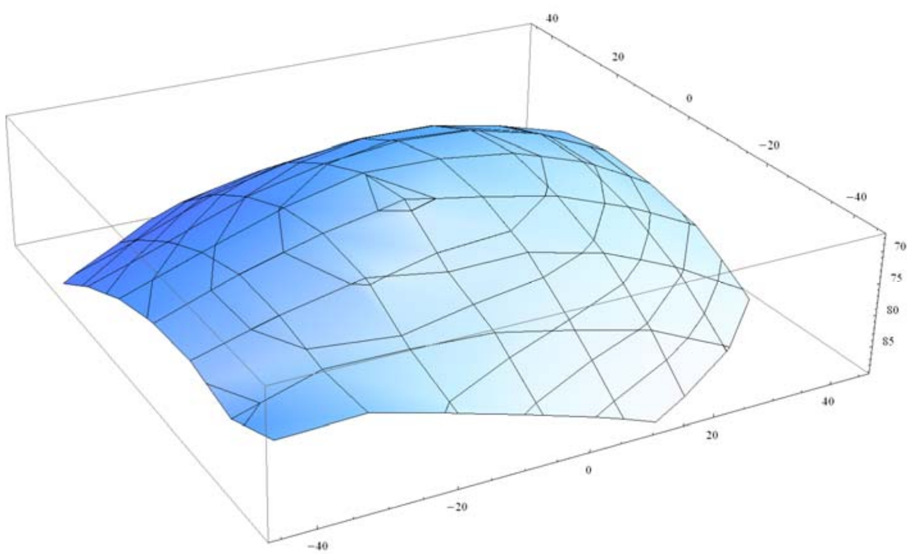

Figure 4.17: The surface generated by the 3D-SPKM

4.9 Summary

In this chapter, the design considerations for the development of a highly accurate 3D-SPKM were described. The design considerations which ensure negligible torsional backlash for the prototype designed have been presented. The design of a two support gimbals joint, which reduces the error in axis definition and improves the torsional rigidity of the leg was presented. The design incorporates two parallel pre-loaded ball splines housed in the reference seat with the ability to increase the torsional rigidity and eliminate angular backlash. These design considerations are essential for the development of a high precision robot required for neurosurgery. The workspace analysis ensures that the manipulability requirements of the surgical tool are fulfilled. The 3D motion simulation was carried out in order to ensure the interference free motion of the mechanism throughout its workspace.

Based on the design solution, a prototype 3D-SPKM has been developed and it was shown that the manipulator exhibits high accuracy and precision. Several experimental results have been presented to determine the repeatability and trajectory following accuracy for various payloads. It is evident from the presented results that the performance of the 3D-SPKM is consistent throughout the workspace. Critical aspects like trajectory following and fine motion control capabilities were observed to be steady in all the experiments. Various experiments have been conducted to show that the 3D-SPKM can be effectively employed in diverse applications. The repeatability achieved and the trajectory following accuracy of the manipulator was within a range of 10 μm and 30 μm respectively. The results were based on the prototype development and are in contrast to the results presented in [119] for a similar 3-UPU mechanism. The accuracy and repeatability measured are in accordance with the preferred accuracy for surgical procedures. The experimental results presented in this chapter validate the 3D-SPKM prototype for conducting frameless stereotactic neurosurgery procedures.

CHAPTER V

Synthesis, Motion Simulation & Prototype Development of 6D-PKM

5.1 Introduction

In the previous chapters, the mobility of passive joints, sensitivity, error and singularity analysis of parallel mechanisms were presented. Based on the analysis and initiation of new design considerations, the development and demonstration of 3D-SPKM prototype has been accomplished. Several experiments were conducted to measure the repeatability and trajectory following accuracy for various payloads for the 3D-SPKM and the results were presented in the previous chapters. The results of the previous chapter demonstrate the choice of parallel kinematic based manipulation for neurosurgical procedures. Almost all surgical trajectories can be conducted using the 3D-SPKM on a standalone basis. To circumvent the custom made patient specific attachments, and to fulfill the additional dexterity to the reachable workspace, a 6 DOF parallel kinematic mechanism to perform stereotactic procedures is analyzed and designed.

This chapter deals with the synthesis, workspace analysis, solid modeling, motion simulation and prototype development of a 6 DOF Parallel Kinematic Mechanism (6D-PKM). The 6D-PKM will be used in the frameless stereotactic neurosurgery for high dexterity. The synthesis of the 6D-PKM is carried out to fulfill the workspace and manipulability requirements. The properties and requirements including engineering design of the robot for frameless stereotactic neurosurgery are presented. The synthesis of the passive composite joints, based on the mobility of the passive joints and error analysis, is presented. This chapter presents the design basis of a 6D-PKM, including workspace requirements; which is established in coordination with neurosurgeons. The workspace analysis ensures that the manipulability requirements of the surgical tool attached to the platform of the 6D-PKM are fulfilled. A 3D motion simulation of the 6D-PKM, which helps to effect corrections for interference free mobility and trajectory planning of the mechanism throughout its workspace, is presented in this chapter.

5.2 Attributes of the Robot for Frameless Stereotactic Neurosurgery

Based on the literature, past surgical experiences and after observing many live neuro-surgeries, the basic attributes of a robot for frameless stereotactic neurosurgery are listed as follows:

1. It should be portable, such that it can be easily mounted near the surgical table, so as to tilt mount in various orientations to serve different various patient postures during the course of the surgery.
2. Higher dexterity is desirable to handle the intricate surgical trajectories. It should have mobility such that it would be able to arbitrarily position and orient the surgical tool in its workspace.
3. It should have good positional accuracy and repeatability throughout its workspace so as to be able to access very small regions (spherical region 1 mm radius)
4. It should have adequate stiffness and load bearing capacity.

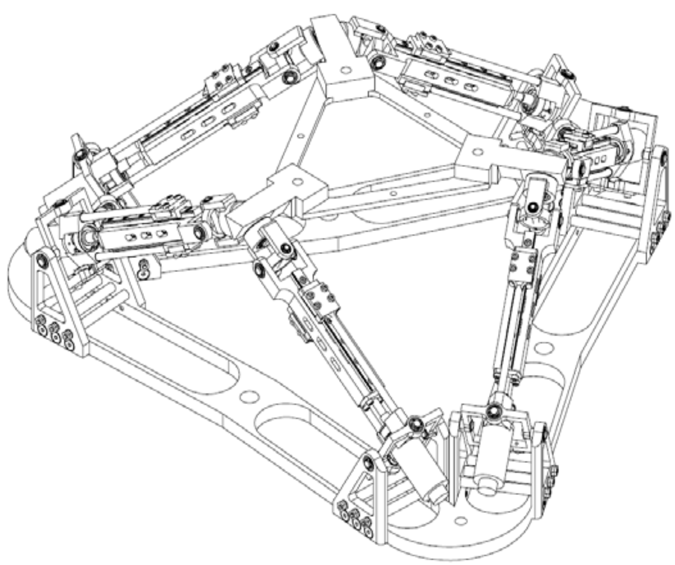

Figure 5.1: Engineering design of the 6D-PKM

The 6D-PKM based architecture has been chosen considering the above mentioned portability, dexterity, precision and rigidity requirements. The kinematic design of the 6D-

PKM has been stated in chapter 3. The engineering design of the 6D-PKM is illustrated in the figure 5.1.

5.3 Synthesis of the 6D-PKM

This section presents the synthesis for the 6D-PKM. The synthesis of the 6D-PKM is carried out to fulfill the workspace and manipulability requirements of neurosurgery. The design is based on the workspace requirements which are set in concurrence with neurosurgeons.

5.3.1 Synthesis of passive composite joints of 6D-PKM

A detailed methodology of the mobility analysis of the passive composite joints for the 6D-PKM has been described in chapter 3. The mobility analysis determines the passive mobility requirement of the universal and spherical joints connected at the base and platform side of the 6D-PKM. The design and the selection of the passive composite joints are carried out based on the passive mobility requirement of the universal and spherical joints. The design considerations, which are presented in section 4.2, are incorporated to design the universal and spherical joints used in 6D-PKM. From the observations made in 3D-SPKM in the previous chapter, it is suggested that two block gimbal joints having distantly separated hinges reduce the error in the axis definition and improve the rigidity of each leg. It also improves the maximum possible mobility of the passive composite joints. Henceforth, the same has been incorporated to develop a high precision 6D-PKM. The mobility analysis of the passive composite joints also indicates that no commercially available universal and spherical joints fulfill the mobility required for the desired motion of the 6D-PKM. Hence the design of novel universal and spherical joints has taken into consideration the mobility required for the passive joints of the mechanism. The kinematics of the universal joint is based on the two orthogonal intersecting axes. Each axis is pre-loaded to arrest the axial clearance and the distant supports to achieve precision in the axis definition. Similarly, the spherical joint is based on the three intersecting axes. The spherical joint designed is a combination of a universal joint and a revolute joint. It aids in reducing the axial clearance and enhances the passive mobility of the spherical joint. The commercially available spherical joints lack in both of the above requirements. Figures 5.2 & 5.3 illustrate the novel design solution for the universal joint connected at the base side and the spherical joint connected at the platform side of each leg of the 6D-PKM.

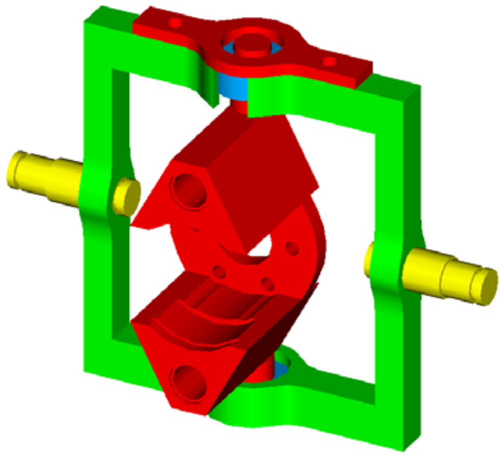

Figure 5.2: 6D-PKM universal joint

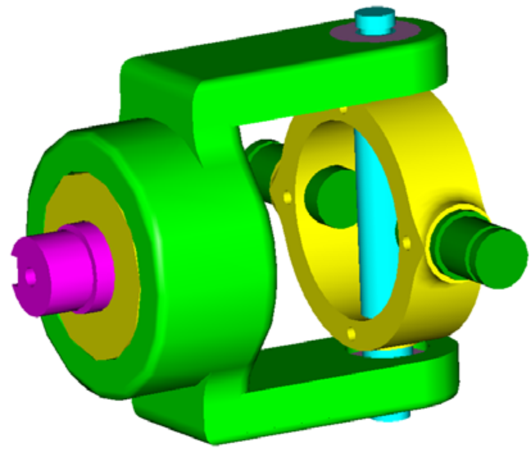

Figure 5.3: 6D-PKM spherical joint

5.3.2 Synthesis for checking the interference between adjacent legs and to determine the optimal offset between them

An important design requirement of the 6D-PKMs is that during the course of any motion of platform, the legs of the mechanism should not interfere with each other. The same can be accomplished by properly choosing the offset distances of the legs from each other. The offset distance and the probability of interference between the legs have an inverse relationship. According to the literature survey (as stated in Chapter 2), the 3-3 architecture based 6 DOF parallel mechanisms, where the offset between the legs is zero, would have the best performance. But the 3-3 architecture based parallel mechanisms are not feasible as the coalescence of the spherical and the universal passive joints severely restricts the mobility of the mechanism. The second best arrangement of the semi-regular hexagonal arrangement of the connection points at both the base and the platform is preferred. The design is preferred from the viewpoint that it is a small deviation from the ideal 3-3 architecture and also it conserves higher symmetry. However, the most symmetrical structure, i.e., the one having both the base and the platform as regular hexagons, would be uncontrollable. Hence, for a good performance, the offset distance between the legs at the base and at the platform should be as small as possible [103]. A finite offset value is a shift from the ideal construction, and the higher offset distance leads closer to singularities of the mechanism. So, the optimal offset distance needs to be determined, keeping the conflicting factors in consideration. The minimum and optimal offset between the legs is determined such that the adjacent legs do not interfere with each other for any of the platform posture in the workspace. The interference between the two adjacent legs of the mechanism depends on the physical dimensions of the associated components of each leg. So the methodology to determine the offset distance should be based on the solid geometry of the legs. Two methodologies have been incorporated to determine the offset distances. The first methodology is using a proximity query package. The second methodology is through motion simulation of the mechanism. The first and second methodology is described in this and the subsequent sections respectively.

Proximity Query Package (PQP): It uses an algorithm presented by Gottschalk et. al. [129] for the efficient and exact detection amongst complex models undergoing rigid motion. The algorithm developed uses a Proximity Query Package (PQP) [130], a library which uses bounding volumes for distance and tolerance queries. The algorithms compute a hierarchical representation using oriented bounding boxes (OBBs). An OBB is a rectangular bounding box at an arbitrary orientation in a 3 DOF space. The resulting hierarchical structure is referred to as an OBB Tree. The PQP is incorporated in the software program to determine the optimal offset distance between the legs.

The various components of the 6D-PKM are modeled in a CAD software package. The models are exported in STL (Stereo Lithography) format. An STL file describes a raw unstructured triangulated surface by the unit normal and vertices (ordered by the right-hand rule) of the triangles using a three-dimensional Cartesian coordinate system. A set of offset distances between the legs is increased from zero to reach the optimal finite value. For a particular workspace position and orientation, the triangulated model of the different legs can be generated. Then the PQP proximity package is used to check for the interference between the two legs. The optimal offset distance between the legs is achieved by an iterative procedure of increasing the offset distance and at each stage checking for interference between the legs.

5.4 Solid Modeling and Motion Simulation of the 6D-PKM

The objective of the motion simulation is to demonstrate the 6D-PKMs interference free mobility and trajectory planning throughout its motion. The run time motion simulation aids the neurosurgeons to visualize the motion of the 6D-PKM robot with respect to the pre-operative imaging data on the computer screen while robotic neurosurgery is being performed. The simulation would aid to visualize the link interference free motion, feasibility of joint limits and verification of inverse kinematic solution in following the given spatial trajectory. If a desired trajectory is specified for the mechanism, the software simulation indicates how the actual mechanism would traverse the trajectory. The optimal offset between the legs for interference free motion is determined by changing the offset distance between the legs in the model. The motion simulation of the spatial parallel mechanism following an intricate trajectory has been implemented. The modeling and simulation serves four important purposes (1) Drawing a feasible assembly sequence to assemble the mechanism from the individual components of the mechanism, (2) Detect the presence of interference, if any, among the members of the mechanism, extent of proximity among members and interference free motion among members during the course of following a trajectory, (3) Visualize the run time simulated motion of the 6D-PKM robot with respect to pre-operative imaging data on the computer screen while performing a neurosurgery, (4) Validation of passive joints mobility requirement for all passive joints for a given trajectory and checking its concurrence with the passive mobility requirement as mentioned in Chapter 3.

The various components of the 6D-PKM are modeled in a CAD software package. Figure 5.4 & 5.5 show the various components of the solid model of the 6D-PKM in an assembly. Subsequently, each component is exported to a software package developed for the simulation. A C++ based software package, using OpenGL library for graphics is used to develop the motion simulation. OpenGL (Open Graphics Library) is a standard specification defining a cross-platform API for writing applications that produce 2D and 3D computer graphics. The interface consists of different function calls which can be used to draw complex three-dimensional scenes from simple primitives. The models were exported from the CAD package in a STL file format. The STL files are given as an input to the graphic simulation. The software simulation package takes the desired translations and rotations as an input and displays the 3D OpenGL simulation model showing the motion sequence of all the translations and rotations. Models can be redrawn by iteratively changing the offsets at the base and the platform. For the given kinematic design parameters that is the values of the base, the platform side and the height of the manipulator, the optimal offsets at the base and the platform were determined.

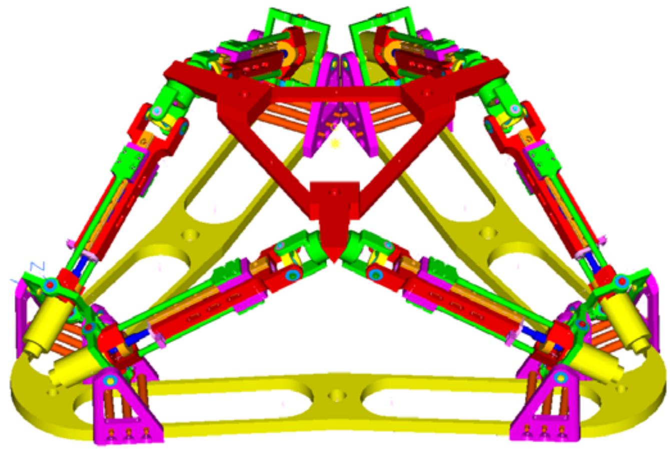

Figure 5.4: A solid model of 6D-PKM used for motion simulation

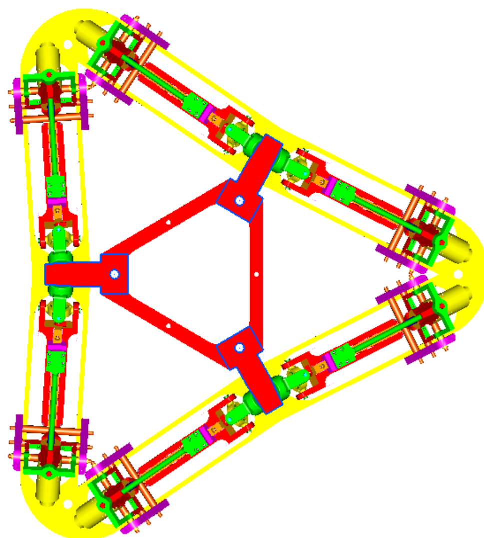

Figure 5.5: A solid model of 6D-PKM showing its top view

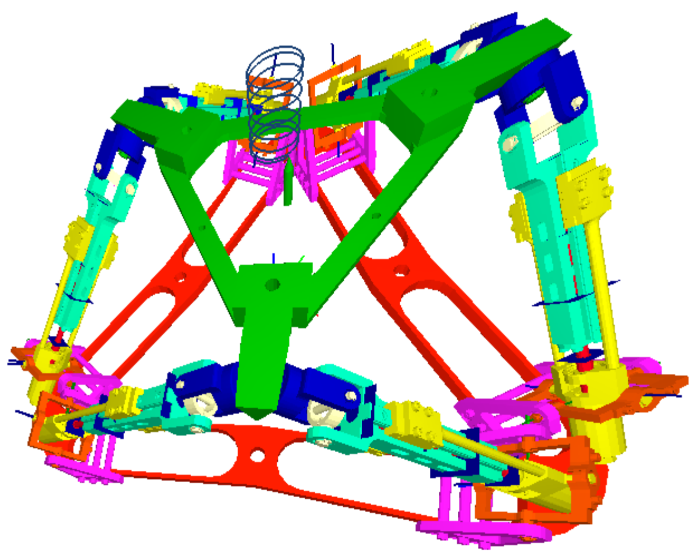

Figure 5.6: 3D motion simulation of 6D-PKM showing helical trajectory

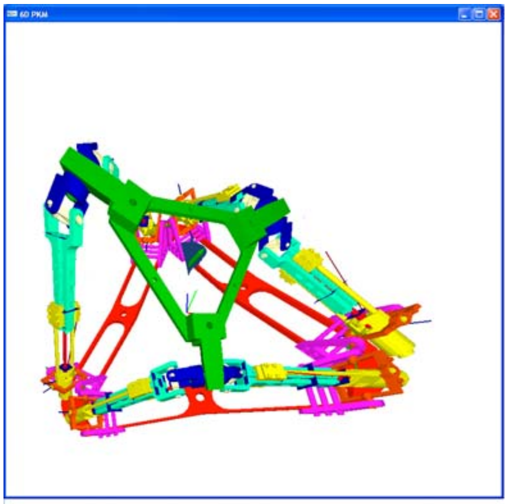

Figure 5.7 (a)

Figure 5.7 (b)

Figure 5.7: 3D motion simulation of 6D-PKM showing rotational motion of platform

The graphics window of the software module shows the 6D-PKM. A snapshot of the motion simulation showing a spiral trajectory of the mechanism is shown in the figure 5.6. An instant of the rotational motion of the platform is captured and represented in figure 5.7. The motion simulation module was tested for the different values of the translations and rotations throughout the workspace. Besides the offset distance between the legs, the passive joints mobility requirement has been verified. The passive joints mobility requirement is in concurrence with the previous sections. The motion simulation illustrated in figures 5.6 and 5.7 shows the interference free motion of the 6D-PKM throughout its workspace.

5.5 Workspace Analysis of 6D-PKM

5.5.1 Translation and rotation workspace of 6D-PKM

The workspace for the neurosurgical requirements is determined. The 6D-PKM design parameters are established based on the desired workspace. The achievable workspace is determined from the constraint of leg ranges, l_{min} and l_{max} (minimum and maximum leg lengths of 6D-PKM). The workspace points have to satisfy the constraints given by the equation.

$$l_{min} \leq \left\|\vec{l_i}\right\| \leq l_{max} \; where \left\|\vec{l_i}\right\| = \left\|\vec{A_i} - \vec{B_i}\right\|, \qquad i = 1, \dots 5,6 \tag{5.1}$$

l_i are the leg lengths connecting the base connection point B_i to the corresponding platform connection point A_i, (i=1,…6) of 6D-PKM (refer section 3.2). For a given rotation of the platform, the inequality equation (5.1) is solved to obtain the equations of 12 spheres, six with minimum leg lengths and six with maximum leg lengths. The workspace is given by the intersection subset of all the 12 spheres. At the minimum height of the mechanism 'h', the coordinates of the geometrical center of the platform with respect to the geometrical center of the base at zero translation is (0, 0, h). The translation of the platform from its minimum height is given by (tx, ty, tz) and henceforth (tx, ty, $tz + h$) are the coordinates of the center of the platform with respect to $\boldsymbol{O}$(XYZ). The rotation of the platform is given by ($rotx, roty, rotz$). The workspace analysis is carried out to determine the maximum possible translation along X and Y at incremental Z coordinates. Similarly, the maximum rotation ranges about X, Y and Z at incremental Z coordinates were found. Figure 5.8 shows the 3D translation workspace of the mechanism. Figure 5.9 & 5.10 illustrates the translational and rotational workspace of the 6D-PKM on different planes. The dimensional values of design parameters (refer section 3.2) and the workspace ranges are shown in table 5.1.

Table 5.1: 6D-PKM dimensions and workspace ranges

Base side (b)	553.9	Length of a side of a base equilateral triangle
Platform side (a)	370	Length of a side of a platform equilateral triangle
Base offset (b_1)	81.3	Offset of base connection point from the nearest vertex.
Platform offset(a_1)	73.9	Offset of platform connection point from the nearest vertex
l_{min}	168	Minimum leg length
l_{max}	253.5	Maximum leg length
Min. height. of platform (h)	55	Distance between geometrical center of base to geometrical center of platform (Refer section 3.2)
Translation (tz_{max})	142	Max. Translation of platform along Z axis (Max. Height – Min. Height)
Translation (tx_{max})	±62	Max. translation of platform along X axes at tz = 77 mm
Translation (ty_{max})	±56	Max. translation of platform along Y axes at tz = 79 mm
Rotation ($rotx_{max}$)	$\pm 27^0$	Max. rotation of platform about X axes at tz = 67 mm
Rotation ($roty_{max}$)	$\pm 29^0$	Max. rotation of platform about Y axes at tz = 67 mm.
Rotation ($rotz_{max}$)	$\pm 22^0$	Max. rotation of platform about Z axes at tz = 72 mm

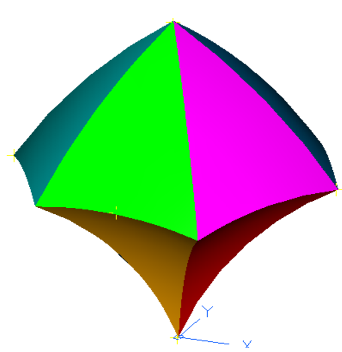

Figure 5.8: 3D translation workspace of 6D-PKM

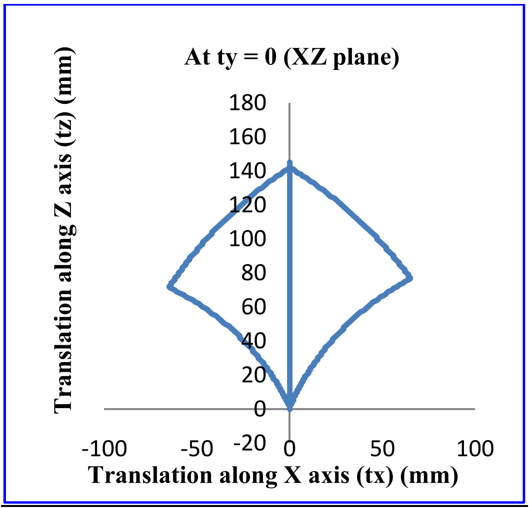

Figure 5.9 (a)

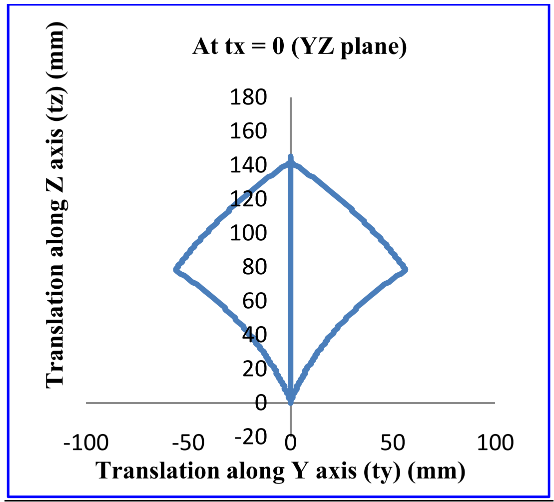

Figure 5.9 (b)

Figure 5.9: Translation workspace of 6D-PKM on a plane

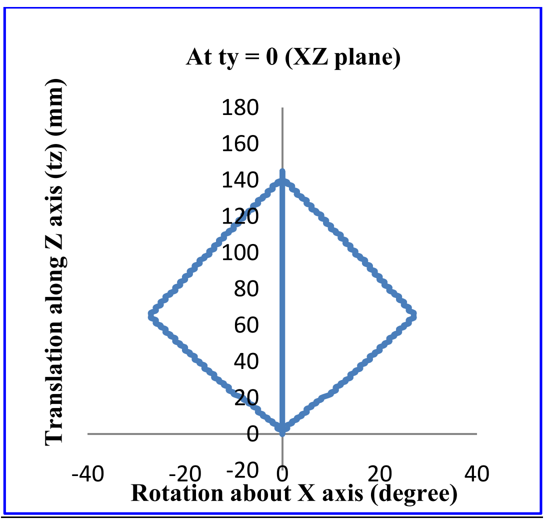

Figure 5.10 (a)

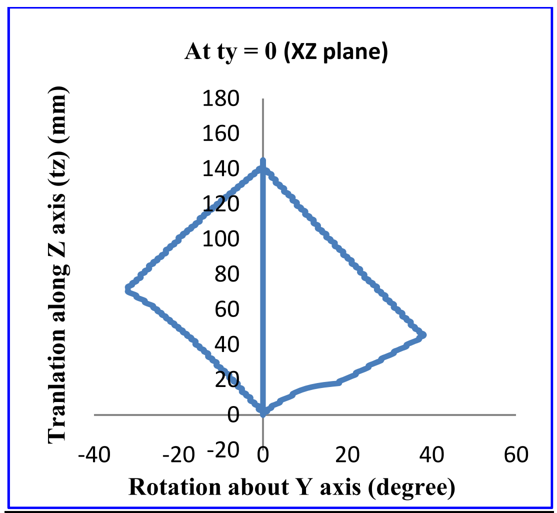

Figure 5.10 (b)

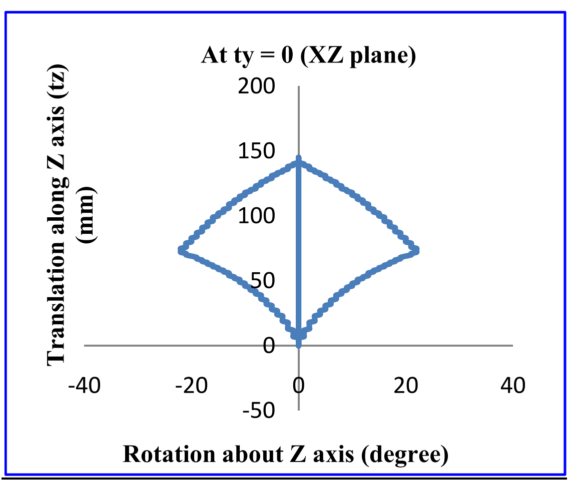

Figure 5.10 (c)

Figure 5.10: Rotational workspace of 6D-PKM on XZ plane (ty = 0)

5.5.2 Combined translation and rotation workspace of platform

The rotation about multiple axes passing through a point or 3D pivoting plays a major role in all kinds of surgeries. A conical sweep about a 3D pivot point is the most common manipulation in minimally invasive surgery. Therefore, understanding the 3D pivot range about a point in the workspace of the 6D-PKM is of utmost importance.

As discussed in the previous subsections, the translation workspace for a given rotation of the 6D-PKM is given by the intersection subset of 12 spheres. To represent the 3D workspace in 2D, slices are cut along the actual workspace with XZ (ty = 0) and YZ (tx = 0) planes. The section of the spheres on the plane would give maximum of 12 circles. The intersection subset of all the circles would give the workspace on the plane. To determine the intersection subset, first, the intersection points of the circles are determined. Then, the intersection points which lie inside or on the maximum radius sphere and on or outside the minimum radius sphere are determined and the rest are eliminated to obtain the workspace boundary points. The reachable workspace consists of the workspace boundary points and the circular arcs connecting them, which lie on any of the 12 circles. A software module is developed which takes the design and motion parameters as input and gives the locus coordinates of the reachable workspace. Figures 5.11, 5.12 & 5.13 illustrates the combined translation and rotation workspace and the maximum pivot region in XZ plane for various rotations of the platform about X, Y, Z axis respectively. Figures 5.14, 5.15 & 5.16 illustrates the combined translation and rotation workspace and the maximum pivot region in YZ plane for various rotations of the platform about X, Y, Z axis respectively. The maximum possible 3D pivot range about a point is obtained by overlapping the translations' workspaces for various orientations. The determined workspace is cross verified by the simulation package described in the previous sections.

A portion of the work in this sub-section was carried out in author's laboratory in coordination with Anubhav Agrawal and Aditya Agrawal, (summer training project students from IIT, Kharagpur, India).

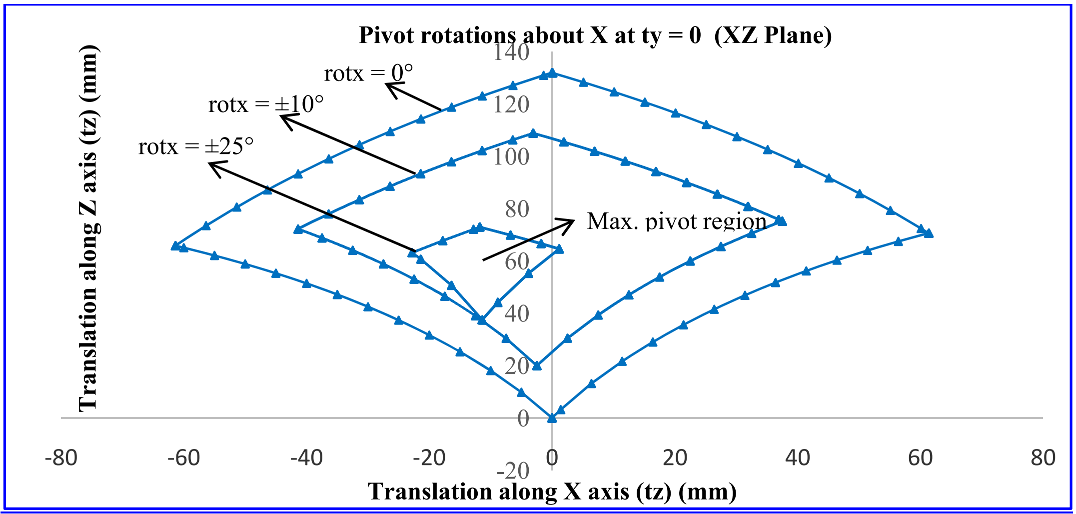

Figure 5.11: XZ translation workspace of 6D-PKM at pivot rotations about X axis

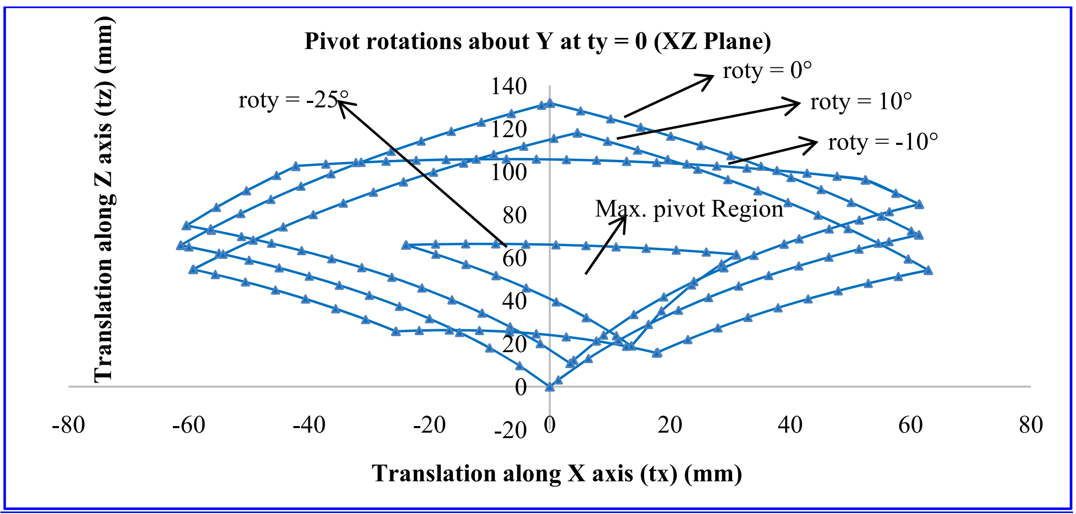

Figure 5.12: XZ translation workspace of 6D-PKM at pivot rotations about Y axis

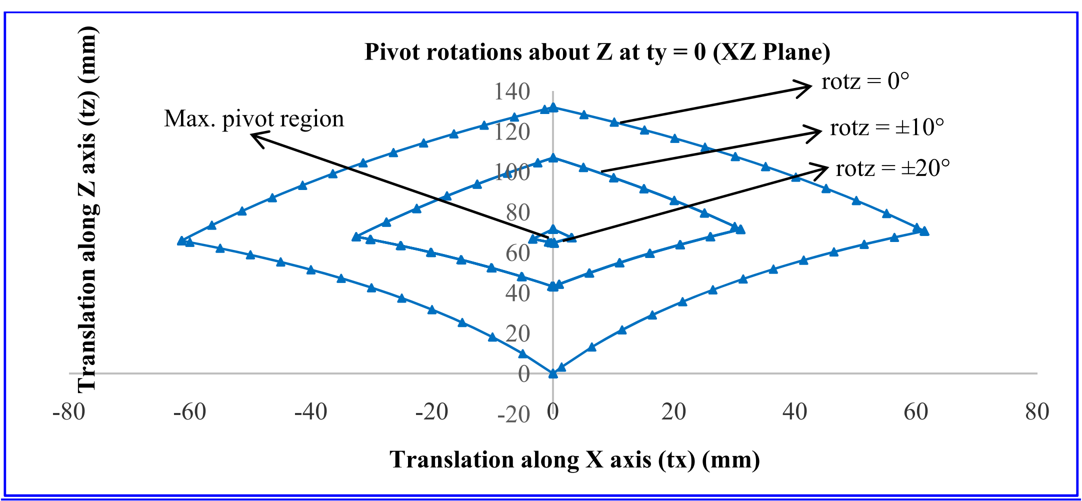

Figure 5.13: XZ translation workspace of 6D-PKM at pivot rotations about Z axis

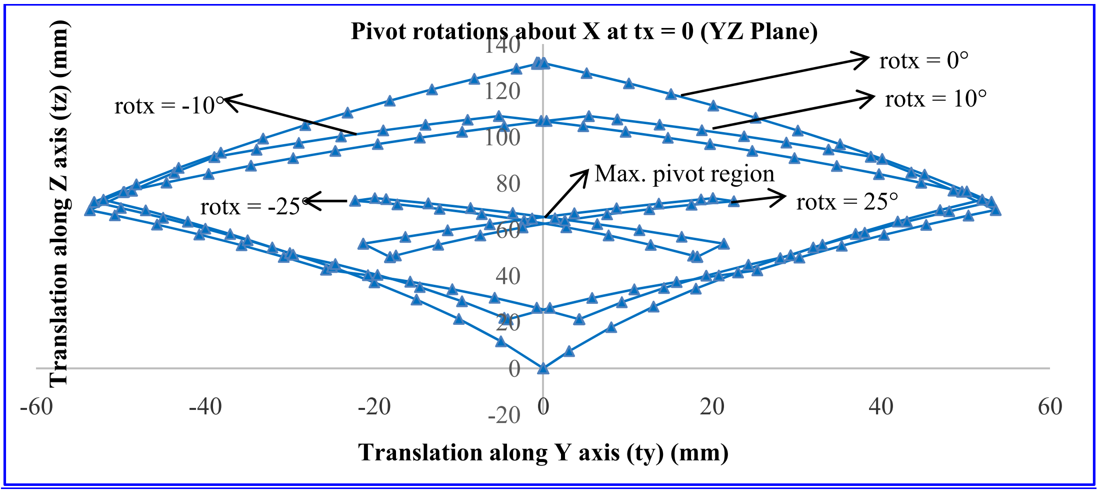

Figure 5.14: YZ translation workspace of 6D-PKM at pivot rotations about X axis

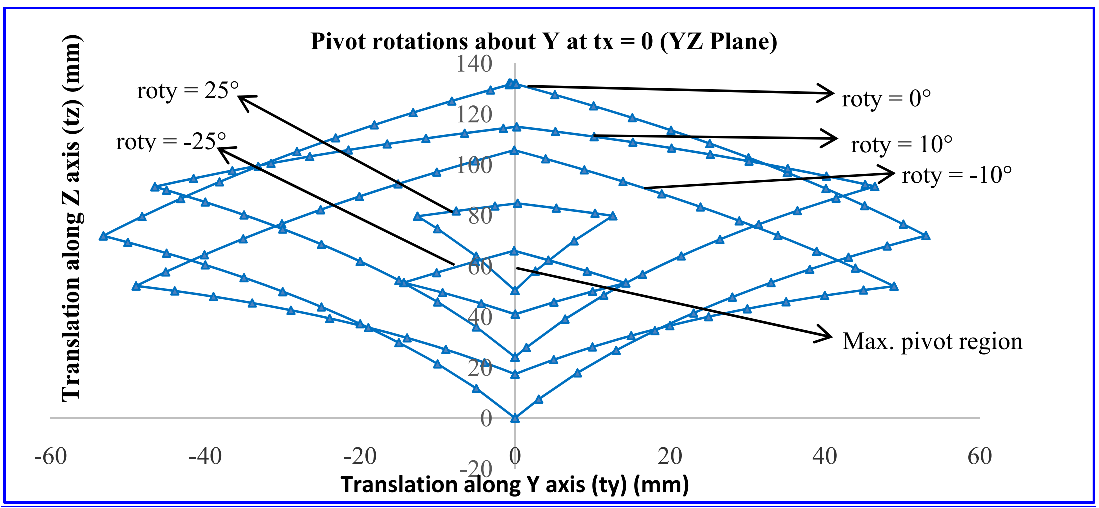

Figure 5.15: YZ translation workspace of 6D-PKM at pivot rotations about Y axis

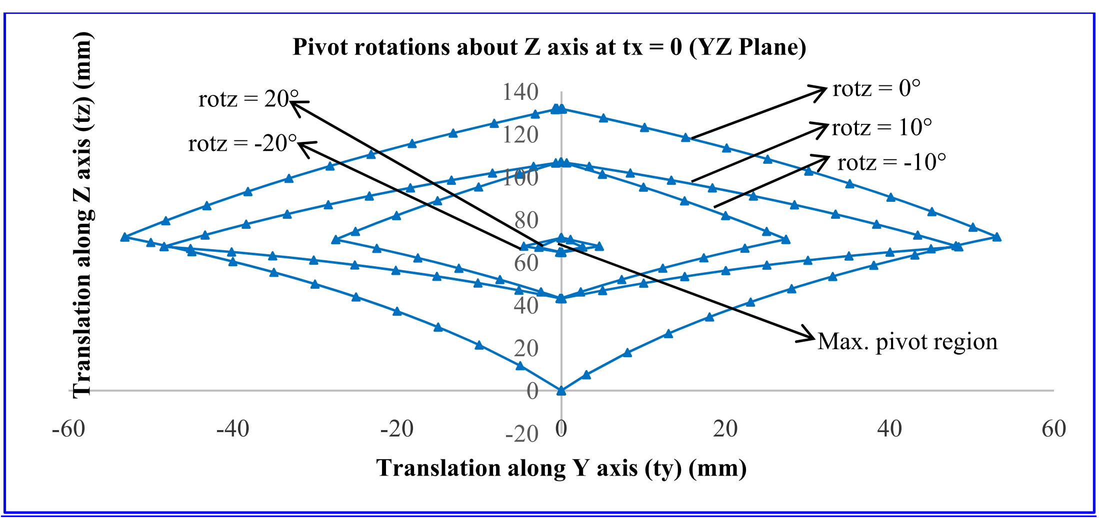

Figure 5.16: YZ translation workspace of 6D-PKM at pivot rotations about Z axis

The figure 5.17 illustrates the 3D translation workspaces for rotations of platform about X axis. The figure 5.17 also shows the maximum pivot region (shown in blue colour) for rotation about X axis. Figures 5.18 & 5.19 illustrate the 3D translation workspace and the maximum pivot region (shown in blue colour) for rotation about Y & Z axes respectively. Figure 5.20 illustrates the maximum pivot regions for rotations about X, Y and Z axis and further their common maximum pivot region (shown in blue color). The platform of the mechanism would have the maximum rotational mobility about any of the axis in the common maximum pivot region. The common maximum pivot region as shown in figure 5.20 is of special interest for neurosurgical manipulation procedures. It helps in understanding the 3D pivot region in the workspace of 6D-PKM. The analysis of the common maximum pivot region gives an insight into the 3D pivot mobility about a point in the workspace of the 6D-PKM. An insight into the 3D pivot mobility at all points in the workspace helps in efficient planning of various neurosurgical procedures. The surgical tool connected to platform can be oriented for maximum orientations in the common maximum pivot region.

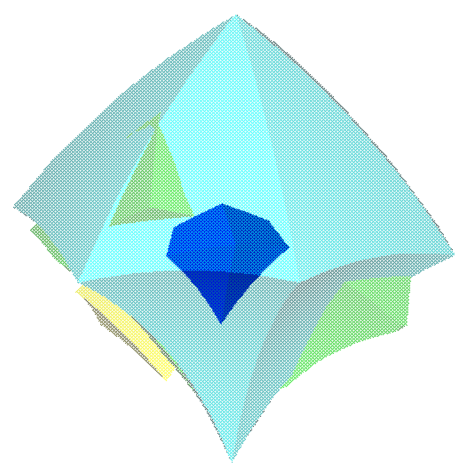

Figure 5.17: 3D model of translation workspace of 6D-PKM at pivot rotations about X axis (blue colour depicts max. pivot region)

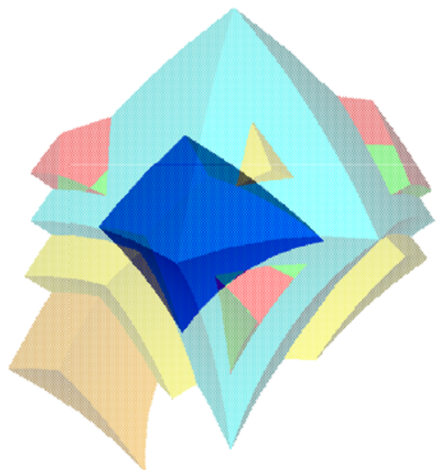

Figure 5.18: 3D model of translation workspace of 6D-PKM at pivot rotations about Y axis (blue colour depicts max. pivot region)

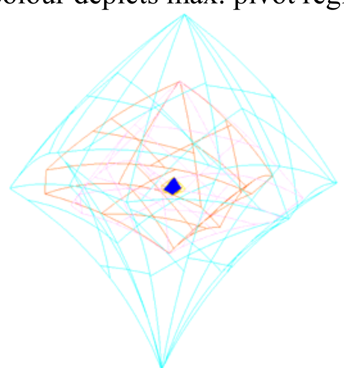

Figure 5.19: 3D model of translation workspace of 6D-PKM at pivot rotations about Z axis (blue colour depicts max. pivot region)

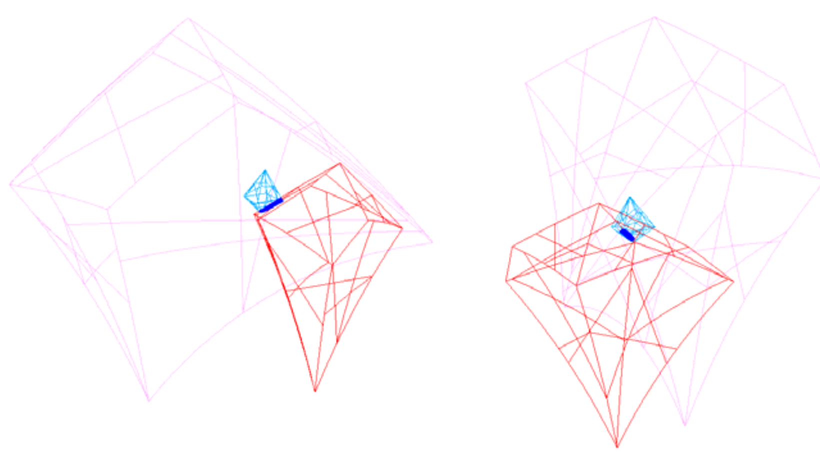

(a) View 1 (b) View 2

Figure 5.20: 3D model of max. pivot region for rotations of 6D-PKM about X, Y and Z axes (blue colour depicts common max. pivot region)

5.6 Prototype Development of 6D-PKM

Figure 5.21: The 6D-PKM prototype developed for performing frameless stereotactic neurosurgery at extended position

After successful testing and demonstration of the prototype of the 3D-SPKM, the scope of the research project is extended and a team is formed to develop the prototype of the 6D-SPKM based on the design given in this chapter. The prototype development of the 6D-PKM is build but its testing is beyond the scope of this thesis. The author is a member of the prototype development team. The prototype of the 6D-PKM is developed based on the kinematic parameters presented in section 5.5. The design considerations mentioned in section 5.3 are incorporated in the prototype. Figure 5.21 illustrates the 6D-PKM in fully extended position. The total height of the mechanism in extended position from the bottom of the base to the top of the platform is 300 mm. Figure 5.22 illustrates the top view of the 6D-PKM. Measurements at the various stages of manufacturing and assembly have been carried out. The exact values of the various kinematic parameters of the 6D-PKM are determined using a high precision Coordinate Measuring Mechanism (CMM) in an accredited metrological laboratory (figure 5.23). The measurement data show that the kinematic design parameters, mobility of all the passive composite joints and the active prismatic range of each of the legs are as prescribed in the design. The testing and demonstration of the 6D-PKM is being carried out. The prototype, as estimated in the analysis section of this chapter is found to satisfy all the motion requirements for the neurosurgical applications with enhanced dexterity.

Figure 5.22: Top view of 6D-PKM prototype developed for performing frameless stereotactic neurosurgery

Figure 5.23 (a)

Figure 5.23 (b)

Figure 5.23: A CMM being used to measure the kinematic parameters of the 6D-PKM

5.7 Summary

The synthesis, solid modeling, and motion simulation of the 6D-PKM has been described in this chapter. The attributes of the robot for the frameless stereotactic neurosurgery are presented. The design and the selection of the passive composite joints, based on the mobility and error analysis were presented. The novel design of the universal and spherical joints has been presented which is based on the mobility requirements of the mechanism. The optimal distance between the leg connection points at the base and the platform of a 6D-PKM is determined to avoid the interference of the legs.

The workspace analysis was presented which determines the translation and rotation ranges of a 6D-PKM. It has been ensured that the translation and rotation ranges are in coordination with the manipulability requirements of the surgical procedures. A new concept of combined translation and rotation workspace of 6D-PKM has been studied and presented. It helps in understanding the 3D pivot region in the workspace of 6D-PKM. The analysis of the common maximum pivot region gives an insight into the 3D pivot mobility about a point in the workspace of the 6D-PKM. An insight into the 3D pivot mobility at all points in the workspace helps in efficient planning of various neurosurgical procedures. The surgical tool connected to platform can be oriented for maximum orientations in the common maximum pivot region. The motion simulation of the 6D-PKM robot was presented to demonstrate its interference free motion throughout the planned trajectory. A software module was presented which takes the specified transformations as input; the OpenGL software model displays the sequence of all the transformations. The software module has been tested for the various trajectories in the workspace. The simulation was carried out which aids to visualize the link interference free motion, feasibility of joint limits and accuracy of the inverse kinematic solution in following the given spatial trajectory. The run time motion simulation would be useful for neurosurgeons to visualize the motion of the robot with respect to the pre-operative imaging data (MRI) on the computer screen while the robot based neurosurgery is being performed. The prototype development of the 6D-PKM has been completed which would be used as a robot for carrying out the frameless stereotactic neurosurgery.

Chapter VI

Neuro-Registration and Neuronavigation Framework for Frameless Stereotaxy

6.1 Introduction

This chapter describes the development of a framework to determine the relationship of the tumor with utmost precision with respect to the robot reference frame. Two relationships are found separately (1) the relationship between the tumor and the patient's body frame of reference (2) the relationship between the patient's body frame of reference and the robot reference frame. The two relationships are used to obtain a direct relationship of the tumor with respect to the robot reference frame. Localizing the tumor with respect to the robot frame of reference is referred to as neuro-registration. The neuro-registration serves as a stage for image guided surgery, which is also termed as neuronavigation. In neuronavigation, the MRI image of the patient along with the real time image of the surgical tool is available on the computer screen to the surgeon. During the surgery, the surgeon can observe in real time the position of the surgical tool along with a MRI image of the patient on the computer workstation. The pre-requisite for neuronavigation is initial registration of the patient with the imaging data. As described in Chapter 2, the optical or camera based tracking techniques are being used in frameless neuronavigation systems. The frame based stereotaxy has much better accuracy in comparison to the camera based frameless stereotaxy procedures. The aim of the research presented in this chapter is to develop a frameless neuronavigation procedure having accuracy comparable to frame based systems. This development combines the ease and comfort of frameless stereotaxy with the accuracy of frame based stereotaxy procedures.

The various standard available digital gauges, which were shortlisted for the precise measurement of the tumor with respect to the body frame of reference, are presented. The experimental setup is prepared to evaluate the performance characteristics of the shortlisted digital gauges. From the results, it is observed and concluded that the standard available digital gauges cannot be used; therefore a customized mechanism is an essential requirement for neuro-registration and neuronavigation.

A portable Surgical Coordinate Measuring Mechanism (SCMM) is designed and developed to measure the coordinates of a point in space. This chapter presents a SCMM; a device which is designed to localize an anatomical reference frame with respect to the robot reference coordinate system. The salient features of the portable SCMM are its compact prototype design and elimination of camera mounts which causes line of sight constraints. The designed SCMM is an articulated serial chain mechanism. Synthesis of the SCMM is carried out in such a manner that it can be fit in the small measurement space and can achieve desired manipulability requirements of the neuro-registration. A solid model and the working model of the SCMM is developed and presented. The control electronics and software for registering the spatial point is implemented. The SCMM would be used to measure the coordinates of the fiducials (radio opaque markers on the skull) with respect to the robot base frame of reference.

Several experiments are performed to evaluate the performance characteristics of the SCMM. A procedure is formulated to determine the relation between the tumor and the body frame of reference using SCMM. The fiducial frame of reference in this chapter is the same as the body frame of reference mentioned in the previous chapters. As the fiducials are affixed on the body, the term 'fiducial frame of reference' is used. Henceforth, the body frame of reference and the fiducial frame of reference are used interchangeably. The chapter presents experimental results of the marker based pair point registration and surface based registration procedures of SCMM. In surface based registration, the accurate measurement employing the SCMM on a human skull phantom has been illustrated. The accuracy of the surface generated by the SCMM is cross verified by comparing it with the surface generated by a high precision 3D-SPKM developed in the laboratory. The demonstration of frameless stereotactic neurosurgery using 3D-SPKM and SCMM is undertaken at author's laboratory.

6.2 Neuro-registration and Neuronavigation Procedure

The main challenge faced by neurosurgeons during surgery is to distinguish between the healthy tissue and the affected tissue. The region of the affected tissue can be spotted and distinguished from the normal tissue in a MRI image only. Hence the surgeons rely on the image to study the location and the extent of the affected region. The tumors which are large in size and near to the surface of the scalp are removed by localizing with respect to the nearby body part and constantly referring to the MRI image. To ensure complete removal of the affected tissue, a negative margin is always kept, thus a layer of healthy tissue along the boundary of the affected region is also removed. However medium, small and deep rooted large tumors cannot be removed by this method. There exists a high risk of losing the reference and thus estimating and localizing the affected region becomes impractical. Surgeons need continuous reference for localizing the surgical tool.

Neuronavigation means to take continuous reference to conduct the neurosurgical procedure. In neuronavigation, the surgeon is in an active feedback loop. While performing the surgery, the neurosurgeon can observe in real time, the current position of the surgical tool and the mechanism carrying the tool, with respect to the patient's MRI image in 3D real time graphics. The surgeon can totally visualize the surgical tool, its movement and location along with the reconstructed graphics model of the MRI image. The surgical tool position can be tracked with respect to the patient throughout the surgery. The surgeon can constantly regulate the tool towards the affected region and can visualize this effect on a monitor of high resolution. The relation between the tumor and the base frame of surgical tool has to be established during the registration procedure before performing neuronavigation. The registration techniques that can be used are either the point to point fiducial based registration or the surface based registration.

Neuro-registration is a process of recording the coordinates of an anatomical point with respect to a surgical/robot frame of reference. Basically, it represents a point in real space that is accessible for measurement. Machine elements have well defined geometrical shapes and references. Geometrical references can be employed or the measuring probe can be guided to access a point uniquely (with very high tolerance). Such referencing or constraints to guide a measuring probe to a specific anatomical point is often unavailable. In order to map the MRI image of the body part with the corresponding anatomical portion of the actual body, specific points on the image are registered with the corresponding real life anatomical points. Highly accurate correspondence cannot be achieved as the point definition is non-existent, and a small regional approximation has to be done. Visual errors in accessing and contacting a point with a probe append to the registration error. These build up errors, increase uncertainty and results in an extended boundary of the surgical portion. In the image guided biopsy for neurosurgery, the registration errors cause the surgical tool reference offset. The translation and orientation shift, offsets the needle from the target, largely, due to the multiplying effect of the traversed length of the needle with the orientation error. A definitive definition for the point has to be obtained in order to minimize the measurement error in registration. Certain simple methods are developed based on the practices in the coordinate measuring methods of the machine elements. A procedure is developed to point to the infinitesimal region repetitively in order to minimize the error in the measurements. Figure 6.1 shows some of the methods to create a nearly exact point definition. The center mark in each figure is constrained and can be identified with a very small deviation (of the order of 15 to 20 μm). The specially designed fiducial to match the measuring probe and the constrained center mark representing a point is illustrated by the magenta colored fixture in figure 6.1.

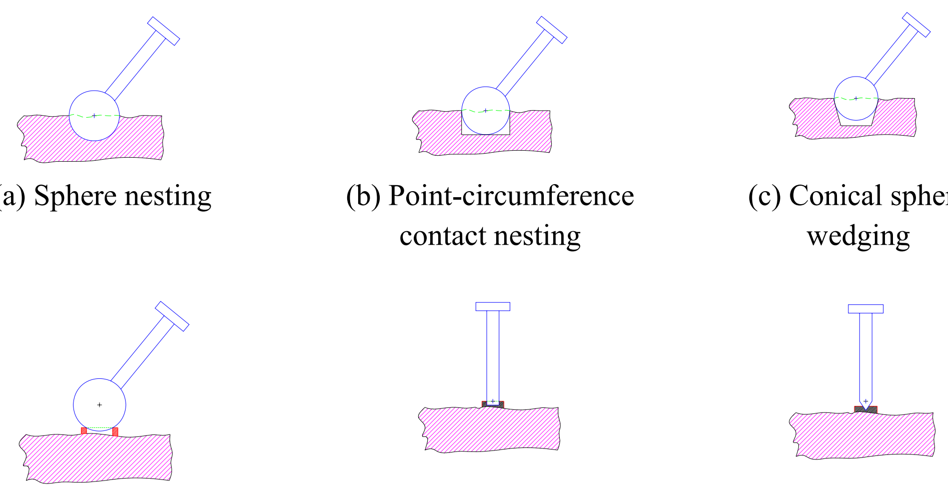

(a) Sphere nesting

(b) Point-circumference contact nesting

(c) Conical sphere wedging

(d) Spherical surface cylinder contact

(e) Cylindrical nesting

(f) Conical nesting

Figure 6.1: Point measuring configuration of the end probe

Three or more fiducials are affixed on the skull prior to the MRI scan in order to aid the coordinate measurement and to establish a high precision reference plane. The fiducial is a radio opaque marker, which resembles a button with a cylindrical hole. The centre of the circle at the top surface of the cylindrical hole is taken as the reference point of the fiducial. The main feature of the radio opaque marker is its visibility in the MRI image. In order to avoid singularity or ill conditioning, it is ensured that no three fiducials should be affixed in a collinear or near collinear manner. In this analysis, four fiducials (points on the skull) are affixed and named as A, B, C and D as represented in the figure 6.2. The MRI is taken along with these fiducials. The MRI scan output is a collection of Digital Imaging and Communications in Medicine (DICOM) images (refer figure 6.3 for illustration) of a section progressing in discrete slices normal to the section. The resolution of the slices depends upon the manufacturer and varies from 0.1 mm to 5 mm.

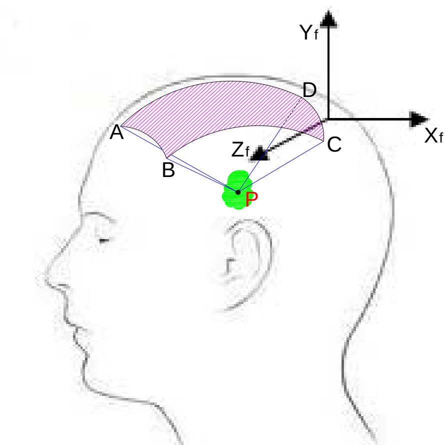

Figure 6.2: Sketch showing fiducial frame, fiducial points A, B, C and D on the scalp and tumor point P

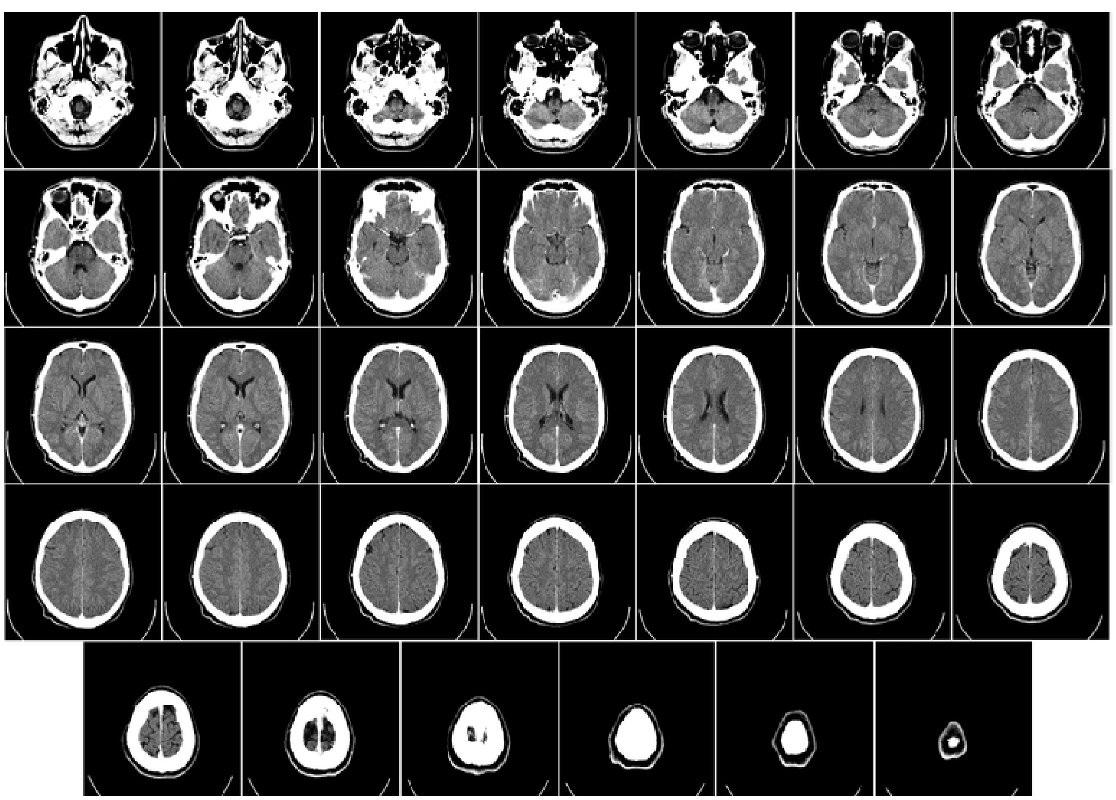

Figure 6.3: CT DICOM images of human brain, from base of the skull to top ([19])

The fiducials and tumor (if present) would appear in the MRI image as a region, with progressively increasing and decreasing contrast depending upon the shape of the tumor. The center point of the tumor is marked in the MRI scan based on the visual estimate of the tumor shape and size. Figure 6.2 illustrates the typical fiducials' point's arrangement, the fiducial frame and a problem point at the estimated centre of the tumor region. A DICOM viewer's software is used to view these MRI images. A common reference frame, termed as a fiducial frame F, is attached in all the images of the section in the viewer software. The viewer software provides a cross-wire cursor with which one can navigate on the image and click at a point of interest to get the coordinates of a point with respect to the fiducial frame F. Fiducial points A, B, C and D are measured with respect to the fiducial frame of reference F.

Fiducial frame to Robot Frame Transformation: From the image, using the DICOM viewer, the coordinates of the fiducial points (in homogeneous coordinates) with respect to the fiducial frame are measured (see figure 6.2).

${}^{f}P_A = \{X_A, Y_A, Z_A, 1\}$, ${}^{f}P_B = \{X_B, Y_B, Z_B, 1\}$, ${}^{f}P_C = \{X_C, Y_C, Z_C, 1\}$ and

${}^{f}P_D = \{X_D, Y_D, Z_D, 1\}$

The coordinates of the fiducial points A, B, C and D with respect to the robot frame of reference are measured using the measuring device.

${}^{R}P_A = \{X_A, Y_A, Z_A, 1\}$, ${}^{R}P_B = \{X_B, Y_B, Z_B, 1\}$, ${}^{R}P_C = \{X_C, Y_C, Z_C, 1\}$ and

${}^{R}P_D = \{X_D, Y_D, Z_D, 1\}$

The transformation matrix, ${}^{R}[T]_f$ which transforms the points that are known in the fiducial frame to the robot frame, is obtained.

$${}^{R}(P_A, P_B, P_C, P_D)_{4\times4} = {}^{R}[T]_{f(4\times4)}\, {}^{f}(P_A, P_B, P_C, P_D)_{4\times4}$$

Writing the above equation in short form, we have

$${}^{R}(P) = {}^{R}[T]_f\, {}^{f}(P) \tag{6.1}$$

The solution of ${}^{R}[T]_f$ for a general case is given as

$${}^{R}[T]_f = {}^{R}(P)\, {}^{f}(P)^T \left[{}^{f}(P)\, {}^{f}(P)^T \right]^{-1} \tag{6.2}$$

The expression ${}^{f}(P)^T \left[{}^{f}(P)\, {}^{f}(P)^T \right]^{-1}$ in equation 6.2 would simplify to $\left[{}^{f}(P) \right]^{-1}$ for the case when fiducial points are four. The equation 6.2 is still valid if the number of fiducial points selected for neuro-registration is more than four. The tumor point is obtained in the robotic frame of reference using the transformation

$$^{R}(P)_{p} = {}^{R}[T]_{f}\, {}^{f}(P)_{P} \tag{6.3}$$

where, ${}^{f}(P)_{P}$ is the position of the tumor point in the fiducial frame of reference. All the fiducial points, tumor point, surgical tool, surgical path of the tool, are determined with respect to the robot frame of reference. The various points are labeled in figure 6.4. The position of the tumor is established with respect to the fiducial frame from the MRI image data and latter transformed to the robot frame of reference. The rigid body motion of a surgical tool is localized with respect to the robot frame.

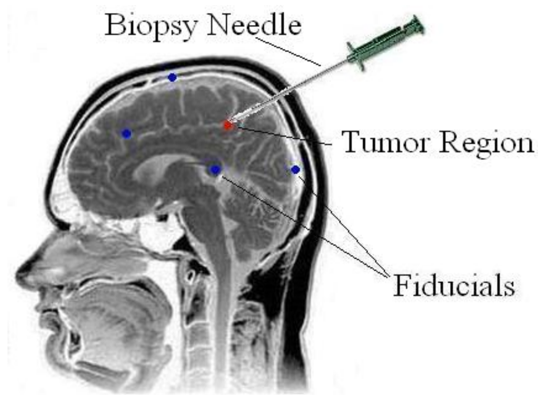

Figure 6.4: Sketch showing the registered fiducial (blue) points, which form a reference frame.

6.3 Standard Available Digital Gauges

This section lists the standard digital gauges for the precise measurement of the fiducial points (fiducial frame of reference) with respect to the robot frame of reference. In order to formulate a relationship of the fiducial frame of reference with respect to the robot frame of reference, various tracking techniques (used to measure linear distances) are studied. The techniques that are studied include mechanical tracking, acoustic tracking, optical tracking and electromagnetic tracking. The basic requirements of the registration system besides the least count in the measurement are that it should be portable, and easy to use. The option of mechanical tracking has been selected for the registration system as per the basic requirements of the registration system. Different digital gauges [131] have been shortlisted and tested and are shown in the figures 6.5 – 6.9.

Figure 6.5: Digital calipers [131]

Figure 6.6: Digital tubular inside micrometers [131]

Figure 6.7: Long stroke linear gage [131]

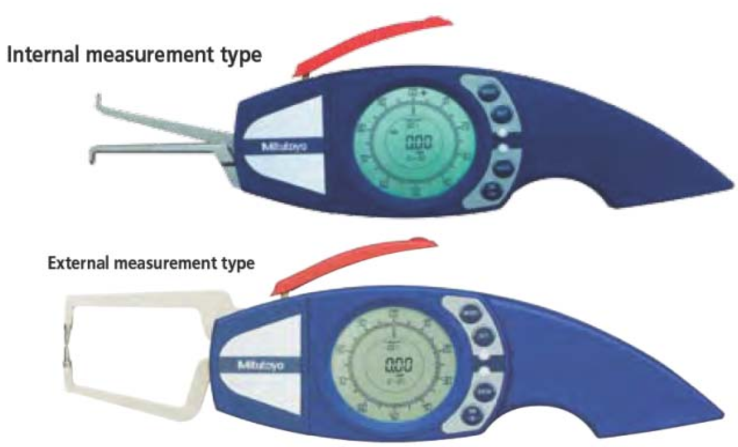

Figure 6.8: Digital caliper gages [131]

Figure 6.9: Digital gage connected to PC data interface device [131]

All the above digital gauges shown in figures 6.5 – 6.8 can be connected to a computer via an interface device (see figure 6.9). The interface device enables transfer of the measured data from a measuring instrument (with the digital output feature) to a computer. The selection is based on the study of various tracking options besides the experience of the actual measuring processes.

An experimental setup was prepared to conduct a trial run to evaluate the standard digital gauges for the purpose of neuro-registration. A hollow spherical glass flask with some fiducial sized markings stuck on the outer side of the glass jar has been taken in order to have similar representation of the skull with the attached fiducials. A set of three mutually perpendicular rods were arranged to represent the X, Y and Z axis of the robot frame of reference. The measurements were carried out separately between the fiducials and the defined robot frame of reference using all the devices shown in figures 6.5 to 6.8. The three linear distances are from the centre point of the fiducial to the pre-determined positions on the robot frame of reference. Further, the resulting distance equations are solved to find the coordinates of the fiducial point. It was observed that taking multiple measurements were very cumbersome and time consuming. Multiple measurements also lead to inaccuracy issues in determining the coordinates of the point. Also, it was observed that there was body interference of the digital gauge with the glass flask during the process of measurement. To take the reading accurately, the measuring tip of the gauge should be normal to the fiducial for accurate measurement. It is not feasible to facilitate such positions and orientation of the fiducials. The process of measurement involved intricate coordinating skills of both the hands, besides maintaining both the hands in a steady posture at the time of measurement. Fulfilling all these requirements is unfeasible for repeated measurement procedures. After this exercise, it was concluded that a simple and one time measuring device, resulting in an accurate coordinates of a point with respect to the reference frame has to be developed. A direct coordinate measurement tool, which would, in a single action give the coordinates of any point with respect to the robot frame of reference, is the essential requirement of the neuro-registration system. On the basis of the above mentioned observations and considerations, a passive serial linkage mechanism has been designed for neuro-registration and neuronavigation purposes.

6.4 Surgical Coordinate Measuring Mechanism (SCMM)

As discussed in the previous section, the standard available digital gauges do not meet the basic requirements of the neuro-registration unit. Synthesis of the Surgical Coordinate Measuring Mechanism (SCMM) has been done such that it can be positioned in the desired measurement space and satisfies the neurosurgical manipulability requirements. The geometry of SCMM workspace resembles a spherical segment with reachable space more than a hemisphere of radius 300 mm. The SCMM satisfies the required accuracy, portability and comfort requirements of the neuro-registration system. The SCMM is made of high strength aluminium alloy to reduce the weight of the mechanism. It is a passive four degree of freedom serial mechanism with encoders mounted at each joint and with a base fixture.

Theoretically, only three DOF device is sufficient to position a point in space. The SCMM has a 4 DOF to give neurosurgeon a flexibility to approach the fiducial points from various directions. Three parallel axes of SCMM are used for much desired redundancy and ease of operation. It is to be noted that SCMM falls under the category of Articulated Arm Coordinate Measuring Mechanism (AACMM). Although AACMM's are commercially available ([132], [133]), none suits the neurosurgical requirements. They are designed to suit the requirements of machine tool measurement. Neurosurgical requirements include the ability of the device to reach the neurosurgical workspace, generation of 3D software model of the measurement device and also the option of interfacing the device with 2D DICOM data of patient along with 3D model of the patient necessary for neuronavigation.

The end link of the SCMM is equipped with an end probe to suit the circumference contact nesting measurements (see figure 6.1(b)). The solid model of the mechanism along with its joint axes orientations is as shown in the figure 6.10. A secure housing design for the end-effector homing reference is shown in figure 6.11. The joint angular displacements sensed at the corresponding rotary joint encoders serve as the input for a Direct Kinematic Problem (DKP). The DKP is solved to compute the coordinates of the reference point on the end-probe with respect to the base frame of the SCMM. The base frame of the SCMM is fixed and is in constant relation with the robot frame.

The measurement can be conducted by resting the end stylus of the probe at the last link on at least three non-collinear fiducial points to establish the relation of the fiducial frame with the robot frame. The last link of the SCMM carries a spring loaded electrode along with the spherical stylus at the end as shown in figure 6.12. The switch of a probe in open condition is shown in figure 6.12(a) and the switch in closed condition is shown in figure 6.12(b). The rigid contact of electrodes ensures exact length of the last link of the SCMM in switch off condition. On contact, it sends a signal to the attached computer to record the encoder readings. The accurate coordinate measurements are obtained on resting a stylus in a nest and with a gentle push to bring the spring loaded electrode in contact with the rigid conducting surface to close the switch.

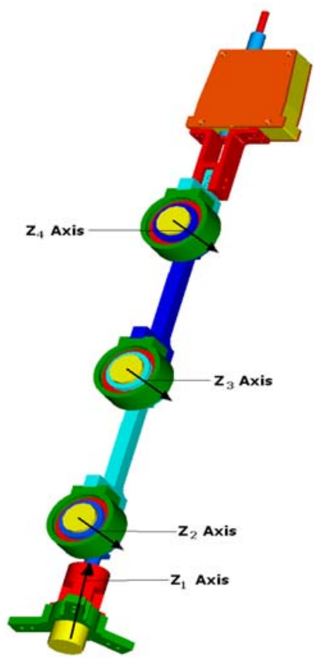

Figure 6.10: Solid model of 4 DOF SCMM

Figure 6.11: SCMM in homing position

Figure 6.12 (a): SCMM end link showing spherical stylus in non-pressed position

Figure 6.12 (b): SCMM end link showing spherical stylus in pressed position and electrodes in activated position

Figure 6.12: SCMM end link showing spring loaded electrodes and spherical stylus

Instant registration of the spatial point in order to avoid uncertainty for a range of points has been considered carefully. The end-probe mechanism and the circuitry are designed in such a manner that the configuration remains same and it results in a single instance of a position. At the instant of closing the switch, the encoder values are recorded and the coordinates of the end reference point are computed. However, on track mode (switch is in closed condition), the encoder values are polled at a high frequency and the coordinates of the end point path are computed continuously in high resolution. Figure 6.11 represents the prototype of the SCMM system with a homing fixture. The SCMM is used to measure the coordinates of the fiducial points with respect to the robot frame of reference. The coordinate measurements are utilized to establish a relation between the fiducial frame and the robot frame.

6.5 Experimental Evaluation of SCMM

Experiments are conducted to evaluate the performance characteristics of the SCMM. The SCMM is evaluated for pair point registration and surface registration techniques. The results are in concurrence with the registration techniques which are currently being used for stereotactic neurosurgery.

6.5.1 Experimentation for pair point registration using SCMM

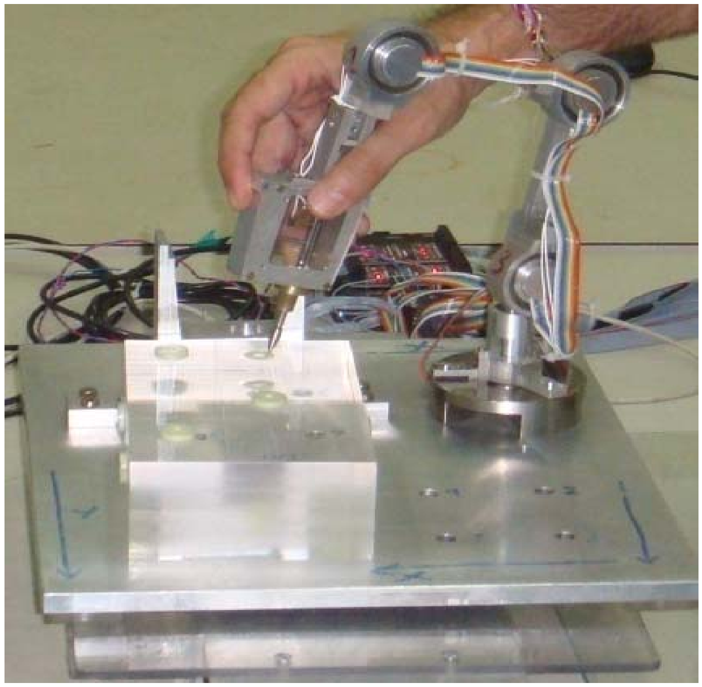

Figure 6.13: SCMM along with a perspex block

A perspex block is chosen as a phantom on which the fiducials are affixed in pre-defined positions. The SCMM along with the perspex block is shown in figure 6.13. The phantom is prepared (with fiducials affixed) and by imaging techniques the relationship of a fixed point on the phantom with respect to the fiducial frame is established. The phantom is subjected to a CT scan; DICOM images are analyzed and from there the coordinates of the fiducials and the fixed point on the phantom with respect to the fiducial frame of reference are determined (as discussed in section 6.2).

Using the same phantom, the accuracy and repeatability analysis of the SCMM is carried out. To check the accuracy of the SCMM, the first set of distances between the fiducials already pasted on the perspex block is measured with it. The same distances are measured separately by using a high precision Coordinate Measuring Machine. The two sets of readings are compared to determine the accuracy of the SCMM. The difference in reading is found to be less than 300 μm. The SCMM is calibrated using a large number of measurements. The measurement repeatability of the SCMM is significantly improved. The maximum precision error, after calibrating the devices is found to be less than 80 μm. The single point articulation test for SCMM is carried out according to ASME Standard B89.4.22 [134] for Articulated Arm Coordinate Measuring Machines (AACMM).

After the calibration of the SCMM using a high precision Coordinate Measuring Machine, the coordinates of the fiducials affixed to the perspex block are determined with respect to the SCMM base frame. Then, using the transformation relationship between the fiducial frame to the robot frame (transformation procedure discussed in section 6.2), the coordinates of the fixed point on the phantom are determined with respect to the SCMM base frame. Thus, the pair point registration procedure using the SCMM is established.

6.5.2 Surface coordinate measurement and registration

In the pair point based registration, there are a relatively small number of point pairs that describe the corresponding locations in the two coordinate frames (robot frame and patient's body frame). In surface registration there are two large sets of points that describe the same surface, but there are no point pairs [21]. The objective of the surface registration is to match the two sets of data for the same surface. Surface coordinate registration of a human skull by SCMM is illustrated in figure 6.14. Typically, in some neurosurgical procedures, certain external anatomical points on the surface have a definite relationship with the inaccessible problem points. Thus mounting the fiducials to create a temporary reference is not required. The geometric relationship between the accessible surface features and the inaccessible problem points is built using the DICOM images of the patient. The coordinates of the accessible external spatial points are to be registered accurately to create a local reference frame. In this application, the accurate measurement and navigation employing the SCMM on a human skull phantom is demonstrated. The surface registration measurement can be achieved by moving the end probe of the last link of the SCMM on the surface of the human skull phantom using a track mode. The angular positions of the encoders are polled at high frequency and the coordinates of the point on the path are computed. Figure 6.15 shows the surface generated by the SCMM.

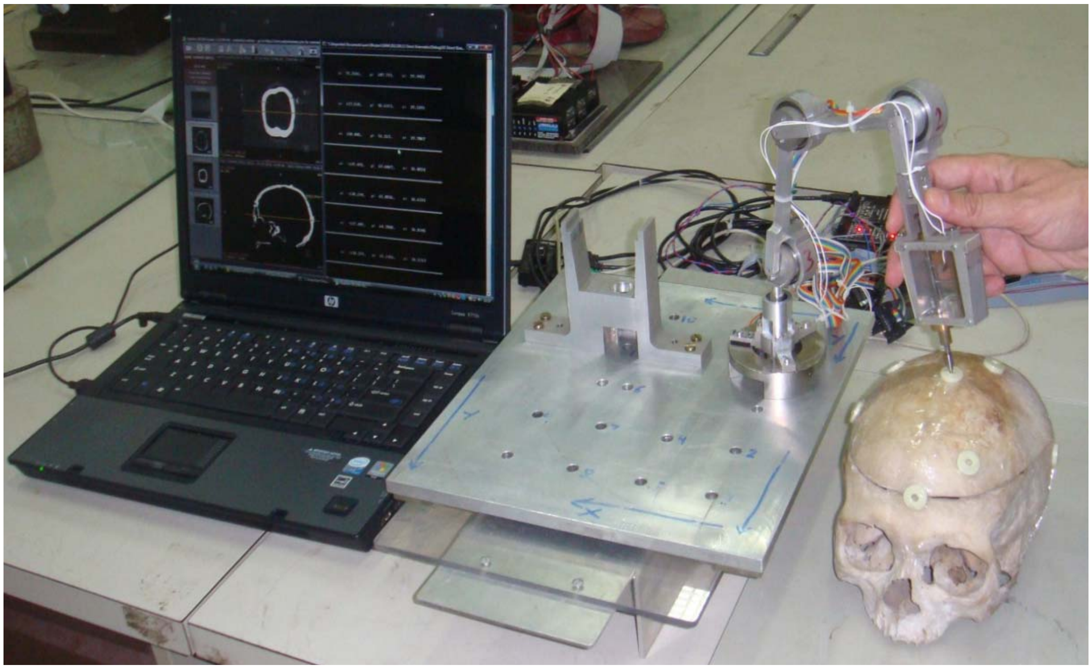

Figure 6.14: Surface coordinate registration of a human skull by SCMM

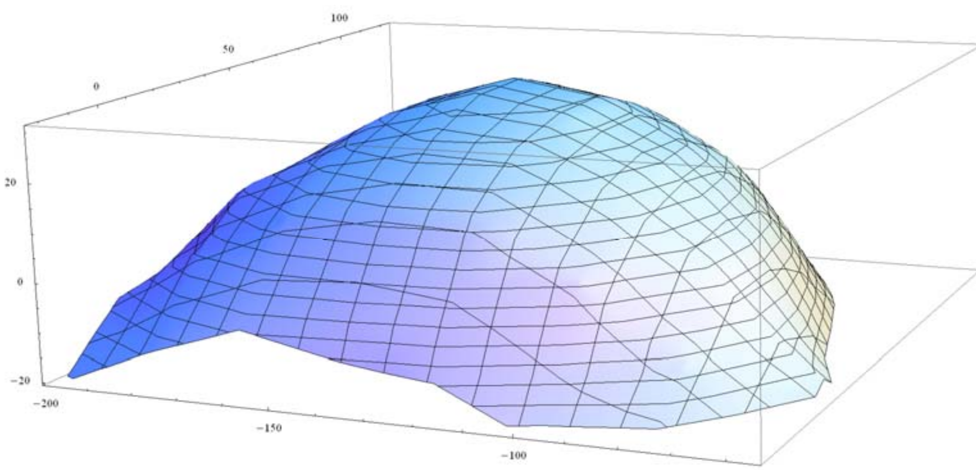

Figure 6.15: The surface generated by the SCMM

The accuracy of the surface generated by the SCMM is verified by comparing it with the surface generated by a high precision 3 DOF Spatial Parallel Kinematic Mechanism (3D-SPKM) developed in the laboratory. The precision of the 3D-SPKM is in the order of 30 μm. Figure 6.16 illustrates the arrangement of the 3D-SPKM measuring the coordinates of the points on the surface of the human skull. The skull is placed on the platform of the highly sensitive 6 axis Force Torque (F-T) sensor developed at author's laboratory [95]. The measuring probe is made to move till the threshold of force magnitude is less than 0.1N. The stop command is activated as soon as the threshold is crossed. The 3D-SPKM successfully stops within a very minute distance exhibiting fine motion control. The compliance corresponding to 0.1 N is estimated to be 20 μm. The coordinates are measured and recorded based on direct kinematics at the rested point. The distance between the several specific points on the skull is repeatedly measured and it is found that the repeatability is within 30 μm over a distance of up to 80 mm. Figure 6.17 shows the surface generated by the 3D-SPKM based measurement. The surface generated by the SCMM was found to be in close agreement with the actual surface as well as the surface generated by 3D-SPKM.

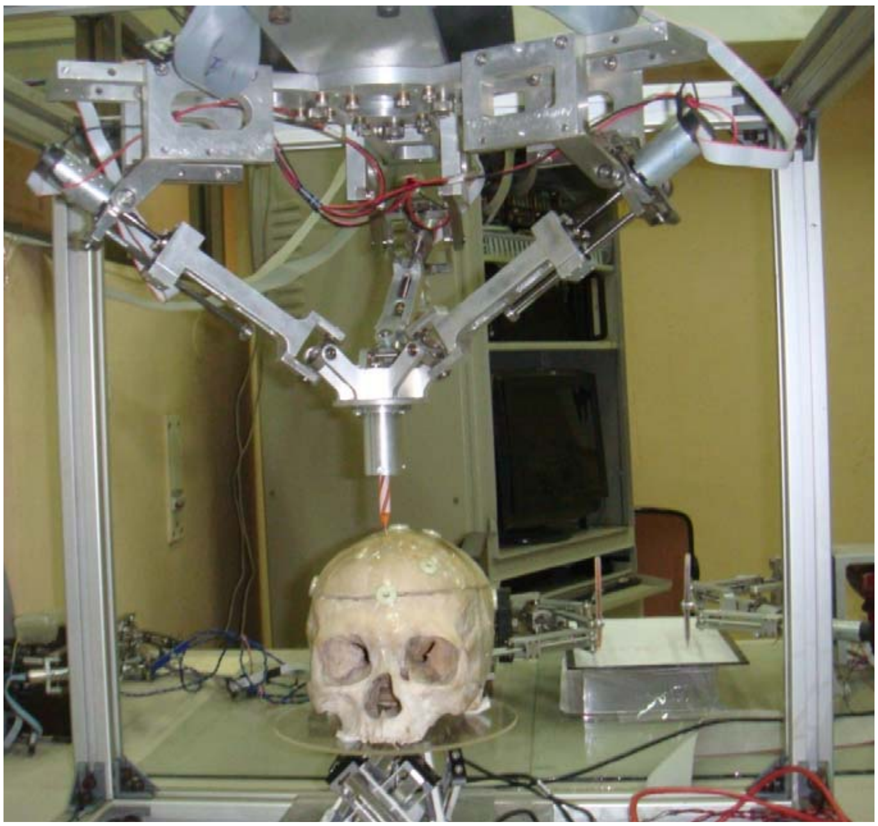

Figure 6.16: 3D-SPKM is being used as a coordinate measuring manipulator and tracing the surface for localization purpose

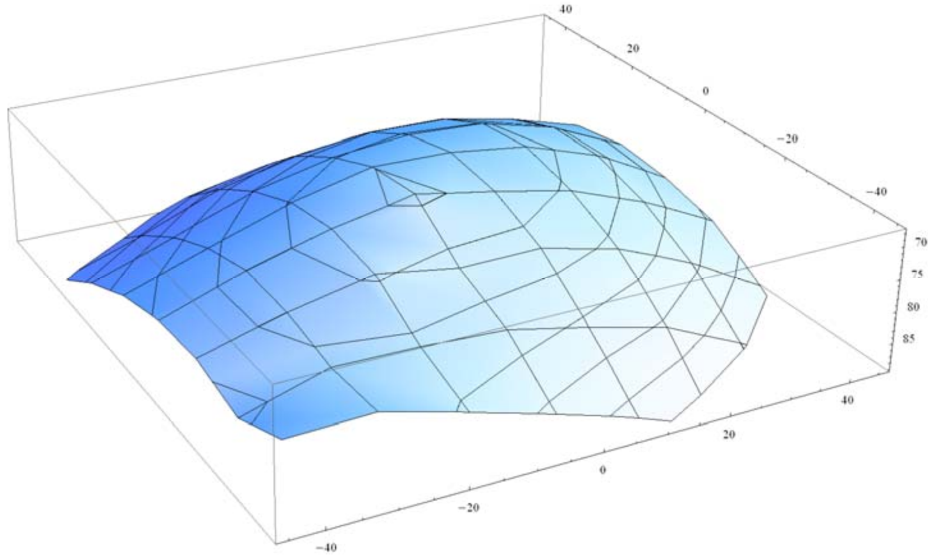

Figure 6.17: The surface generated by the 3D-SPKM

In the surface registration, the first set of data is generated from the preoperative MRI scan data and the second set is generated from the SCMM which is traversed on the patient's skull. A surface to surface matching algorithm is used to calculate the transformation which matches and aligns two sets of points generated. This calculated transformation can be used by the neurosurgeon to perform an image guided surgery.

6.6 Experimentation of Neuronavigation at Laboratory

A point to point fiducial based neuro-registration and neuronavigation is demonstrated in the laboratory. Neuronavigation experiments are conducted using a human skull phantom to evaluate the performance characteristics of the SCMM. The human skull phantom is prepared for a CT scan by affixing the fiducials on the surface of the skull. The phantom is subjected to a CT scan and the relation of the fiducials with respect to the fiducial frame is established using DICOM images. The relation between the tumor (a fixed point on the skull phantom) with respect to the fiducial frame is established. Using the transformation formulated, the coordinates of the tumor with respect to the SCMM base frame are determined. Subsequent to the registration, the neuronavigation procedure is performed.

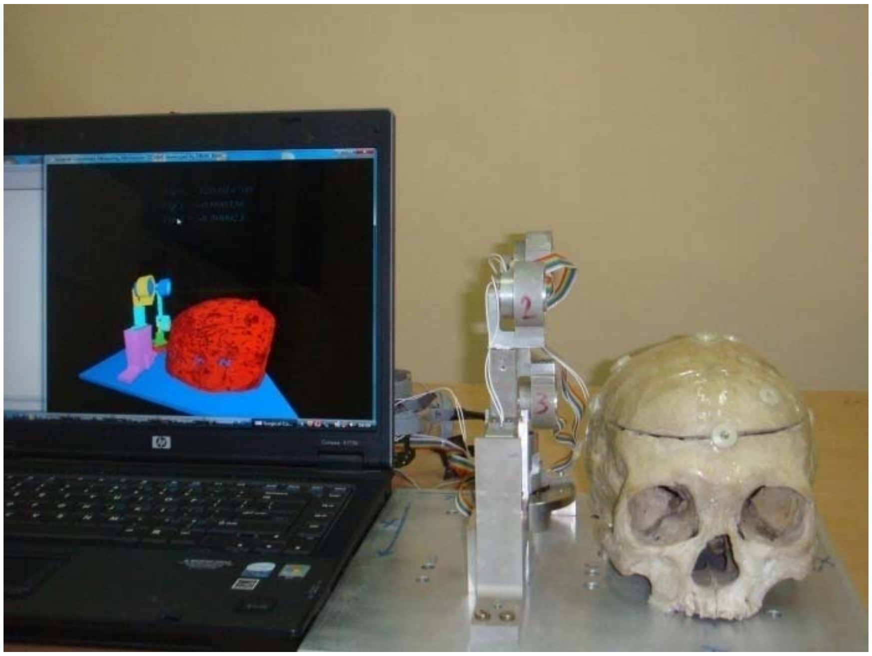

Figure 6.18 (a) SCMM in home position

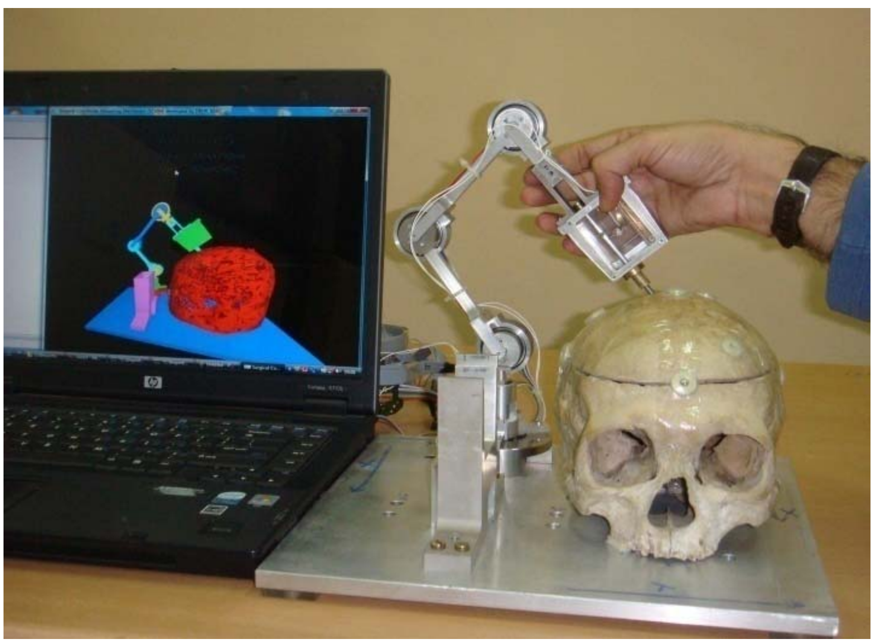

Figure 6.18 (b) SCMM end tool traversing skull surface

Figure 6.18: Neuronavigation procedure demonstrated for SCMM

In the neuronavigation procedure, the passive SCMM is used to navigate the surgical tool. When the user manually navigates the end tool fixed to the SCMM (as represented in figure 6.18), he can visualize on the computer screen: the actual configuration of the SCMM, tool movement relative to the 3D model of the actual skull built using a CT image and also the tip of the tool with respect to the tumor region. The implementation of the SCMM based neuronavigation is illustrated in the figure 6.18. The figure 6.18 shows CT image converted into a transparent 3D model and the SCMM graphic model based on its actual size. The software developed is having a pan, tilt and a zoom feature to visualize the 3D model of the SCMM from different views and to determine its position with respect to the skull phantom. The values from the simulated input data of the joint encoder are taken for conducting neuronavigation. Figure 6.18 (a) shows the SCMM and its simulated model in the home position. Figure 6.18 (b) shows the SCMM and its simulated model when the user is traversing the surface of the skull.

6.7 Demonstration of Frameless Stereotactic Neurosurgery using 3D-SPKM and SCMM at Author's Laboratory

Experiments are conducted to interface the SCMM and the 3D-SPKM to validate the robot based frameless stereotaxy. An experimental setup is prepared in which the 3D-SPKM and SCMM are arranged close to each other. Figures 6.19 and 6.20 illustrate the experimental setup comprising of all the subsystems for the robot based frameless stereotactic neurosurgery. The 3D-SPKM and the SCMM are fixed to a rigid aluminum frame at pre-defined positions such that the relationship of the 3D-SPKM base frame and the SCMM base frame is established.

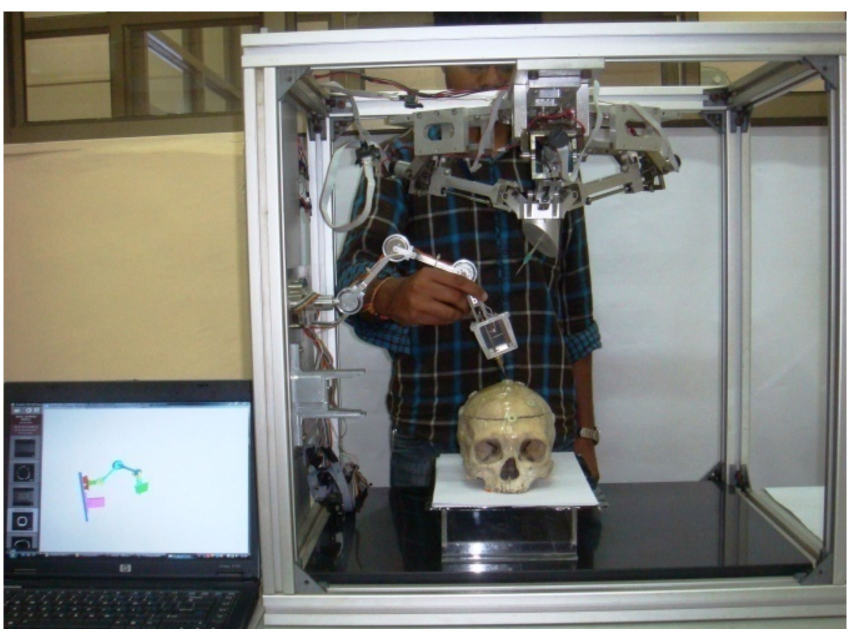

Figure 6.19: Experimental demonstration showing the position of tumor being determined using SCMM

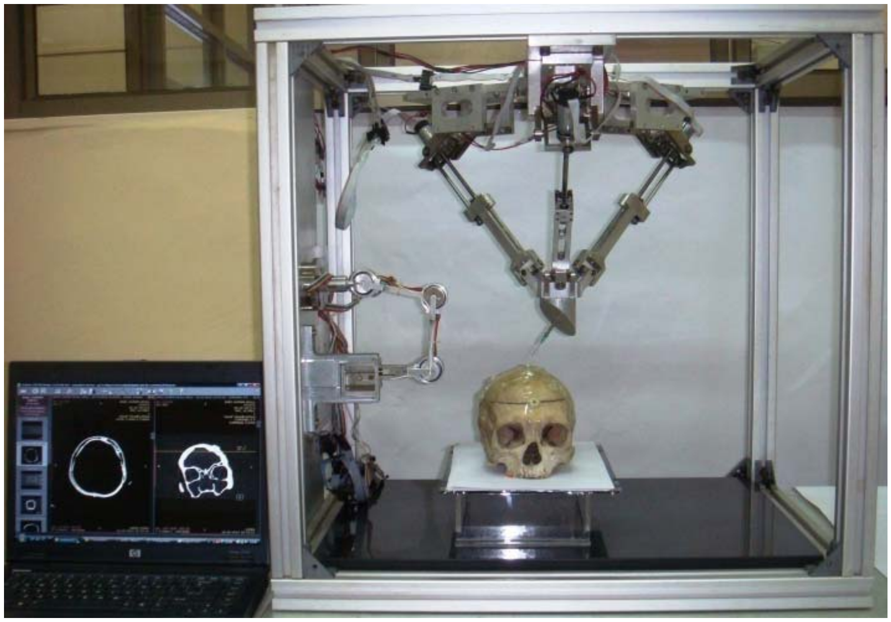

Figure 6.20: Motion of 3D-SPKM while it is approaching tumor point

The coordinates of a dummy tumor point fixed on the surface of the skull are determined with respect to the SCMM base frame. Figure 6.19 illustrates the position of the dummy tumor point being determined with respect to the SCMM base frame by a human operator. The figure 6.19 also presents the computer graphics interface showing the current position of the SCMM. The transformation between the SCMM and the 3D-SPKM frames is used to determine the coordinates of the tumor point with respect to the 3D-SPKM base frame. The inverse kinematics is solved and the SPKM is navigated to reach the tumor point. Figure 6.20 shows the motion of the 3D-SPKM while it is approaching the tumor point. In figure 6.20, the graphics interface shows the CT scan images of the phantom. The frameless stereotactic neurosurgery is validated using the 3D-SPKM and SCMM. Figure 6.21 illustrates the thesis in a nutshell; the proposed robot based frameless stereotactic neurosurgery using 3D-SPKM and SCMM.

Figure 6.21 (a): SCMM based registration carried out by an human operator

Figure 6.21 (b): 3D-SPKM approaching patient for neurosurgery

Figure 6.21: A robot based frameless stereotactic neurosurgery using SCMM and 3D-SPKM (for illustration purpose only)

6.8 Summary

Neuro-registration and neuronavigation are explained in a detailed manner. A thorough analysis of the point representation and measurement was presented which is incorporated in the neuro-registration procedures. The methodology to determine the position of the tumor with respect to the fiducial frame and hence the robot frame of reference was explained. The standard available digital gauges were evaluated for the neuro-registration system. It was concluded that taking the measurement was time consuming and inconvenient using digital gauges and hence a simple coordinate measuring device has been developed for the neuro-registration and neuronavigation.

The SCMM is a direct coordinate measurement tool; which in a single action gives the coordinates of any point with respect to the robot frame of reference. The implementation and use of the portable SCMM for neurosurgical procedures was established. The accuracy of the developed SCMM unit in the pair point based registration method was presented. The localization of the region representing the tumor was done by conducting the experiments on a phantom. The localization algorithm was described. The experiments and the results of successful mapping from the fiducial frame of reference to the robot frame of reference were described in detail. Surface registration experiments were carried out using the SCMM and were validated using a high precision 3D-SPKM developed at the author's laboratory.

Further, the effectiveness of the SCMM in neuronavigation was explained. The SCMM based image guided surgical procedure was exhibited on the skull phantom. The experiments have been established to validate the SCMM based successful neuro-registration and neuronavigation procedure. The actual configuration of the SCMM was visualized on the computer screen along with the tool movement relative to the 3D model of the skull phantom when the user manually navigates the end tool fixed to the SCMM. The demonstration of frameless stereotactic neurosurgery using 3D-SPKM and SCMM was undertaken at author's laboratory. The procedure presented eliminates the line of sight problem which is a constraint of the current neuronavigation procedures. The SCMM based neuro-registration and neuronavigation is an economical and a promising substitute over the current optical tracking based neuronavigation systems. The developed SCMM based frameless stereotaxy system has an accuracy comparable to the frame based stereotaxy system and at the same time patient comfort levels equivalent to the optical tracking based frameless stereotaxy systems.

Chapter 7

Conclusion and Future Work

7.1 Conclusion

The research was carried out with the aim of modeling, designing and development of a robot assisted frameless stereotactic neurosurgery. A prototype of a robot and the associated setup which aid the neurosurgeons in frameless stereotactic neurosurgery has been developed. The system, which has been developed, has the following features: (i) accuracy analogous to frame based stereotaxy (ii) comfort levels for the patient equivalent to frameless stereotaxy (iii) eliminates the line of sight problem in registration and in navigation, in comparison with optical based frameless stereotaxy. The research issues accomplished to implement the system are as follows:

7.1.1 Parallel mechanism based robot for frameless stereotactic neurosurgery

A detailed analysis of the parallel mechanism was carried out in order to find the influence of choice of the design parameters on the performance characteristics of the mechanism. The mobility analysis ensured that the mobility of the passive composite joints meet the mobility requisites of the surgical tool during neurosurgery. The locations of the central axis of the solid angle (cone angle) of the passive composite joints were optimized. Two numerical examples have been presented considering realistic dimensions to attain the optimum mobility range of the passive joints at the platform and at the base. The design synthesis has been presented with an objective of enhancing the utility of the passive joint mobility which improves the neurosurgical workspace reach of the parallel mechanisms. The novel options for the design of passive composite joints have been presented. This reduces the error in axis definition, enhances the passive mobility and improves the torsional rigidity of the leg. The sensitivity analysis has been presented which establishes the best performing region of the robot's workspace in order to perform the neurosurgery. The sensitivity analysis determines the variations of the sensitivity in the workspace with respect to the input range parameters. The singularity analysis ensures that the workspace boundary is farthest from the singularity surfaces. The results presented were in contrast to the generalized observations presented in [119] for the similar three axis U$\underline{P}$U based translational parallel manipulator. The error analysis arrives at the platform posture error due to the inaccuracies in the passive composite joints for a specified workspace of the 3D-SPKM. It was observed and concluded from the error analysis results that the sum of the absolute of maximum individual errors at each joint pairs of all the legs as reported by [122] and [123] give a highly exaggerated figure. Hence it cannot be taken as a fair estimate. The analysis and algorithms enhanced the micro-management of the operative space of the workspace of the robot. The analysis is an essential requirement for the development of a 6 DOF robot which would maneuver the surgical tool with utmost precision to the tumor point.

Design considerations have been presented which ensure negligible torsional backlash for the highly accurate 3D-SPKM prototype. The 3D motion simulation has been presented which ensures the interference free motion of the mechanism throughout its workspace. The synthesis of the robot was carried out to meet the workspace and manipulability requirements of the neurosurgery. The design and development of the 3D-SPKM has been carried out on the basis of the analysis. Several experimental results have been presented to determine the repeatability and trajectory following accuracy for various payloads. It was evident from the presented results that the performance of the 3D-SPKM is consistent throughout the workspace. Critical aspects like the trajectory following and the fine motion control capabilities were observed to be steady in all the experiments. Experimental results show the repeatability achieved by the 3D-SPKM is around 10 μm and the trajectory following accuracy of the manipulator is within 30 μm. The accuracy and repeatability measured are better than the preferred accuracy for neurosurgical procedures. The experimental results presented validate the frameless stereotactic neurosurgery procedure using the 3D-SPKM.

The stated analysis and design of the 3D-SPKM has been extended to develop a higher degree of freedom Parallel Kinematic Mechanism. A 6D-PKM has been analyzed and designed to fulfill the additional dexterity to the reachable workspace required for performing stereotactic neurosurgery procedures. The workspace analysis presented ensures that the manipulability requirements of the surgical tool attached to the platform of the 6D-PKM are achieved. 3D motion simulation of the 6D-PKM, which verifies interference free mobility and trajectory planning of the mechanism throughout its workspace, has been presented. The

3D motion simulation in runtime would aid neurosurgeons to visualize the motion of the robot with respect to the pre-operative imaging data (MRI) during the course of neurosurgery. The 6D-PKM based robot has been designed, simulated and developed to illustrate all the features required for a successful stereotactic neurosurgical procedure.

7.1.2 Neuro-registration and neuronavigation framework for frameless stereotaxy

A methodology has been developed to provide a realistic design solution to determine the relation of the tumor with respect to the robot frame of reference. A new representation for the neuro-registration and neuronavigation for the frameless stereotaxy has been established through the development of a 4 DOF SCMM. The SCMM determines the relation of the tumor with respect to the surgical tool; which is kept in known relationship with respect to the 6D-PKM based robot. The SCMM has resulted in a simpler and accurate system for registration and tracking purposes. Experiments have been conducted in order to evaluate the performance characteristics and to validate the mechanism. The accuracy of the developed SCMM unit in the fiducial and surface based registration procedures has been presented. The localization of the region representing the tumor was obtained by conducting the experiments on a phantom. Experiments and the results of successful mapping from the image frame with respect to the robot frame of reference were described. Surface registration experiments were carried out using SCMM and were validated using a high precision 3D-SPKM developed at the laboratory.

SCMM based image guided surgical procedure was exhibited on the skull phantom. The experiments have been established to validate the SCMM based successful neuro-registration and neuronavigation procedure. The actual configuration of the SCMM was visualized on the computer screen along with the tool movement relative to the 3D model of the skull phantom when the user manually navigated the end tool fixed to the SCMM. The presented procedure eliminates the line of sight problem, which is a main constraint of the current neuronavigation procedures. SCMM based neuro-registration and neuronavigation is an economical and a promising substitute over the current optical tracking based neuronavigation systems. The developed SCMM based frameless stereotaxy system has accuracy comparable to frame based stereotaxy systems and the patient comfort levels equivalent to the optical tracking based frameless stereotaxy systems.

7.2 Future Work

Any research is complete only when it meets its application. In this thesis, the frameless stereotactic neurosurgery procedure is validated using the developed 3D-SPKM. Further, the validation of the frameless stereotactic neurosurgery procedure has to be carried out using the 6D-PKM. It includes the development of end tooling and appropriate fixtures for the 6D-PKM and SCMM. After the successful validation at the laboratory, the frameless stereotactic neurosurgery framework, which includes the 6D-PKM and SCMM can be used for hospital trials. The application of parallel manipulator as a tele-manipulator in surgery can be explored.

As discussed in chapter 2, research is being carried out in the area of intra-operative imaging to incorporate the brain shift. The next phase of the work would be to develop a 6D-PKM based stereotactic neurosurgery, which uses intra-operative images. In the intra-operative imaging, MRI or ultrasound based imaging is done during the intermediate stages of neurosurgery. Further work is required to estimate the brain shift and to develop an algorithm based modification of the registration with respect to the intra-operative imaging data from pre-operative imaging data.

The research and recent publications significantly point towards robots aiding or taking over more and more surgical procedures in the next ten years. Active research interest may be observed in classifying surgeries for robot based surgery. Many surgical procedures need co-operation of multiple tools at the surgical site. Setting up objectives for co-operation to generate a functional relationship among the co-operative tools to achieve successful and fail safe surgery may find enhanced research attention. Rapid convergence of imaging techniques and robot based measurement may lead to autonomous registration, navigation and eventually to surgery.

References

[1] Clinical Trials and Noteworthy Treatments for Brain Tumors, http://www.virtualtrials.com/Schulder.cfm (last accessed November 15, 2014)

[2] Zheng J., "An Accurate and Efficient Target Localization method for Stereotactic Neurosurgery of Parkinson's Disease," *PhD Thesis*, The State University of New Jersey, October 2006.

[3] Wikipedia: Stereotactic surgery, http://en.wikipedia.org/wiki/Stereotactic_surgery (last accessed November 15, 2014)

[4] Gildenberg P. L., "General concepts of Stereotactic surgery," *Modern Stereotactic Neurosurgery*, Lunsford L. D. Ed., Martinus Nijhoff Publishing, Boston, 1988.

[5] Gildenberg P. L., "Stereotactic Surgery: Present and Past," *Stereotactic Neurogurgery*, Heilbrun M. P. Ed., Baltimore, Williams & Wilkins, 1988.

[6] Horsley V., Clarke R. H., "The structure and functions of the cerebellum examined by a new method," *Brain*, Vol. 31, pp. 45-124, 1908.

[7] Marshall L. H., Magoun H. W., "The Horsley-Clarke Stereotaxic instrument: the beginning," *Kopf Carrier Newsletter*, Patterson M. M. (ed). Published by David Kopf Instruments, Tujunga, California, October 1990.

[8] Marshall L. H., Magoun H. W., "The Horsley-Clarke Stereotaxic Instrument: The First Three Instruments," *In Kopf Carrier Newsletter,* Patterson MM(ed). Published by David Kopf Instruments, Tujunga, California, May 1991.

[9] Bertrand G, "Stereotactic surgery at McGill: The early years," *Neurosurgery,* Vol. 54, pp. 1244-1252, 2004.

[10] International Parkinson and Movement Disorder Society http://www.movementdisorders.org/james_parkinson/anatomy.html (last accessed August 1, 2011)

[11] Spiegel E. A., Wycis H. T., Marks M., Lee A., "Stereotaxic apparatus for operations on the human brain," *Science,* Vol. 106, pp. 349-350, 1947.

[12] Gildenberg P. L., "Spiegel and Wycis: the early years," *Stereotactic Functional Neurosurgery*, Vol. 77, pp. 11-16, 2001.

[13] Leksell L., “Stereotactic Apparatus for Intracerebral Surgery,” *Act Chir Scand*, Vol. 99, pp. 229-223, 1949.

[14] Leksell L, “The stereotaxic method and radiosurgery of the brain,” *Act Chir Scand*, Vol. 102, pp. 316-319, 1951.

[15] Elekta Systems, http://www.elekta.com/healthcare-professionals/products/elekta-neuroscience/stereotactic-neurosurgery/leksell-stereotactic-system.html (last accessed November 15, 2014)

[16] Leksell Stereotactic System, Elekta Instrument AB, Manual. (Document number 1007063 Rev. 02 (2008/10))

[17] Brain and Mind, Electronic magazine on Neuroscience: Stereotactic Neurosurgery, http://www.cerebromente.org.br/n02/historia/stereotactic.htm (last accessed November 15, 2014)

[18] HowStuffWorks: CT Scan, http://science.howstuffworks.com/cat-scan.htm (last accessed November 15, 2014)

[19] Wikipedia: X ray computed tomography, http://en.wikipedia.org/wiki/X-ray_computed_tomography (last accessed November 15, 2014)

[20] Neurosurgical Medical Clinic, Inc, http://www.sd-neurosurgeon.com/practice-stereotactic-surgery.php (last accessed November 15, 2014)

[21] G Eggers, J. Muhling, R Marmulla, “Image-to-patient registration techniques in head surgery,” *International Journal of Oral and Maxillofacial Surgeons*, Vol. 35, pp. 1081-1095, 2006.

[22] NDI Medical, http://www.ndigital.com/medical/polarisfamily.php (last accessed November 15, 2014)

[23] Brainlab Surgery Products, http://www.brainlab.com/ (last accessed November 15, 2014)

[24] Frey S., Comeau R., Hynes B., Mackey S. and Petrides M., “Frameless Stereotaxy in the nonhuman primate,” *NeuroImage*, Vol. 23, pp. 1226-1234, 2004.

[25] Doward N. L., “Frameless Stereotactic biopsy with the EasyGuide,” *Medicamumdi*, Vol. 42, Issue 1, March 1998.

[26] thamburaj.com: Article on Stereotactic Neurosurgery,

http://www.thamburaj.com/stereotactic_neurosurgery.htm
(last accessed November 15, 2014)

[26A] Ganslandt O., Behari S., Gralla J., Fahlbusch R., Nimsky C., "Neuronavigation: Concept, Techniques and Applications," *Neurology India*, Vol. 50(3), pp. 244-255, 2002.

[27] Wikipedia: Robot-assisted surgery,
http://en.wikipedia.org/wiki/Robot-assisted_surgery
(last accessed November 15, 2014)

[28] Kwoh Y. S., Hou J., Jonckheere E. A. and Hayall S., "A robot with improved absolute positioning accuracy for CT guided stereotactic brain surgery", *IEEE Transactions on Biomedical Engineering*, Vol. 35(2), pp. 153–161, 1988.

[29] Pransky J., "ROBODOC: Surgical Robot Success Story", *Industrial Robot*, Vol. 24(3), pp. 231-233, 1997.

[30] ROBODOC Curexo Technology Corporation,
http://www.robodoc.com/index.html
(last accessed August 1, 2011)

[31] Wikipedia: da Vinci Surgical System
http://en.wikipedia.org/wiki/Da_Vinci_Surgical_System
(last accessed November 15, 2014)

[32] Intuitive Surgical, Incorporation, http://www.intuitivesurgical.com/
(last accessed November 15, 2014)

[33] Gomes P., *Medical Robotics: Minimally Invasive Surgery*, Woodhead Limited Publication, 2012, ISBN 978-0-85709-739-2 (online).

[34] Ballantyne G. H. and Moll F., "The da Vinci telerobotic surgical system: the virtual operative field and telepresence surgery", *Surgical Clinics of North America*, Vol. 83(6), pp. 1293–1304, 2003.

[35] Davies B., "A review of robotics in surgery", *Proceedings Institution of Mechanical Enggineers, Part H: Journal of Engineering in Medicine*, Vol. 214, pp. 129–140, 2000.

[36] Low S. C. and Phee L., "A review of master–slave robotic systems for surgery", *IEEE Conference on Robotics, Automation and Mechatronics*, pp. 37–42, 2004.

[37] Mack M. J., "Minimally invasive and robotic surgery", *Journal of American Medical Association*, Vol. 285(5), pp. 568–572, 2001.

[38] Gomes P., "Surgical robotics: Reviewing the past, analyzing the present, imagining the future", *Robotics and Computer-Integrated Manufacturing*, Vol. 27(2), pp. 261–266, 2011.

[39] STS Team H, https://sts09-teamh.wikispaces.com/Packaging+%26+Energy (last accessed November 15, 2014)

[40] Wikipedia: ZEUS robotic surgical system, http://en.wikipedia.org/wiki/ZEUS_robotic_surgical_system (last accessed November 15, 2014)

[41] Computer Motion, http://biomed.brown.edu/Courses/BI108/BI108_2000_Groups/Heart_Surgery/Robotics.html#CompMo (last accessed November 15, 2014)

[42] Edgar Online, http://sec.edgar-online.com/intuitive-surgical-inc/8-k-current-report-filing/2003/03/07/Section10.aspx (last accessed November 15, 2014)

[43] odec.ca: Robotic Surgery, http://www.odec.ca/projects/2008/brai8z2/Dates.html (last accessed November 15, 2014)

[44] Sunga G. T., Gill I. S., "Robotic laparoscopic surgery: a comparison of the da Vinci and Zeus systems", *Urology*, Vol. 58(6), pp. 893–898, 2011.

[45] Phys.org, http://phys.org/news67222790.html (last accessed November 15, 2014)

[46] (e) science news, http://esciencenews.com/articles/2008/11/20/surgeons.perform.worlds.first.pediatric.robotic.bladder.reconstruction (last accessed November 15, 2014)

[47] biomed.brown.edu, http://biomed.brown.edu/Courses/BI108/BI108_2005_Groups/04/neurol (last accessed August 1, 2011)

[48] Taylor R. H., Dan Stoianovici D., "Medical Robotics in Computer-Integrated Surgery," *IEEE Transactions on Robotics and Automation*, Vol. 19(5), pp. 765-781, 2003.

[49] Zamorano L., Li Q., Jain S., Kaur G., "Robotics in neurosurgery: state of the art and future technological challenges," *International Journal of Medical Robotics*

and Computer Assisted Surgery, Vol. 1(1), pp. 7-22, 2004.

[50] Renishaw: neuromate stereotactic robot, http://www.renishaw.com/en/neuromate-stereotactic-robot--10712 (last accessed November 15, 2014)

[51] Benabid A. L., Cinquin P., Lavallee S., Le Bas JF, Demongeot J., de Rougemont J., "Computer driven robot for stereotactic surgery connected to CT scan and magnetic resonance imaging," *Technological design and preliminary results, Appl Neurophysiol*, Vol. 50, pp. 153-154, 1987.

[52] Integrated Surgical Systems, http://robodoc.com/_oldfiles/eng/neuromate.html (last accessed November 15, 2014)

[53] Prosurgics Limited, http://prosurgics.com/prosurgics_pathfinderkey.htm (last accessed November 15, 2014)

[54] Deacon G., Harwood A., Holdback J. et. al., "The pathfinder image-guided surgical robot," *Proceedings of the Institution of Mechanical Engineers*, Vol. 224(5), pp. 691–713, 2010.

[55] Morgan P., Carter T., Davis S. et. al., "The application accuracy of the pathfinder neurosurgical robot," *International Congress Series*, Elsevier Publications, Vol. 1256, pp. 561–567, 2003.

[56] Beasley R. A., "Medical Robots: Current Systems and Research Directions," *Journal of Robotics*, Vol. 2012, Article ID 401613, 2012.

[57] Wikipedia: NeuroArm, http://en.wikipedia.org/wiki/NeuroArm (last accessed November 15, 2014)

[58] Sutherland G. R., McBeth P. B., Louw D. F., "NeuroArm: An MR Compatible Robot for Microsurgery", *Computer Assisted Radiology and Surgery,* Vol. 1256, pp. 504-508, 2003.

[59] McBeth P. B., Louw D. F., Rizun P. R., Sutherland G. R., "Robotics in Neurosurgery", *American Journal of Surgery*, Vol. 188, pp. 68S-75S, 2004.

[60] Rizun P. R., Sutherland G. R., "A Tactile-Feedback Laser System for Robotic Surgery", *Proceedings of the World Haptics Conference,* pp. 426 – 431, 2005.

[61] Sutherland G. R., Newhook P., Feil G., Fielding T., Greer A.D., Latour I., "An image-guided MR compatible surgical robot", *Neurosurgery,* Vol. 62, pp. 286-293, 2008.

[62] Image Guided Therapy Solutions, http://www.imris.com/

(last accessed November 15, 2014)

[63] NeuroArm, http://www.neuroarm.org/
(last accessed November 15, 2014)

[64] Science Notes: Doctors used robot to do brain surgery,
http://sciencenotes.wordpress.com/2008/05/17/doctors-use-robot-to-do-brain-surgery/
(last accessed November 15, 2014)

[65] McBeth P. B., Louw D. F., Rizun P. R. and Sutherland G. R., "Robotics in neurosurgery," *The American Journal of Surgery*, Vol. 188, pp 68S-75S, 2004.

[65A] PI Instruments,
http://www.pi-usa.us/news/newsletter/old/25/hexapod_operation_robot.html
(last accessed November 15, 2014)

[65B] ParalleMIC: The true origins of parallel robots by Bonev I.,
http://www.parallemic.org/Reviews/Review012.html
(last accessed November 15, 2014)

[66] Dasgupta B., "Advanced Topics in Robotics", a report on a short term course during July 27-31, Indian Institute of Technology Kanpur, 1998.

[67] Dasgupta B. and Mruthyunjaya T, "The Stewart Platform Manipulator: A Review*,"* *Mechanism and Machine Theory*, Vol. 35, pp. 15-20, 2000.

[68] Merlet J. P., *Parallel Robots*, 2nd Edition, Springer Publications, 2006.

[69] Duffy J., *Statics and Kinematics with Applications to Robotics*, Cambridge University Press, 1996.

[70] ParalleMIC: The true origins of parallel robots by Bonev I.,
http://www.parallemic.org/Reviews/Review007.html
(last accessed November 15, 2014)

[71] sop.inria.fr: Merlet J. P.,
http://www-sop.inria.fr/members/Jean-Pierre.Merlet/merlet_eng.html
(last accessed November 15, 2014)

[72] Gwinnett J. E., "Amusement device", United States Patent No 1,789,680, January, 20, 1931.

[73] Pollard W. L. V., "Position controlling apparatus", United States Patent No 2,286,571, 16 June 1942.

[74] Gough V. E., "Contribution to discussion of papers on research in automobile

stability, control and tyre performance", *Proceedings of Automobile Division Inst. Mechanical Eng.,* pp. 392-394, 1956-1957.

[75] Gough V. E. and Whitehall S. G., "Universal tire test machine", *In Proceedings 9th Int. Technical Congress F.I.S.I.T.A.,* Vol. 117, pp. 117–135, May 1962.

[76] Stewart D, "A platform with 6 degrees of freedom", *Proceedings of the Institution of mechanical engineers*, Vol. 180(Part 1, 15), pp. 371–386, 1965.

[77] Cappel K. L., "Motion simulator", *United States Patent No. 3,295,224 The Franklin Institute,* January 3, 1967.

[78] Hunt K. H., *Kinematic Geometry of Mechanisms*, *Clarendon Press,* Oxford, 1978.

[79] Earl C. F. and Rooney J., "Some kinematics structures for robot manipulator designs", *Journal of Mechanisms, Transmissions and Automation in Design*, Vol. 105(1), pp. 15–22, 1983.

[80] K.H. Hunt K. H., "Structural Kinematics of In-Parallel-Actuated Robot Arms," *ASME Journal of Mechanisms Transmissions and Automation in Design,* Vol. 105 (4), pp. 705-712, 1983.

[81] Fichter E. F. and McDowell E. D., "Determining the motions of joints on a parallel connection manipulator", *Proceedings of 6th World Congress on Theory of Machines and Mechanisms,* New Delhi*, India, pp.* 1003-1006*, 1983.*

[82] Mohamed M. G., Sanger J., Duffy J., "Instantaneous kinematics of fully parallel devices", *Proceedings 6th World Congress on the Theory of Machines and Mechanisms*, pp. 77-80, 1983.

[83] Mohamed M. G. and Duffy J., "A direct determination of the instantaneous kinematics of fully parallel robot manipulators", *Journal of Mechanisms, Transmissions and Automation in Design*, Vol. 107(2), pp. 226–229, 1985.

[84] Yang D. C. H. and Lee T. W., "Feasibility study of a platform type of robotic manipulators from a kinematic viewpoint", *Journal of Mechanisms, Transmissions and Automation in Design,* Vol. 106, pp. 191-198, 1984.

[85] Fichter E. F., "A Stewart Platform-Based Manipulator: General Theory and Practical Construction," *International Journal of Robotic Research,* Vol. 5 (2), pp. 157-182, 1986.

[86] Merlet J. P., "Parallel manipulators. Part I: Theory design, kinematics, dynamics and control", *INRIA Research Report* No. 646, 1987.

[87] Raghavan M., “The Stewart Platform of General Geometry Has 40 Configurations,” *ASME Journal of Mechanical Design*, Vol. 115(2), pp. 277–282, 1993.

[88] Ronga F. and Vust T., “Stewart Platforms without Computer?”, *Proceedings of the International Conference on Real Analytic and Algebraic Geometry*, (Trento, Sept. 21–25, 1992), Walter de Gruyter Verlag, Berlin, pp. 197–212, 1995.

[89] Husty M. L. “An algorithm for solving the direct kinematic of Stewart-Gough-type platforms”, *Mechanism and Machine Theory*, Vol. 31(4), pp. 365–380, 1996.

[90] Gaillet A. Reboulet C., “An Isostatic Six Component Force and Torque Sensor”, *Proceedings of the 13th International Symposium on Industrial Robotics*, Chicago, IL, USA, pp. 102–111, 1983.

[91] Griffis M. and Duffy J., “Kinestatic Control: A Novel Theory for Simultaneously Regulating Force and Displacement”, *Transactions of ASME, Journal of Mechanical Design,* Vol. 113(4), pp. 508-515, 1991.

[92] Dasgupta B., Reddy S., Mruthyunjaya T. S., “Synthesis of a force-torque sensor based on the Stewart platform mechanism”, *Proceedings of National Convention on Industrial Problems in Machines and Mechanisms (IPROMM)'94, Bangalore, India*, pp. 14-23, 1995.

[93] Dwarakanath T. A., Dasgupta B. and Mruthyunjaya T. S., "Design and Development of Stewart Platform based Force-Torque Sensor”, *Mechatronics,* Vol. 11, Issue 7, pp. 793-809, 2001.

[94] Dwarakanath T. A. and Venkatesh D., “Simply supported, 'Joint less' Parallel Mechanism based Force-Torques Sensor”, *Mechatronics,* Vol. 16, pp. 565-575, 2006.

[95] Dwarakanath T. A. and Bhutani G., “Beam type hexapod structure based six component force-torque sensor”, *Mechatronics*, Volume 21, Issue 8, pp. 1279 – 1287, 2011.

[96] Ghosal A., “Six component force-torque sensors Gough-Stewart platform manipulators”, *Annals of the Indian National Academy of Engineering,* Vol. 8, pp. 79-88, 2011.

[97] Ranganath R., Nair P. S., Mruthyunjaya T. S. and Ghosal A., “A force-torque sensor based on a Stewart Platform in a near-singular configuration”, *Mechanism*

and Machine Theory, Vol. 39, pp. 971-998, 2004.

[98] Gosselin C. and Angeles J., “Singularity analysis of closed-loop kinematic chains”, *IEEE Transactions on Robotics and Automation*, Vol. 6(3), pp. 281–290, 1990.

[99] Chowdhury P. and Ghosal A., “Singularity and controllability analysis of parallel manipulators and closed-loop mechanisms”, *Mechanism and Machine Theory*, Vol. 35, pp. 1455-1479, 2000.

[100] Ghosal A. and Ravani B., “Differential geometric analysis of singularities of point trajectories of serial and parallel manipulators", *Transactions of ASME, Journal of Mechanical Design,* Vol. 123, pp. 80-89, 2001.

[101] Bandyopadhyay S. and Ghosal A., “Analysis of configuration space singularities of closed-loop mechanisms and parallel manipulators”, *Mechanism and Machine Theory,* Vol. 39, pp. 519-544, 2004.

[102] Bandyopadhyay S. and Ghosal A., “Geometric characterization and parametric representation of the singularity manifold of a 6-6 Stewart platform manipulator”, *Mechanism and Machine Theory*, Vol. 41, pp. 1377-1400, 2006.

[103] Lee J., Duffy J, Hunt K. H., “A Practical quality index based on the octahedral manipulator,” *International Journal of Robotic Research,* Vol. 17 (10), pp. 1081-1090, 1998.

[104] Waldron K. J., Hunt K. H., “Series-Parallel dualities in actively co-ordinated mechanisms,” *International Journal of Robotics Research,* Vol. 10 (5), pp. 473-480, 1991.

[105] Di Gregorio R., Parenti-Castelli V., “Mobility Analysis of the 3-UPU Parallel Mechanism Assembled for a Pure Translational Motion,” *Journal of Mechanical Design*, Vol. 124(2), pp. 259-264, 2002.

[106] Di Gregorio R., “Statics and Singularity Loci of the 3-UPU Wrist,” *IEEE transactions on robotics*, Vol. 20 (4), pp. 630-635, August 2004.

[107] Gosselin C., “Determination of the workspace of 6-DOF parallel manipulators,” *ASME Journal of Mechanical Design*, Vol. 112, pp. 331–336, 1990.

[108] Wang Zhe, Wang Zhixing, Liu W., Lei Y., “A study on workspace, boundary workspace analysis and workpiece positioning for parallel machine tools,” Mechanism *and Machine Theory*, Vol. 36, pp. 605-622, 2001.

[109] Pernkopf F. and Husty M. L., “Workspace analysis of Stewart Gough

manipulators using orientation plots", *Proceedings of MUSME, The International Symposion of Multibody Simulation and Mechatronics*, Mexico, September 2002.

[110] Ciprian L., Vistrian M., Olimpiu H., "Workspace Analysis and Design of a 6-DOF Parallel Robot," *Proceedings of the 8th WSEAS International Conference on Signal Processing, Robotics and Automation,* pp. 337-340, 2009.

[111] Merlet J. P., "Determination of the orientation workspace of parallel manipulators," *Journal of Intelligent and Robotic Systems*, Vol. 13, pp. 143-160, 1995.

[112] Cai G. Q., Wang Q. M., Hu M., Kang M. C., Kim N. K., "A study on the kinematics and dynamics of a 3-DOF parallel machine tool," *Journal of Materials Processing Technology*, Vol. 111, pp. 269-272, 2001.

[113] Gosselin C. M., Jean M., "Determination of the workspace of planar parallel manipulators with joint limits," *Robotics and Autonomous Systems*, Volume 17, pp. 129-138, 1996.

[114] Merlet J. P., Gosselin C. M., Mouly N., "Workspaces of planar parallel manipulators," *Mechanism and Machine Theory*, Vol. 33, pp. 7-20, 1998.

[115] Tsai L. W., Walsh G. C., and Stamper R. E., "Kinematics of a Novel Three DOF Translational Platform," *Proceedings of the 1996 IEEE International Conf. On Robotics and Automation*, Minneapolis, MN, pp. 3446–3451, 1996.

[116] Tsai L. W., Joshi S., "Kinematics and Optimization of a Spatial 3-UPU Parallel Manipulator," *Journal of Mechanical Design,* Vol. 122 (4), pp. 439-446, 2000.

[117] Joshi S., Tsai L. W., "Jacobian Analysis of Limited-DOF Parallel Manipulators," *Journal of Mechanical Design*, Vol. 124, pp. 254-258, 2002.

[118] Hu B. and Lu Y., "Solving stiffness and deformation of a 3-UPU parallel manipulator with one translation and two rotations," *Robotica*, Vol. 29, pp. 815-822, 2011.

[119] Han C., Kim J., Kim J., Park F. C., "Kinematic sensitivity analysis of the 3-UPU parallel mechanism," *Mechanism and Machine Theory,* Vol. 37, pp. 787–798, 2002.

[120] Merlet J. P., "Jacobian, Manipulability, Condition Number, and Accuracy of Parallel Robots," *Journal of Mechanical Design*, Vol. 128(1), pp. 199-206, 2006.

[121] Walter D. R., Husty M. L. and Pfurner M., "A Complete Kinematic Analysis of the SNU 3-UPU Parallel Manipulator", *Contemporary Mathematics*, volume 496,

chapter pp. 331-346, American Mathematical Society, 2009.

[122] Venanzi S. and Parenti-Castelli V., “A New Technique for Clearance Influence Analysis in Spatial Mechanisms,” *Journal of Mechanical Design*, Vol. 127(5), pp. 446-455. 2005.

[123] Meng J., Zhang D., Li Z., “Accuracy Analysis of Parallel Manipulators With Joint Clearance,” *Journal of Mechanical Design*, Vol. 131(1), pp. 1-9, 2009.

[124] Di Gregorio R., Castelli V. P., "A Translational 3-DOF Parallel Manipulator," *Advances in Robot Kinematics: Analysis and Control*, J. Lenarcic and M. L. Husty, eds., Kluwer Academic, pp. 49–58, 1998.

[125] Joshi S., Tsai L. W., “A Comparison Study of two 3 DOF Parallel Manipulators: One with three and another with four supporting legs,” *IEEE Transactions on Robotics and Automation*, Vol. 19(2), pp. 200-209, 2003.

[126] Li Y., Xu Q., “Kinematic Analysis and Design of a new 3-DOF Translational Parallel Manipulator,” *Journal of Mechanical Design*, Vol. 128, pp. 729-737, 2006.

[126A] Walter D. R., Husty M. L., “Kinematic Analysis of the TSAI 3-UPU Parallel Manipulator using Algebraic Methods,” *13th IFToMM World Congress*, Guanajuato, Mexico, June 19–25, 2011.

[126B] Barequet G., Elber G., “Optimal bounding cones of vectors in three dimensions,” *Information Processing Letters Vol.* 93, pp. 83-89, 2005.

[126C] Shirmun L. A., Abi-Ezzi S. S., “The cone of normals technique for fast processing of curved patches,’ *Comput. Graphics Forum*, Vol. 12, pp. 261–272, 1993.

[126D] Lawson C., “The Smallest Covering Cone or Sphere,” *SIAM Reviews,* Vol. 7(3), pp. 415-417, 1965.

[127] Gosselin C. and Angeles J., “Singularity analysis of closed-loop kinematic chains,” *IEEE Transactions on Robotics and Automation*, Vol. 6(3), pp. 281-290, 1990.

[128] Blanding D. L., *Exact Constraint: Machine Design Using Kinematic Principles*, *ASME Press*, New York, 1999.

[129] Gottschalk S., Lin M. C. and Manocha D., “OBBTree: A Hierarchical Structure for Rapid Interference Detection,” *Proceedings of ACM SIGGRAPH, 23rd annual conference on Computer Graphics and interactive techniques*, pp. 171-180, 1996.

[130] Geometric Algorithms for Modeling, Motion and Animation: Proximity Query Package, http://gamma.cs.unc.edu/SSV/ (last accessed November 15, 2014)

[131] Mitutoyo South Asia Pvt. Ltd., http://www.mitutoyoindia.com/msapl/index (last accessed November 15, 2014)

[132] Faro India, http://www.faro.com/en-in/products/metrology/faroarm/overview (last accessed November 15, 2014)

[133] Cimtrex Systems, http://www.cimtrix.com/baces-3d.htm (last accessed November 15, 2014)

[134] ASME Standard: *Methods for Performance Evaluation of Articulated Arm Coordinate Measuring Machines (CMM)*, ASME B89.4.22 Standard.